

Zentrum für Sonnenenergie-
und Wasserstoff-Forschung Ulm



Universität Ulm
Fachbereich Chemie

Towards the Realization of Powerful and Energetic Electrochemical Double Layer Capacitors

Dissertation zur Erlangung des Doktorgrades
Doktor der Naturwissenschaften (Dr. rer. Nat.)
an der Fakultät der Naturwissenschaften Universität Ulm

vorgelegt von
Xu Tian

Ulm 2015

Dissertation eingereicht: 07. 2015
Tag der Promotion: 10.11. 2015
Amtierender Dekan: Prof. Dr. Joachim Ankerhold
Gutachter: 1. Prof. Dr. Werner Tillmetz
2. Prof. Dr. Mika Lindén

Declaration

The work described in this dissertation was carried out in ZSW Ulm (Zentrum für Sonnenenergie- und Wasserstoff-Forschung Baden-Württemberg), under the supervision of Prof. Werner Tillmetz, from 01.03.2011 to 31.08.2014.

Hereby I declare that this dissertation was independently made by the author and it has not been submitted for any other degree or qualification at any academic institution. No external sources and aids are used unless they are listed in the bibliography.

Karlsruhe, 11.11.2015 **Xu Tian**

Acknowledgement

First of all I would like to express my deep appreciation to Prof. Werner Tillmetz who is my first examiner. We met each other regularly and he gave me a lot of useful advices. In the end of my PhD work, he helped me with the correction of this dissertation.

I am also grateful to Prof. Mika Lindén who is so kind to be my second examiner and contributed to the improvement of this work.

Then I want to express my great gratitude to Dr. Margret Wohlfahrt-Mehrens, head of the ECM (Material research) department, for offering me the opportunity to write my dissertation in her group. She gave me lots of practical advices and has answered all my questions during the whole three and half years.

I would like to especially thank Dr. Sonia Dsoke who is the group leader of supercapacitor research in ZSW. She concerned very much about my work. Every time when I asked her questions, she was really patient and always had novel ideas which helped me a lot. She has contributed significantly to the correction of this dissertation.

Now I would like to thank all the colleagues in ZSW who helped me with my dissertation, especially the following people:

- Bettina Fuchs and Tong Zhang. We have been working together in the project of “NovaCap” and were having everyday fruitful discussions both in science and in free time.
- Gerda Dörfner for wonderful SEM/EDX pictures.
- Thomas Meinecke for helping me by using the calibrating calender.
- Paul Drews for the gas adsorption measurements.
- Marcel Wilka for numerous interesting discussions.
- Michael Kasper and Rainer Stern for all their help in technical fields.
- Agnese Birrozzi, Marco Secchiaroli, Emanuele Gucciardi and other Italian colleagues. It was always a lot of fun when talking with them. Grazie!

The German Federal Ministry of Education and Research (BMBF) and the German Ministry for Economic Affairs and Energy receive my sincere appreciation for their financial support throughout my whole PhD period.

A special thank goes to my soulmate Min Zhang, who has been always supporting me physically and mentally. It was destiny who brought us together.

In the end I would like to sincerely thank my parents. They are always the greatest help.

Abstract

In the last years, electrochemical double layer capacitors (EDLCs) have attracted a lot of interest because of their promising performances in terms of energy storage and power supply. Their ability of providing much higher power output in comparison to other devices (e.g. batteries) makes this technology suitable for many applications.

Within the framework of this dissertation, the influence of the active material, the electrode preparation and the electrode mass ratio on the performances of an EDLC has been investigated in depth.

A completely solvent-free electrode preparation route has been developed. The manufacturing parameters have been proved to be essential for obtaining electrodes with low equivalent series resistance (ESR) and diffusion resistance. The optimized hot-pressing condition has been found as 200 °C and 10 bar. Study on electrode recipe has shown that adding carbon black as conductive additive is unnecessary if the new solvent-free preparation method is employed. Furthermore, the PTFE binder content can be decreased as low as 5%. Moreover, the optimized mass ratio between the positive and negative electrodes has been found to be $m_+/m_- = 1.086$.

In the second part, six carbonaceous materials have been tested as electrode active materials in order to obtain better understanding of the correlation between physical properties of the carbons and their electrochemical performances. The carbon types SV and S0 have the highest gravimetric and volumetric capacitance, respectively. They are considered as suitable candidates for high energy applications. On the other hand, the carbon type CB possesses the lowest total resistance and is considered as a good choice for high power applications.

Table of Contents

Abstract ..... **i**

Table of Contents ..... **x**

List of Figures ..... **xiii**

List of Tables ..... **xix**

List of Abbreviations ..... **xxi**

1. General introduction **1**

2. Goal of the dissertation **6**

2.1 resistance sources control during the electrode preparation for EDLCs 6

2.2 Investigation of various carbonaceous materials for EDLC applications 6

3. Introduction to supercapacitor technology **8**

3.1 Classification of supercapacitors 8

3.2 Pseudocapacitor 10

3.2.1 Construction and Working principle 10

3.2.2 Materials 10

3.3 Hybrid capacitor 13

3.3.1 Concept and classification 13

3.3.2 Internal series hybrid 14

3.3.3 Internal parallel hybrid 15

3.4 Electrochemical double layer capacitor 17

3.4.1 Construction and working principle 17

3.4.2 Electrode active materials 20

3.4.3 Electrolyte 28

3.4.4 Separator 30

3.4.5 Current collector 31

3.5 Application fields of supercapacitors 32

4. Experimental 35
4.1 Raw materials 35
4.2 Electrode preparation 36
4.3 Cell assembly 38
4.4 Characterization methodologies 39
4.4.1 Gas sorption measurements and pore property analysis 39
4.4.2 Scanning electron microscopy (SEM) and image analysis 45
4.4.3 Electronic conductivity measurements 46
4.4.4 Electrochemical characterization 47
5. Results and discussion part I: Effects of electrode preparation, recipe and mass ratio 59
5.1 Effects of electrode preparation techniques 59
5.1.1 General effects of the Hot-pressing method 60
5.1.2 Hot-pressing effect – varying pressure 70
5.1.3 Hot-pressing effect – varying temperature 78
5.1.4 Laminating effect – varying rolling force 81
5.2 Effects of electrode recipe 89
5.3 Effects of electrode mass ratio 99
6. Results and discussion part II: Effects of electrode active materials 111
6.1 Physical properties affecting high energy performance 112
6.2 Physical properties affecting high power performance 124
6.2.1 Electrical conductivity and resistivity of carbon electrodes 124
6.2.2 Effects of mesoporous structure of carbon materials 126
7. Conclusion and outlook 134
7.1 Conclusion 134
7.1.1 Improvement of electrode preparation 134

7.1.2 Selection of proper carbons as EDLC active material for various applications 136
7.2 Outlook 138
Bibliography 139

List of Figures

FIGURE 1. SPECIFIC POWER AGAINST SPECIFIC ENERGY, ALSO CALLED A RAGONE PLOT, FOR VARIOUS ELECTRICAL ENERGY STORAGE DEVICES [4]. 3
FIGURE 2. SCHEMATIC OF CLASSIFICATION OF SUPERCAPACITORS [13]. 9
FIGURE 3. PROPOSED PSEUDOCAPACITOR MATERIALS IN LITERATURE [11]. 11
FIGURE 4. CLASSIFICATION OF HYBRID CONFIGURATIONS OF SUPERCAPACITORS AND BATTERIES, SEPARATORS ARE NOW DRAWN FOR SIMPLICITY [15]. 14
FIGURE 5. CONSTRUCTION OF A CONVENTIONAL ELECTRIC CAPACITOR. 17
FIGURE 6. PRINCIPLE CONSTRUCTION OF AN EDLC: 1. EXTERNAL POWER SOURCE, 2. CURRENT COLLECTOR, 3. ELECTRODE, 4. HELMHOLTZ DOUBLE LAYER, 5. ELECTROLYTE, 6. SEPARATOR [29]. 18
FIGURE 7. SIMPLE SKETCH OF THE HELMHOLTZ DOUBLE LAYER [28]. 20
FIGURE 8. SCHEMATIC OF THE POROUS STRUCTURE OF ACTIVATED CARBON [32]. 22
FIGURE 9. SCHEMATIC OF THE STRUCTURE OF SWCNT AND MWCNT [38]. 24
FIGURE 10. SCHEMATIC OF PREPARATION PROCEDURE OF ORDERED MESOPOROUS CARBON (OMC) [41]. 25
FIGURE 11. SCHEMATIC OF THE STRUCTURE OF GRAPHENE LAYER [45]. 27
FIGURE 12. CAPABUS (SUPERCAPACITOR BUS) IN SHANGHAI COMPLETELY POWERED BY SUPERCAPACITORS [59]. 33
FIGURE 13. SCHEMATIC DEMONSTRATION OF THE SOLVENT-FREE ELECTRODE PREPARATION PROCEDURE. 38
FIGURE 14. SKETCH OF A SWAGELOK CELL (ADAPTED FROM [64]). 39
FIGURE 15. SIX TYPICAL ISOTHERMS OF POROUS MATERIALS [65]. 40
FIGURE 16. FOUR TYPICAL HYSTERESIS PATTERNS OF ISOTHERMS OF POROUS MATERIALS [65]. 41
FIGURE 17. TYPICAL T-PLOT OF A POROUS MATERIAL WITH PRESENCE OF BOTH MESO- (A) AND MICROPORES (B) [67]. 45
FIGURE 18. IMAGE PROCESSING STEPS FOR CHARACTERIZATION OF THE PORES [73]. . 46

FIGURE 19. EXPERIMENTAL SETUP FOR MEASURING THE VOLUME ELECTRONIC CONDUCTIVITY OF ELECTRODES. (A) SCHEMATIC OF THE DEVICE AND (B) DETAILED VIEW OF THE 4-WIRE SENSING SETUP [64]. 47
FIGURE 20. SCHEMATIC OF CURRENT EXCITATION IN A GCPL MEASUREMENT [64]..... 48
FIGURE 21. TYPICAL CHARGING-DISCHARGING CURVE OF AN EDLC CELL. 49
FIGURE 22. SCHEMATIC OF VOLTAGE EXCITATION IN A CV MEASUREMENT [64]. 51
FIGURE 23. TYPICAL CYCLIC VOLTAMMOGRAM OF AN EDLC..... 52
FIGURE 24. SINUSOIDAL EXCITATION AND RESPONSE IN AN EIS EXPERIMENT [64]..... 54
FIGURE 25. TYPICAL NYQUIST PLOT FOR A CARBON/CARBON EDLC..... 54
FIGURE 26. EXPERIMENTAL NYQUIST PLOT AND CORRESPONDING SIMULATION. THE INSET SHOWS THE EQUIVALENT CIRCUIT USED FOR THE SIMULATION. 55
FIGURE 27. THE STANDARD TEST PROTOCOL USED IN THIS STUDY..... 58
FIGURE 28. RESISTANCE SOURCES IN AN EDLC ELECTRODE [73]..... 60
FIGURE 29. N_2 ADSORPTION AND DESORPTION ISOTHERMS OF POWDERS (A) AND ELECTRODES (B) OF SIX CARBONACEOUS MATERIALS..... 61
FIGURE 30. PORE SIZE DISTRIBUTION PATTERNS OF POWDERS (A) AND ELECTRODES (B) FROM SIX CARBONACEOUS MATERIALS OBTAINED BY BOTH N_2 AND CO_2 ADSORPTION MEASUREMENTS. THE MODEL USED FOR COMPUTATION WAS BASED ON NLDFT..... 64
FIGURE 31. SCHEMATIC OF A PROCESS IN WHICH MICROPORES JOIN TOGETHER TO FORM MESOPORES, ONLY THE TRANSITION PROCESS INSIDE THE RED CIRCLE IS DEPICTED FOR SIMPLICITY. 67
FIGURE 32. RELATIONSHIP BETWEEN DIFFUSION RESISTIVITY AND EXTERNAL SURFACE PROPORTION OF ELECTRODES MADE FROM SIX CARBON MATERIALS. 68
FIGURE 33. RELATIONSHIP BETWEEN DIFFUSION RESISTIVITY AND MESOPOROUS VOLUME PROPORTION OF ELECTRODES MADE FROM SIX CARBON MATERIALS. 69
FIGURE 34. SPECIFIC CAPACITANCE VERSUS CELL VOLTAGE OF CARBON ELECTRODES PREPARED AT VARIOUS PRESSURES. THE DATA ARE OBTAINED FROM CV AT 10 MV

S^{-1} BY DIVIDING THE SPECIFIC CURRENT BY THE SCAN RATE. ELECTROLYTE: $TEABF_4$ IN ACETONITRILE.....70
FIGURE 35. (A) GALVANOSTATIC CYCLE AT 1 A G^{-1} OF CARBON ELECTRODES PRESSED ON A TREATED AL FOIL AT 160 °C AND AT 10, 30, AND 50 BAR. (B) MAGNIFICATION OF THE CURVES AT MORE POSITIVE POTENTIALS. ELECTROLYTE: $TEABF_4$ IN ACETONITRILE.....72
FIGURE 36. NYQUIST PLOTS OF CELLS ASSEMBLED WITH ELECTRODES PRESSED ON A TREATED AL FOIL AT 160°C AND AT 10, 30, AND 50 BAR. ELECTROLYTE: $TEABF_4$IN ACETONITRILE. THE INSET SHOWS THE NYQUIST PLOTS MAGNIFICATION.....72
FIGURE 37. IMPEDANCE SPECTRA OF ELECTRODES PRESSED USING THE SAME CONDITIONS (160 °C AND 50 BAR) BUT ONTO DIFFERENT CURRENT COLLECTORS.73
FIGURE 38. ORIGINAL AND WITH IMAGEJ-CONVERTED MICROGRAPHS OF THE ELECTRODES PRESSED AT 160 °C AND DIFFERENT PRESSURES. 74
FIGURE 39. PORES AREA CALCULATED BY USING IMAGEJ ANALYSIS OF THE ELECTRODES OF FIGURE 38.....75
FIGURE 40. SEM IMAGES AT HIGHER MAGNIFICATION OF CARBON ELECTRODES PRESSED AT 160 °C AND AT VARIOUS PRESSURES. THE AREAS MARKED WITH DASHED LINE INDICATE THE BINDER.....77
FIGURE 41. NYQUIST PLOTS OF CELLS ASSEMBLED WITH ELECTRODES PRESSED ON A TREATED AL FOIL AT 10 BAR AND AT DIFFERENT TEMPERATURES. ELECTROLYTE: TEABF4 IN ACETONITRILE. THE INSET SHOWS THE NYQUIST PLOTS MAGNIFICATION. 78
FIGURE 42. ORIGINAL AND WITH IMAGEJ-CONVERTED MICROGRAPHS AFTER THRESHOLD OF ELECTRODES PRESSED AT 10 BAR AND DIFFERENT TEMPERATURES. 79
FIGURE 43. (A) PORE AREA AVERAGE CALCULATED BY SEM IMAGES USING IMAGEJ SOFTWARE AND (B) DIFFUSION RESISTIVITY AS CALCULATED FROM THE EIS SIMULATION.....80

FIGURE 44. NYQUIST PLOTS (FRESH ELECTRODES) OF SUPERCAPACITOR CELLS LAMINATED WITH DIFFERENT FORCES IN COMPARISON WITH THE ONE PROCESSED BY HOT-PRESS. 82
FIGURE 45. NYQUIST PLOTS (AFTER 200 CYCLES) OF SUPERCAPACITOR CELLS LAMINATED WITH DIFFERENT FORCES IN COMPARISON WITH THE ONE PROCESSED BY HOT-PRESS. 83
FIGURE 46. GRAVIMETRIC CAPACITANCE OF SUPERCAPACITOR CELLS LAMINATED WITH DIFFERENT FORCES IN COMPARISON WITH THE ONE PROCESSED BY HOT-PRESS (SCAN RATE 10 MV S^{-1}). 84
FIGURE 47. GALVANOSTATIC CYCLING CURVES OF SUPERCAPACITOR CELLS LAMINATED WITH DIFFERENT FORCES IN COMPARISON WITH THE ONE PROCESSED BY HOT-PRESS (CYCLING CONDITION: 1 A G^{-1}). 86
FIGURE 48. SCANNING ELECTRON MICROSCOPY (SEM) IMAGES AND THE ANALYSIS THEREOF FROM SUPERCAPACITOR ELECTRODES LAMINATED WITH DIFFERENT FORCES..... 88
FIGURE 49. NYQUIST PLOTS OF FRESH CARBON ELECTRODES WITH DIFFERENT CARBON BLACK CONTENT. 90
FIGURE 50. DEVELOPMENT OF INTERFACE CONTACT RESISTANCE OF CARBON ELECTRODES CONTAINING DIFFERENT PERCENTAGE OF CARBON BLACKS DURING ELECTROCHEMICAL TESTING. 91
FIGURE 51. DEVELOPMENT OF APPARENT DIFFUSION RESISTANCE OF CARBON ELECTRODES CONTAINING DIFFERENT PERCENTAGE OF CARBON BLACKS DURING ELECTROCHEMICAL TESTING. 92
FIGURE 52. SEM PICTURES OF UNCOMPACTED MIXTURE (ACTIVATED CARBON, CARBON BLACK AND BINDER) AND FREE STANDING ELECTRODE. 94
FIGURE 53.DEVELOPMENT OF APPARENT DIFFUSION COEFFICIENT OF CARBON ELECTRODES CONTAINING DIFFERENT PERCENTAGE OF PTFE BINDER DURING ELECTROCHEMICAL TESTING. 96

FIGURE 54. SEM IMAGES OF EDLC ELECTRODES WITH THREE DIFFERENT PTFE BINDER CONTENT. 97
FIGURE 55. RELATIONSHIP OF SURFACE PORE FRACTION AND PTFE BINDER CONTENT OF THE CARBON ELECTRODES (OBTAINED FROM SEM PHOTOS ANALYSIS BY IMAGEJ). 98
FIGURE 56. SCHEMATIC OF TEA^+ AND BF_4^- IONS [86]..... 99
FIGURE 57. COMPARISON OF SYMMETRIC AND ASYMMETRIC EDLCS: DIFFERENCE ON THE WIDTH OF ELECTROCHEMICAL STABILITY WINDOWS [87]..... 100
FIGURE 58. INDIVIDUAL CONTRIBUTIONS OF BOTH ELECTRODES IN A SYMMETRIC CELL IN THE CONVENTIONAL POTENTIAL RANGE (2.5 V). 102
FIGURE 59. DETERMINATION OF THE ELECTROLYTE ESW IN HALF CELL..... 103
FIGURE 60. SCHEMATIC OF CALCULATION METHOD FOR FARADAIC FRACTION IN ANODIC TERRITORY [88]..... 104
FIGURE 61. FARADAIC FRACTION UNDER VARIOUS POTENTIALS AND TWO DIFFERENT CRITERIA OF DETERMINING ESW OF AN ELECTROLYTE..... 106
FIGURE 62. CAPACITANCE LOSSES OF EDLCS WITH DIFFERENT OPERATING VOLTAGES AFTER 1500 CYCLES..... 108
FIGURE 63. RELATIONSHIP BETWEEN TOTAL FARADAIC FRACTION AND CAPACITANCE LOSS AFTER CYCLING..... 109
FIGURE 64. SEM PHOTOS OF SIX CARBON MATERIALS..... 111
FIGURE 65. N_2 ADSORPTION AND DESORPTION ISOTHERMS OF SIX CARBONACEOUS MATERIALS..... 113
FIGURE 66. CHARGING/DISCHARGING CURVES OF CAPACITOR CELLS BASED ON SIX CARBONACEOUS MATERIALS. CYCLING CURRENT DENSITY = 1 A G^{-1}..... 114
FIGURE 67. RELATIONSHIP BETWEEN SPECIFIC SURFACE AREA OF CARBON AND GRAVIMETRIC CAPACITANCE OF ELECTRODE (ADAPTED FROM [93]). 116
FIGURE 68. RELATIONSHIP BETWEEN BETSSA AND GRAVIMETRIC CAPACITANCE OF THE CARBONACEOUS MATERIALS TESTED AT ZSW AND KÖTZ'S GROUP [93]..... 117

FIGURE 69. RELATIONSHIP BETWEEN DFT SSA AND GRAVIMETRIC CAPACITANCE OF THE CARBONACEOUS MATERIALS TESTED AT ZSW AND KÖTZ'S GROUP [93]..... 118
FIGURE 70. EFFECT OF PORE SIZE ON THE AREA SPECIFIC CAPACITANCE FOR THE CARBONS IN $TEABF_4$-BASED ELECTROLYTE, ADAPTED FROM [97]: (A) THE NORMALIZED CAPACITANCE INCREASES IN SUB-NM PORES; (B TO D) SCHEMATIC ILLUSTRATION OF SOLVATED IONS IN PORES WITH DISTANCE BETWEEN ADJACENT PORE WALLS (B) > 2 NM, (C) 1 NM - 2 NM, AND (D) < 1 NM..... 120
FIGURE 71. PORE SIZE DISTRIBUTION PATTERNS OF SIX CARBONACEOUS MATERIALS OBTAINED FROM BOTH N_2 AND CO_2 ADSORPTION MEASUREMENTS. THE MODEL USED FOR COMPUTATION WAS BASED ON NLDFT..... 121
FIGURE 72. LINEAR FIT OF C_{SEXT} VERSUS $S_{MICRO}S_{EXT}$ FOR VARIOUS CARBONACEOUS MATERIALS..... 123
FIGURE 73. NYQUIST PLOTS OF FRESH CAPACITOR CELLS USING DIFFERENT CARBON MATERIALS AND A ZOOM-IN OF THE SEMICIRCLES..... 126
FIGURE 74. RELATIONSHIP BETWEEN DIFFUSION RESISTIVITY AND EXTERNAL SURFACE PROPORTION OF SIX CARBON MATERIALS..... 127
FIGURE 75. RELATIONSHIP BETWEEN DIFFUSION RESISTIVITY AND MESOPOROUS VOLUME PROPORTION OF SIX CARBON MATERIALS..... 128
FIGURE 76. RAGONE PLOTS (ENERGY DENSITY VS. POWER DENSITY) OF EDLC CELLS MADE FROM SIX CARBON MATERIALS. 129
FIGURE 77. PLOT OF SPECIFIC CAPACITANCE VERSUS TESTING FREQUENCY, DERIVED FROM EIS MEASUREMENTS. 131
FIGURE 78. PLOT OF C' RETENTION AGAINST MESOPOROUS VOLUME FRACTION OF SIX CARBON POWDERS..... 132
FIGURE 79. PLOT OF C' RETENTION AGAINST MESOPOROUS VOLUME FRACTION OF ELECTRODES MADE FROM SIX CARBON MATERIALS..... 133

List of Tables

TABLE 1. PROPERTIES AND CHARACTERISTICS OF VARIOUS CARBONACEOUS MATERIALS AS SUPERCAPACITORS ELECTRODE MATERIALS [30]. 21
TABLE 2. RAW MATERIALS USED IN THIS DISSERTATION. 35
TABLE 3. PRECURSOR MATERIALS AND ACTIVATION METHODS OF SIX CARBONS 36
TABLE 4. COMPARISON OF THE SPECIFIC SURFACE AREA DATA FROM BOTH PURE CARBON POWDERS AND READY ELECTRODES BY EMPLOYING THE BET AND NLDFT MODELS 63
TABLE 5. MICROPOROUS SURFACE AREA AND MICROPOROUS VOLUME FRACTION OF SIX CARBONACEOUS MATERIALS (POWDER FORM AND ELECTRODE FORM) 65
TABLE 6. MESOPOROUS SURFACE AREA AND MESOPOROUS VOLUME FRACTION OF SIX CARBONACEOUS MATERIALS (POWDER FORM AND ELECTRODE FORM) 66
TABLE 7. GRAVIMETRIC SPECIFIC CAPACITANCES OF SUPERCAPACITOR ELECTRODES LAMINATED WITH DIFFERENT FORCES IN COMPARISON WITH THE ONE PROCESSED BY HOT-PRESS (CALCULATED FROM CV). 85
TABLE 8. GRAVIMETRIC SPECIFIC CAPACITANCES OF SUPERCAPACITOR ELECTRODES LAMINATED WITH DIFFERENT FORCES IN COMPARISON WITH THE ONE PROCESSED BY HOT-PRESS (CALCULATED FROM GCPL). 87
TABLE 9. PORE FRACTION AND AVERAGE PORE SIZE VALUES OF SUPERCAPACITOR ELECTRODES LAMINATED WITH DIFFERENT FORCES. 88
TABLE 10. FARADAIC FRACTION (R), Δn AND $\Delta n + 1 - \Delta n$ AT DIFFERENT POTENTIALS. 107
TABLE 11. SUMMARY OF THE EXPERIMENTAL RESULTS FROM INVESTIGATION OF THE RELATION BETWEEN MASS RATIO AND CAPACITANCE LOSS. 110
TABLE 12. SPECIFIC GRAVIMETRIC AND VOLUMETRIC CAPACITANCE OF THE SIX CARBON ELECTRODES DERIVED FROM GCPL MEASUREMENTS (CYCLING RANGE: 0-2.5 V, CURRENT DENSITY = 1 A G^{-1}). 115

TABLE 13. COMPARISON BETWEEN THE PORE SIZES OF THE CARBON MATERIALS TESTED IN THIS STUDY AND THE SIZES OF THE MOST COMMONLY USED IONS [97][101]... 122
TABLE 14. ELECTRICAL RESISTIVITY AND CONDUCTIVITY OF ELECTRODES PREPARED FROM SIX DIFFERENT CARBONS..... 125
TABLE 15. ENERGY RETENTION OF EDLC CELLS PREPARED FROM SIX CARBONACEOUS MATERIALS..... 130

List of Abbreviations

AC	Activated Carbon
ACF	Activated Carbon Fibre
AN	Acetonitrile
BET	Brunauer–Emmett–Teller
CDC	Carbide Derived Carbon
CE	Counter Electrode
CNT	Carbon nanotube
CPD	Constant Power Discharge
CV	Cyclic Voltammetry
DB	Denka Black
DFT	Density Functional Theory
EDLC	Electrochemical Double Layer Capacitor
EIS	Electrochemical Impedance Spectroscopy
EPH	External Parallel Hybrid
ESH	External Series Hybrid
ESR	Equivalent Series Resistance
ESW	Electrochemical Stability Window
GCPL	Galvanostatic Cycling with Potential Limitation
GO	Graphene Oxide
HEV	Hybrid Electric Vehicle
IHP	Inner Helmholtz Plane
IL	Ionic Liquid
IPH	Internal Parallel Hybrid
IR-Drop	Voltage drop
ISH	Internal Series Hybrid
ITO	Indium Tin Oxide

LIB	Lithium Ion Battery
LTO	Lithium Titanate ($Li_4Ti_5O_{12}$)
MWNT	Multi Walled Nanotube
NLDFT	Non-Local Density Functional Theory
OHP	Outer Helmholtz Plane
PANI	Polyaniline
PC	Propylene Carbonate
PSD	Pore Size Distribution
PTFE	Polytetrafluoroethylene
RE	Reference Electrode
SEM	Scanning Electron Microscopy
SC	Supercapacitor
SSA	Specific Surface Area
SWNT	Single Walled Nanotube
WE	Working Electrode
wt%	Weight percent

1. General introduction

Referring to the World Energy Outlook 2013 written by the International Energy Agency, the global total primary energy demand from 2011 to 2035 will increase double the quantity as the growth from 1987 to 2011. In simple words, our energy consumption increases with accelerating speed [1].

In recent years, the great success that the Americans and Canadians achieved in the exploitation of shale gas has brought us illusion that it looks like always possible for human being to find new fossil energy sources. However, no matter how promising a fossil energy source may appear to be, the reserves of them are limited. There must come one day that all resources in our beautiful planet are depleted. What we need is renewable, affordable and reliable energy sources which have unlimited reservoir.

Renewable energy sources, as the name itself explains, can be continually replenished on a human time scale. Typical examples are wind, sunlight, geothermal heat and biomass etc. [2]. However, the wind isn't blowing without seconds of interruption; the sun doesn't shine in the night. There comes the problem that energy supply which is based 100% on renewable sources is not stable. Sometimes excessive electricity is generated and sometimes only very limited amount of energy can be supplied. This is exactly the reason why electric energy storage is now under the spotlight.

Electric energy storage technologies can be classified into two categories, stationary and mobile. For stationary applications lead-acid battery, fuel cell, redox-flow battery, lithium-ion-battery etc. are currently widely used, whereas in the case of mobile electric energy storage, or more precisely, for pure electric vehicles, fuel cells, batteries and electrochemical double-layer capacitors (EDLCs) are the three main candidates.

A fuel cell is an electrochemical energy conversion device that has a continuous

supply of fuel such as hydrogen or methanol (for anodic consumption) and an oxidant such as oxygen or simply air (for cathodic consumption) [3].

A battery is one or more electrically connected electrochemical cells having contacts to supply electrical energy. A secondary battery, in contrast to a primary battery, can be recovered to its charged state by means of flowing of electric current in the opposite direction as the current flow during discharge. In the field of E-mobility, normally such rechargeable batteries are employed as the energy source [3].

An EDLC is a device that stores electrical energy in the electrical double layer that forms at the interface between an electrolytic solution (electrolyte) and an electronic conductor (electrode) [3].

EDLCs are very often compared with other electric energy storage devices. Shown below in Figure 1 is a comparison of power densities and energy densities among many popular devices [4]. It can be clearly observed from the graph that EDLC possesses lower energy density in comparison with batteries and lower power density when compared with traditional capacitors. Written below is a detailed analysis of the problems that EDLC is currently facing.

1. The power density

The term "Power density" describes the fast charging-discharging capability of an electric energy storage device. The higher the power density of the device is, the faster it can be charged and discharged. This characteristic is essential for practical applications.

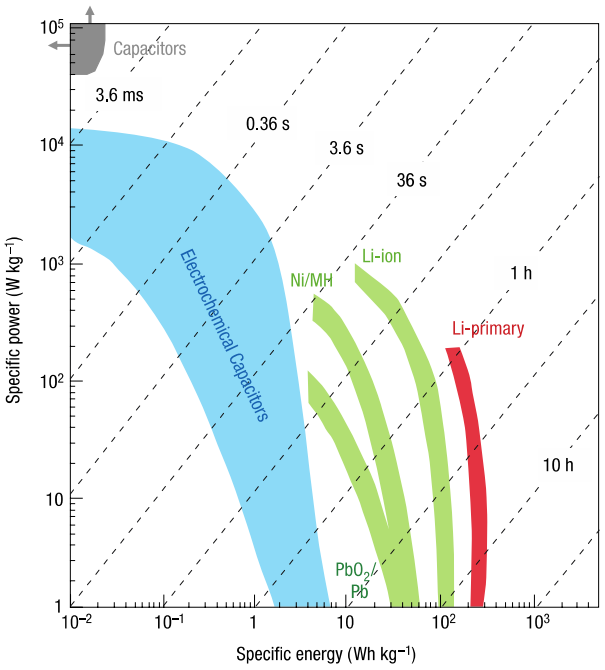


Figure 1. Specific power against specific energy, also called a Ragone plot, for various electrical energy storage devices [4].

When we speak about a typical EDLC application, the role of EDLC as a temporary storage device to catch the braking energy and further transfer it to the main battery of a car is very often mentioned. A normal battery in comparison would be not able to do this job. However, it is very often the case that even EDLCs don't function satisfactorily if the design of the capacitor cells is not optimized. Therefore it is obviously necessary to look close to the scientific background and find out proper solution to improve the power density of EDLCs. The maximum power density of an EDLC can be calculated by applying the formula: $P_{max} = V^2/4R$, in which V stands for the operating voltage of the capacitor cell and R is the Equivalent Series Resistance (ESR) [5]. In order to achieve a maximum power density, it is obvious that the voltage of the capacitor has to be as high as possible and its resistance has to be kept to the minimum

value. However in reality, due to various reasons (e.g. improper mass balance of the cathode and the anode, use of electrolytes with narrow Electrochemical Stability Window (ESW), insufficient contact between the current collector and the electrode active material etc.), the power density of an EDLC is very often not achieving the optimum.

2. The energy density

"Energy density" is another very important parameter describing energy storage devices and it's a measure of how much electrical energy can be stored in them. In practice, this property of an electrical energy storage device has significant meaning because it determines directly how many hours you can play with your cellphone and how many kilometers you can drive with your electric car.

It is generally believed that EDLCs feature only 5-10% the energy density comparing to LIBs [6]. Therefore in order to compete with batteries, the energy density of EDLCs must be significantly increased. Referring to the formula $E = 1/2\ CV^2$, the energy density of an EDLC is determined by the specific capacitance of the active material and the cell operating voltage [5]. With the goal of achieving a maximum energy density, both the specific capacitance and operating voltage have to be maximized. However, very often in the real life, derived from various origins (e.g. improper mass balance of the cathode and the anode, use of electrolytes with narrow Electrochemical Stability Window (ESW), use of active materials with low specific capacitance etc.), the energy density of EDLCs is not very much satisfactory.

3. Electrode preparation technique

Furthermore, what should be also mentioned in this chapter is the electrode preparation technique. Traditionally the EDLC electrodes are prepared by the wet slurry method including mixing process of raw materials in N-Methyl-2-pyrrolidone (NMP). NMP is an organic solvent which is toxic and environmental unfriendly. Furthermore, electrodes produced by the slurry method are known to

have generally low compaction degree and density, the surface of electrodes shows sometimes cracks. Therefore this preparation method still presents some problematic which has to be solved.

2. Goal of the dissertation

2.1 RESISTANCE SOURCES CONTROL DURING THE ELECTRODE PREPARATION

In order to maximize the power density of an EDLC, its operating voltage has to be as high as possible and its electric resistance has to be as low as possible.

Nowadays the operating voltages of commercial EDLCs lie in the range of 2.3 – 2.7 V, they are mainly determined by the electrolytes that are employed [7][8]. As long as the same electrolyte is employed, the operating voltage of the cell remains unchanged.

One goal of this dissertation is to obtain deep understanding of the origin of the resistance sources in capacitor electrodes and control the resistance. This can be done by employing active material with low electrical resistivity and controlling the resistance sources during the electrode preparation. It is planned to develop a new environmental friendly electrode preparation route which is able to manufacture supercapacitor electrodes with excellent power performances and overcome the drawbacks of the traditional method which employs toxic solvent like N-Methyl-2-pyrrolidone.

Furthermore, a fast diffusion of the electrolyte inside the carbon pores is of great importance for the power density of the capacitor. This is also greatly influenced by the electrode preparation and formulation. Physical and electrochemical characterization techniques allow correlating and understanding the ion adsorption mechanism in the porous structure of the active materials.

Moreover, good electrode balancing insures high energy density of the cell and improved cycling stability. Thus the effect of mass ratio between the cathode and anode has been also studied.

2.2 INVESTIGATION OF VARIOUS CARBONACEOUS MATERIALS FOR EDLC APPLICATIONS

There are great numbers of various materials that can be used in EDLCs, e.g. activated carbon, transition metal oxides, electric conducting polymers, carbon

nanotubes, graphene etc. [4]. However, activated carbon is presently still the most widely used active material for EDLCs thanks to their high surface area, controllable pore size and relatively low cost [9]. In this dissertation, several activated carbons featuring different physical properties (surface area, pore size distribution etc.) are supposed to be physically and electrochemically characterized. From these results and also the help of an optimized electrode preparation technique it is possible to find out the ones suitable for high power, high energy and universal applications, respectively. Furthermore, one could also understand the correlations between the electrochemical performances (i.e. resistance and capacitance) with the physical properties of the specific carbonaceous material.

3. Introduction to supercapacitor technology

3.1 Classification of supercapacitors

Supercapacitor (SC) is usually considered as the general term for a family of electrochemical capacitors [8][13]. There are three main categories of SCs: Electrochemical double layer capacitors, Pseudocapacitors and hybrid capacitors (see Figure 2) [10]. This classification is made based on different charge storage mechanisms of the capacitors. EDLCs store electric charge pure electrostatically; pseudocapacitors store electric charge electrochemically whereas the charge is stored both electrostatically and electrochemically in hybrid capacitors. The detailed working principles of every individual class are explained in following sections.

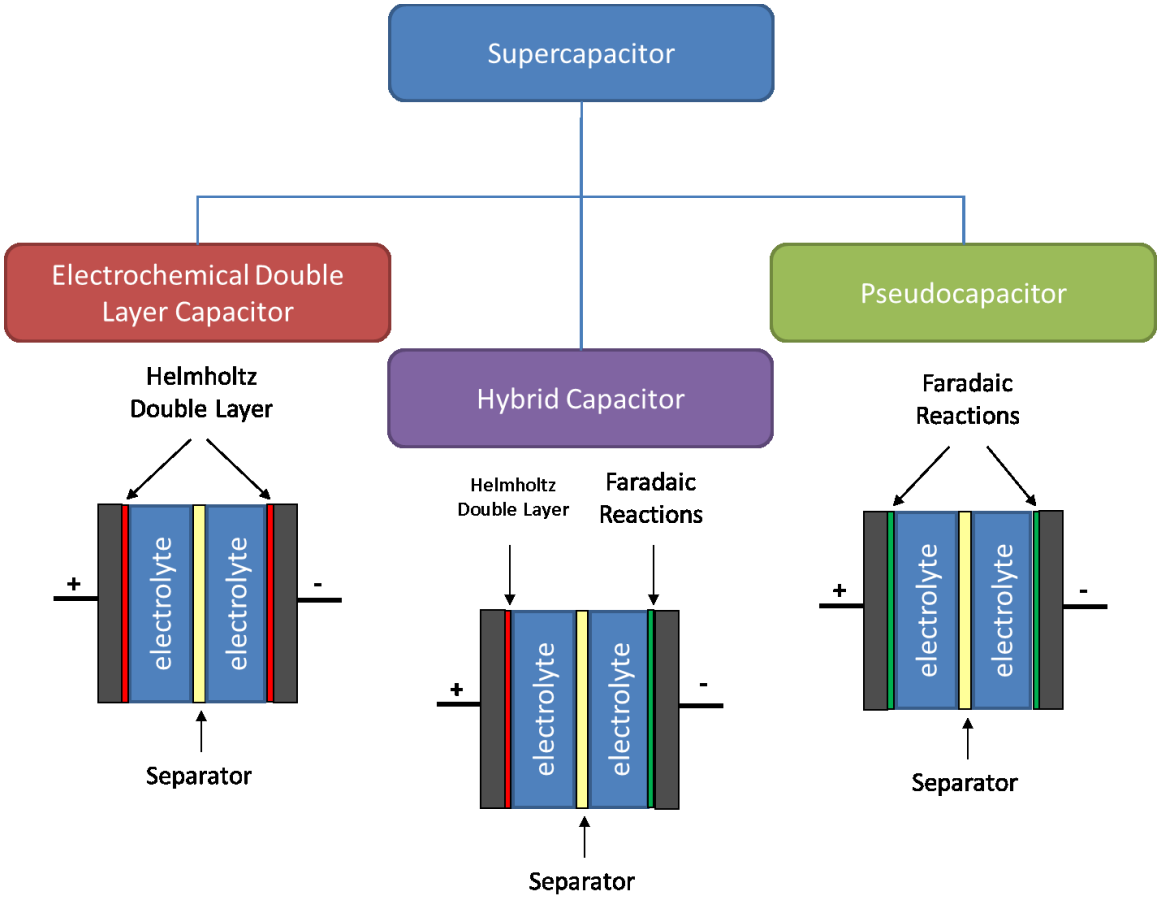


Figure 2. Schematic of classification of supercapacitors [13].

3.2 PSEUDOCAPACITOR

3.2.1 Construction and Working principle

Pseudocapacitor stores electrical energy in a dynamic way. Fast reversible faradaic reactions at the electrode-electrolyte interface facilitate the charge transfer and normally the specifically adsorbed ions on the electrode surface are responsible for these reactions. However, a pseudocapacitance occurs always together with double-layer capacitance and they contribute to the total capacitance at the same time. The pseudocapacitance may achieve a capacitance value 10 or 100 times bigger than the static double-layer capacitance, this is fully depending on the reaction mechanisms that happen on the electrode surface and within the electrode structure [5].

A pseudocapacitor is normally built on the basis of an EDLC by replacing carbon electrodes with electrodes which enable the pseudocapacitance, typical materials used in such electrodes are metal oxides and conducting polymers [10]. Examples of possible active materials are given in the following section.

3.2.2 Materials

Researchers have investigated plenty of active materials which can be used for EDLC and pseudocapacitor applications. The specific capacitances of them are compared in Figure 3.

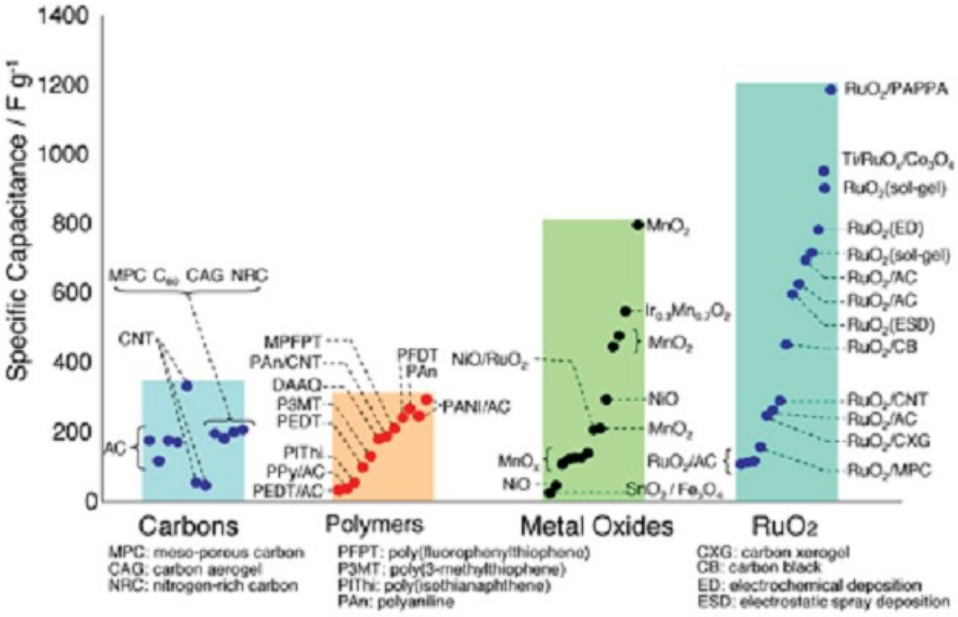


Figure 3. Proposed pseudocapacitor materials in literature [11].

Metal oxides have been proposed long ago as the possible electrode materials for pseudocapacitors. The main advantages of such materials are their high specific capacitance and excellent electric conductivity [10].

Researchers all over the world have been studying candidates like MnO_2, NiO, SnO_2, Fe_3O_4, RuO_2 etc. [11]. Among all of them, ruthenium oxide is attracting the most attention due to its extremely high specific capacitance. The capacitance of ruthenium oxide is achieved through the intercalation-deintercalation process of protons into its structure [12]. For instance, the group of Naoi has reported a composite made from highly dispersed nano-sized (0.5 to 2 nm) hydrous RuO_2/Ketjen black, the composite shows a high specific capacitance of 821 F g^{-1} [13].

Although the electrochemical properties of ruthenium oxide are really attractive, the high cost of this material still hinders its wide success. A lot of researches are going on trying to reduce the material and processing cost of it [10].

For pseudocapacitors with metal oxide as active material, water based-electrolyte like NaOH or H_2SO_4 is the state-of-the-art.

Conducting polymers, another category of important pseudocapacitor materials, have attracted a lot of attention as well. This group of materials has also relatively high capacitance and conductivity which make them suitable candidates for pseudocapacitor applications. Popular materials are polyaniline, polypyrrole and polythiophene etc. [11]. The pseudocapacitance of conducting polymers arises from fast and reversible redox processes of the π-conjugated polymer chains [14]. The n/p-type polymer configuration with one n-doped and one p-doped polymer electrode has considerable energy and power densities; however, an efficient n-doped conducting polymer material has not been found yet [10]. Moreover, cycling stability of this group of materials remains uncertain due to the mechanical stress induced by the charging-discharging process, this is hindering the development of conducting polymer pseudocapacitors [13][41].

The electrolytes which can be used in conducting polymer pseudocapacitors are similar to those employed in EDLCs, such as H_2SO_4, NaOH, $TEABF_4$ in PC etc. [14][10].

3.3 HYBRID CAPACITOR

3.3.1 Concept and classification

The hybridization of various electrochemical energy storage devices has been always one of the most interesting topics for researchers worldwide. In order to realize a hybrid configuration, one has to bring at least two different energy storage mechanisms together into one single device. In practice, EDLC technology is very often combined with pseudocapacitor or battery. According to the classification method proposed by Cericola et al., hybrid systems are devided into two categories and subsequently four subcategories (see Figure 4) [15].

External hybridization can be realized by hardwire-connecting two energy storage devices with different storage mechanisms together (e.g. an EDLC with a lithium ion battery), either series connected (ESH) or parallel connected (EPH). These kinds of devices are rather irrelevant for chemists and will not be discussed further in this dissertation.

On the other hand, internal hybrid devices are developed by hybridization on the electrode level. For instance, a device with one EDLC electrode and one battery electrode is considered as internal series hybrid (ISH); a device with the property that each electrode consists of at least two active materials is defined as internal parallel hybrid (IPH) [15].The goal of building such hybrid capacitors is to greatly increase the energy density of the wholedevice while keeping the high power density advantage of the EDLC material.

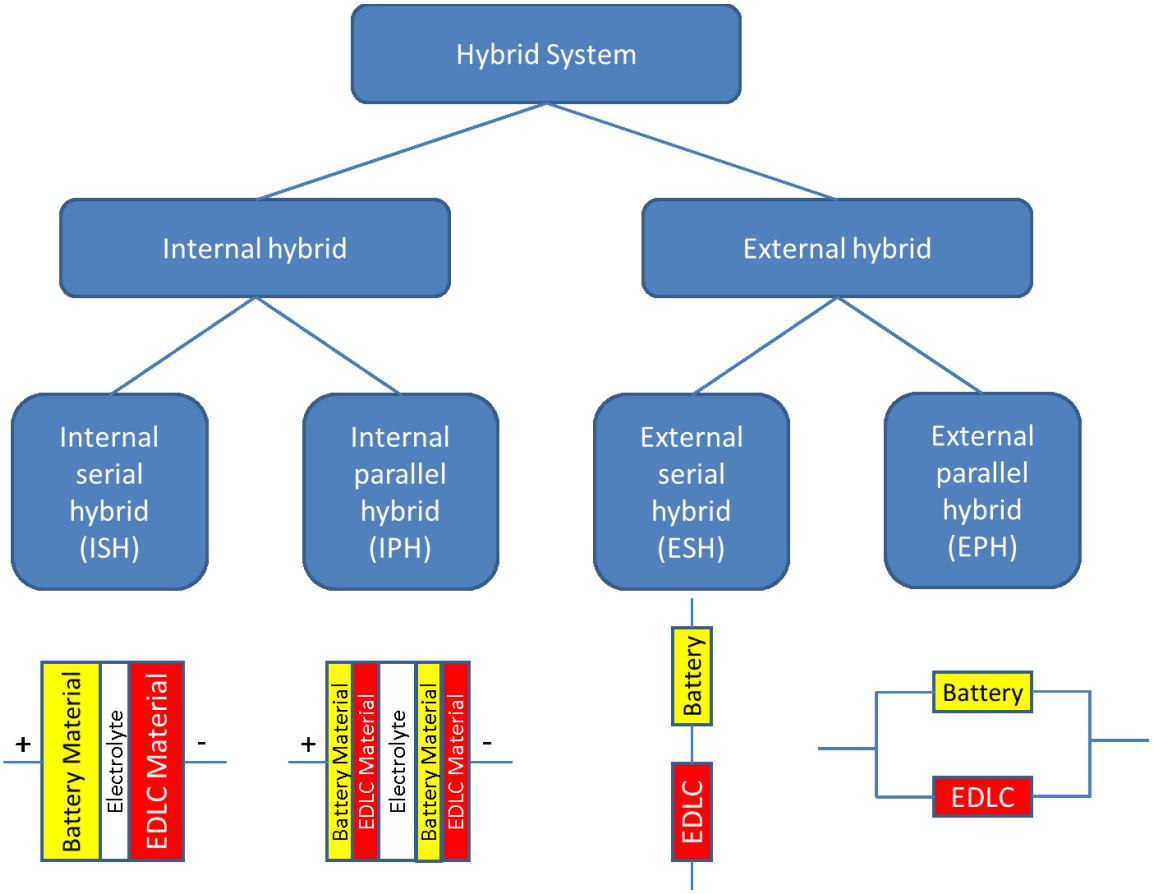


Figure 4. Classification of hybrid configurations of supercapacitors and batteries, separators are now drawn for simplicity. This graph is adapted from [15]. License received from Elsevier under the license Number 3747000025199.

3.3.2 Internal series hybrid

An internal series hybrid system consists of one electrode enabling faradaic reaction and another electrode where the charge is stored in the EDL. For the EDL storage mechanism is normally carbonaceous materials (mainly activated carbon) responsible. But for the faradaic reactions researchers have been investigating countless materials. Typical examples are metal oxides, conducting polymers and lithium insertion materials.

Manganese oxides are studied widely as active materials for hybrid capacitors. In such configuration, activated carbon is used as negative electrode material; MnO_2 is used in the positive electrode; aqueous solutions like Na_2SO_4, K_2SO_4 and KOH are employed as electrolytes [15].

Moreover, conductive polymers are also used in supercapacitors due to their excellent specific capacitance and rate capability. In a conducting polymer-based hybrid capacitor, the negative electrode is usually activated carbon and the positive electrode is composed of a polymer like Polyaniline, Polyfluorene or various Polythiophene-based materials. Furthermore, the electrolytes can be selected from a broad spectrum ranging from aqueous solutions, organic electrolytes to ionic liquids [15].

In order to include the high energy characteristic of a lithium ion battery and the high power property of an EDLC, various configurations of hybrid Li-ion capacitors have been proposed. Unlike metal oxides- and conducting polymer-based hybrid capacitors, Li-insertion materials can be used in either the negative electrode or the positive electrode.

$Li_4Ti_5O_{12}$ (LTO) is the most frequently used negative electrode material which features high rate capability and moderate energy density. Nano crystalline LTO is able to maintain about half the original specific capacity at 100C cycling rate [16] [17] [18] [19].

Unlike the case of negative electrode materials, there are plenty of choices when lithium insertion materials are used for the positive electrode of a hybrid capacitor. Typical examples among them are $LiMnO_4$, $LiNi_{0.5}Mn_{1.5}O_4$, $Li(Ni_{1/3}Mn_{1/3}Co_{1/3})O_2$, $LiCrTiO_4$ etc. [15] [20] [21] [22].

3.3.3 Internal parallel hybrid

An internal parallel hybrid capacitor must have at least one bi-material electrode, faradaic reaction and double-layer effect function within a single electrode at the

same time. Researches on this topic started just several years ago, pioneer works have been done by Cericola et al., they have compared IPH and ISH configurations based on LTO, LMO and AC materials. The IPH capacitors showed better electrochemical performances than the ISH ones. The highest energy density and power density achieved were 71 Wh kg^{-1} and 27 kW kg^{-1}, respectively [23]. In general, the IPH devices still have great potential to be exploited and they are now very hot research topics in the field of supercapacitor technology [24] [25] [26].

3.4 ELECTROCHEMICAL DOUBLE LAYER CAPACITOR

3.4.1 Construction and working principle

The construction of a conventional electric capacitor is fairly uncomplicated (Figure 5). It consists of two metal plates as the electrodes and there is a piece of insulating material called “dielectric” in between separating them. If external voltage is applied on the capacitor, positive and negative charges will be accumulated on the surface of corresponding electrodes. Thereby the electric charges are stored in the capacitor [10].

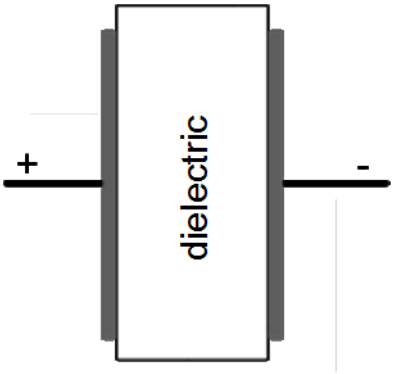


Figure 5. Construction of a conventional electric capacitor.

Capacitance C is defined as the ratio of stored charge Q to the applied voltage V as $C = \frac{Q}{V}$. For a capacitor, it is determined by the formula:

$$C = \varepsilon_0 \varepsilon_r \frac{A}{d} \quad (1)$$

where C is the capacitance, ε_0 is the dielectric constant of vacuum, ε_r stands for the dielectric constant of the insulating material between two electrodes, A stands for the surface area of each electrode and d is the distance between two electrodes. This formula is valid for conventional electrostatic capacitors as well as electrochemical double layer capacitors [10].

A typical EDLC consists of two electrodes made from high surface activated carbon, a separator in between avoiding short-circuit and electrolyte solution enabling the ion transport. Furthermore, current collectors are attached firmly to the electrodes for a good contact and thereby low electric resistance (see Figure 6) [10]. The capacitance of the whole cell derives from both electrodes, as contribution of two series connected capacitors. It is determined by the following formula [27]:

$$\frac{1}{C_{cell}} = \frac{1}{C_1} + \frac{1}{C_2} \quad (2)$$

The electric charges are stored at the interface between the electrode and the electrolyte. A so-called Helmholtz double layer forms at this interface and serves as the dielectric which separates opposite charges and thus enables the electric energy storage of EDLCs [28].

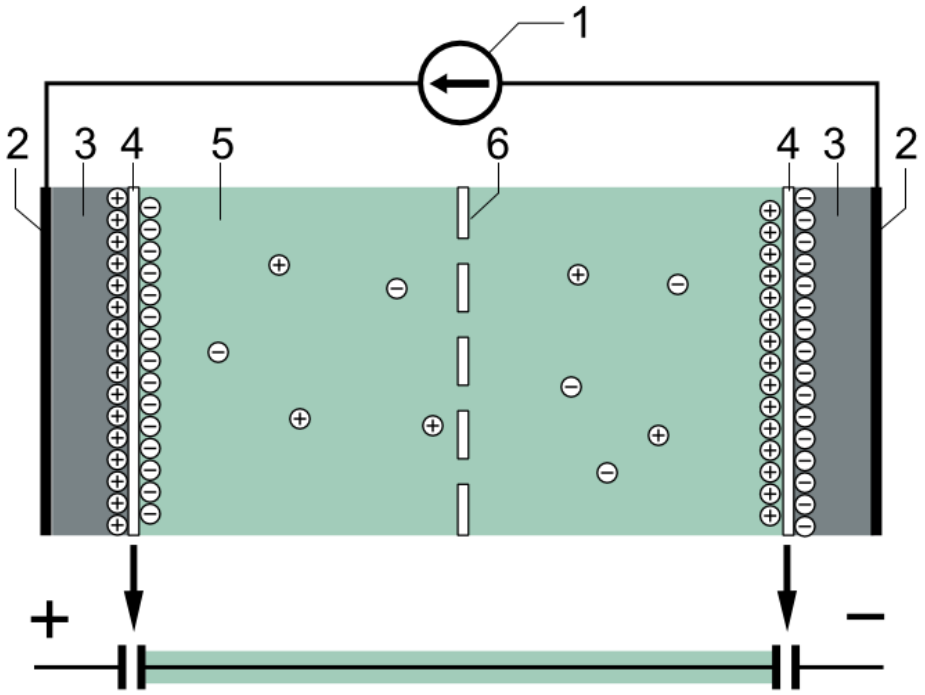


Figure 6. Principle construction of an EDLC: 1. External power source, 2. Current collector, 3. Electrode, 4. Helmholtz double layer, 5. electrolyte, 6. Separator [29].

3.4.1.1 The Helmholtz double layer capacitance

The Helmholtz double layer is formed when the surface of an electrode is in contact with electrolytes. Thanks to the various contributions from Helmholtz, Gouy, Chapman and Stern, the modern model of Helmholtz double layer is sophisticated and can precisely describe the capacitive behavior of it. It is generally believed that the Helmholtz layer contains several parts (see Figure 7). Most closely to the electrode surface locates a layer of solvent dipoles and specifically adsorbed ions, the so-called inner Helmholtz plane (IHP) goes through them. Some nanometers further the solvated ions accumulate together and the outer Helmholtz plane (OHP) is formed at the average radius of the ions. Up to this point, the potential profile $\varphi\ vs.d$ is linear. By going further in the bulk of the electrolyte, an incompact diffusive layer of solvated ions could be observed; the potential decreases exponentially until the level of the liquid electrolyte [28].

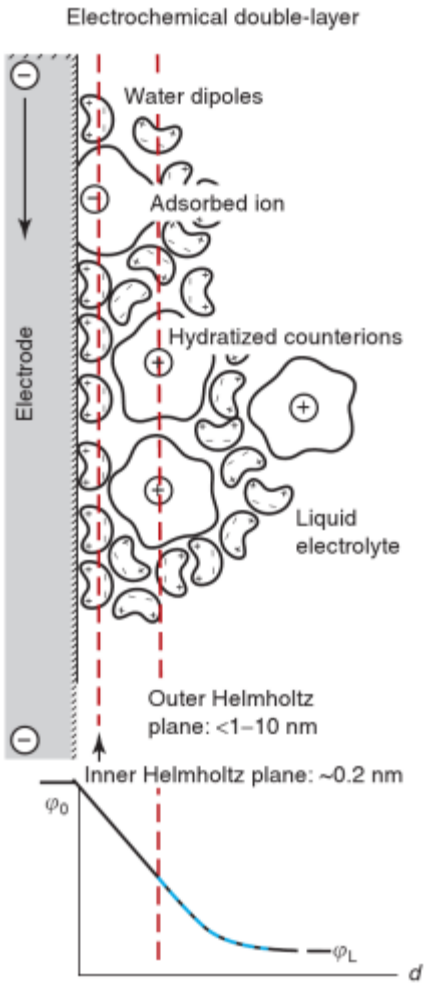


Figure 7. Simple sketch of the Helmholtz double layer [28].

3.4.2 Electrode active materials

A big number of carbonaceous materials are proposed for EDLC applications. Activated carbon, carbon black, carbon aerogel, carbon fiber, carbon nanotube, graphene, carbide derived carbon etc. are all possible candidates for this technology and every individual of them possesses unique properties [7]. A list of the characteristics of various carbonaceous materials which can be used in supercapacitors is shown below:

Table 1. Properties and characteristics of various carbonaceous materials as supercapacitors electrode materials [30].

Carbon Materials	Specific surface area/m^2 g^{-1}	Density /g cm^{-3}	Aqueous electrolyte (e.g. K_2SO_4 solution)		Organic electrolyte (e.g. $TEABF_4$ in Acetonitrile)	
			F g^{-1}	F cm^{-3}	F g^{-1}	F cm^{-3}
Activated Carbons (ACs)	1000-3500	0.4-0.7	<200	<80	<100	<50
Activated Carbon fibers (ACFs)	1000-3000	0.3-0.8	120-370	<150	80-200	<120
Carbon Aerogels	400-1000	0.5-0.7	100-125	<80	<80	<40
Carbon Nanotubes (CNTs)	120-500	0.6	50-100	<60	<60	<30
Graphene	2630	>1	100-205	>100-205	80-110	>80-110
Templated Porous Carbon	500-3000	0.5-1	120-350	<200	60-140	<100

Properties of several important materials are discussed in detail in the following paragraphs.

3.4.2.1 Activated carbon

Activated carbon was the material selected by SOHIO as the main electrode component in the world-first-commercialized EDLC in 1966 [31]. It is nowadays still the most

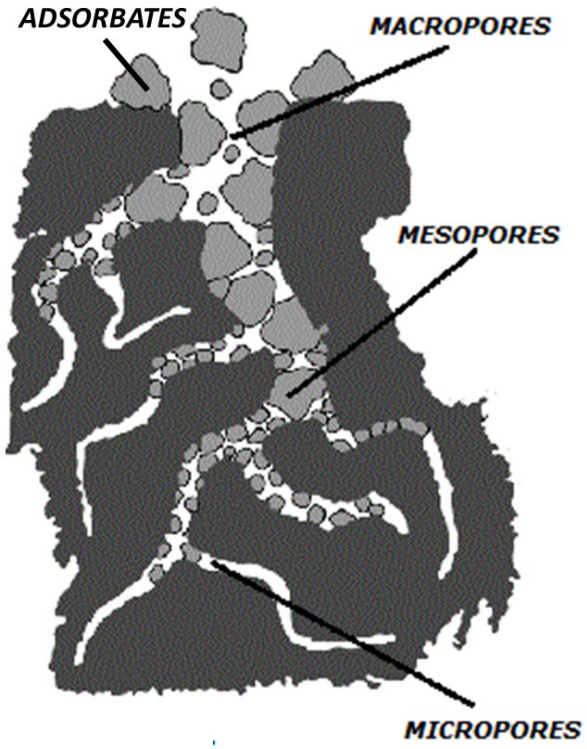


Figure 8. Schematic of the porous structure of activated carbon [32].

popular material for EDLCs due to their moderate cost, large surface area, availability and mature technology [33][34]. Activated carbons possess highly porous structure which comprises macropoes (>50 nm), mesopores (2-50 nm) and micropores (<2 nm). The electrolyte ions can adsorb on the porous surface (Figure 8).

ACs are generally prepared by means of physical and/or chemical activation of various types of carbon materials (e.g. wood, coal, coconuts shell etc.). Physical

activation is generally considered as a process of treating carbon precursors under elevated temperature (700-1200 °C) in the presence of oxidizing gases (e.g. steam, air). The chemical activation in contrast is performed at relatively lower temperature (400-700 °C); the commonly used activation agents include KOH, NaOH, and H_3PO_4 etc. The produced ACs can have very high specific surface area (SSA) up to 3000 m^2g^{-1}. If one recalls the formula $C = \varepsilon_0 \varepsilon_r \frac{A}{d}$, large value of surface area contributes significantly to the capacitance. However, the specific capacitance of an AC is not only influenced by its SSA; the pore size distribution, pore shapes and type of functional groups play also very important role on its electrochemical properties [34].

It is generally believed that EDLCs with AC electrodes show higher capacitance (100 F g^{-1} to 300 F g^{-1}) when aqueous electrolytes are used. In contrast, organic electrolytes offer lower values normally less than 150 F g^{-1}. One essential factor leading to this phenomenon is considered as the effective solvent ion size. Normally the ion size of an organic solvent is bigger than that of water molecule, thus the solvated cations and anions in organic electrolytes are not able to enter the small pores in the carbon material which leads to a relatively lower capacitance value. However, organic electrolytes are presently preferred in commercial EDLCs because they enable much higher operating voltage of the capacitors which contributes greatly to their energy density [34].

In order to achieve a maximum of capacitance, the pore size distribution of an AC has to fit the individual electrolyte that is employed. Study from Salitra et al. shows that 0.4 nm is the lower limit for size of pores which are active for electrochemical double layer (EDL) capacitance in aqueous electrolytes [35]. In the case of organic electrolytes, Béguin's group concluded that 0.8 nm is the optimal pore size [36]. Furthermore, Largeot et al. prepared carbide derived carbons (CDCs) with precise pore size distribution and demonstrated that the

maximum capacitance is achieved when the pore size of the carbon approximates the ion size [37].

3.4.2.2 Carbon nanotube

Carbon nanotubes (CNTs) have attracted plenty of attention since they were discovered more than 20 years ago. Their excellent electrical, mechanical and thermal properties

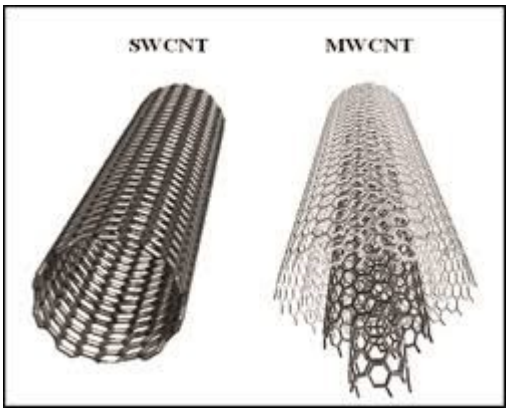


Figure 9. Schematic of the structure of SWCNT and MWCNT [38].

give them the potential to fit numerous practical applications. Unsurprisingly, they are also good candidates as EDLC electrode material [34]. Single-walled carbon nanotubes (SWCNTs) and multi-walled carbon nanotubes (MWCNTs) are the two main classes of CNTs, both of them have been extensively studied as electrode material for energy storage applications (Figure 9). Thanks to their excellent electrical conductivity and readily accessible surface area, CNTs are usually considered suitable for high-power devices. However, their energy density is usually lower than that of ACs due to their smaller SSA (see Table 1). In order to improve their SSA, chemical activation is a possible solution. Frackowiak et al. have reported an increase of the BET SSA of MWNTs from an

initial value of 430 to 1035 m^2 g^{-1} by activation with KOH [39]. Furthermore, Bordjiba and co-workers managed to synthesize a CNT-aerogel composite material which exhibits high SSA of 1059 m^2 g^{-1} and extremely high specific capacitance of 524 F g^{-1} in 5 M KOH electrolyte [40]. However, the preparation route of this complex material is very tedious and a mass production is not expected in the near future. In fact, carbon nanotubes are generally much more expensive than activated carbons and thus less competitive.

3.4.2.3 Templated porous carbon

Porous carbons produced with help of proper templates possess well-controlled pore size distribution, ordered pore structures, large SSAs and interconnected pore network. Such carbons are good candidates for various applications including active materials for EDLCs. Generally templated carbons are prepared in the following way: at first, a carbon precursor is intruded into the porous structure of the template; secondly, the carbon precursor is carbonized and; in the end, the template is removed and the porous carbon with desired structure is obtained (Figure 10) [34].

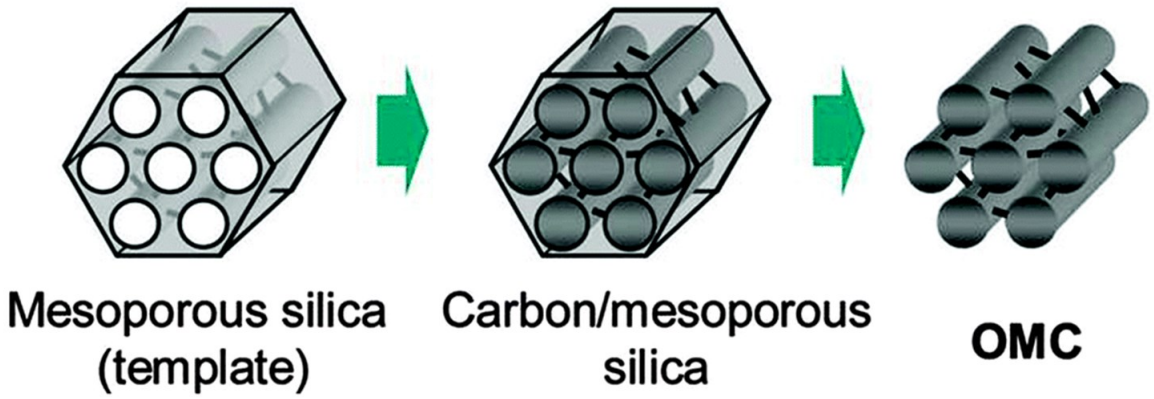


Figure 10. Schematic of preparation procedure of ordered mesoporous carbon (OMC) [41].

In order to guarantee the defined physical and chemical properties of the carbons, the preparation procedure has to be carefully controlled, including: selection of the template material and the carbon precursor, controlling of the carbonization process etc.

It has been reported in literature that the mesopores in porous carbons facilitate the ion transport in the electrodes and thus play essential role for high power characteristic of the capacitor cell. On the other hand, micropores with proper pore size contribute greatly to the specific capacitance of the carbon and therefore also the energy density of the cell [42][43][44]. By following this conclusion, Wang et al. designed a 3D hierarchical porous graphitic carbon material which features macroporous cores, mesoporous walls and micropores for high rate EDLC applications [44]. The macropores work as ion-buffering reservoirs; the mesoporous structure accelerates the kinetic process in porous electrodes; the micropores are mainly responsible for charge storage.

3.4.2.4 Graphene

Graphene is single carbon layer which is only one atom thick. Its simple structure is shown in Figure 11.

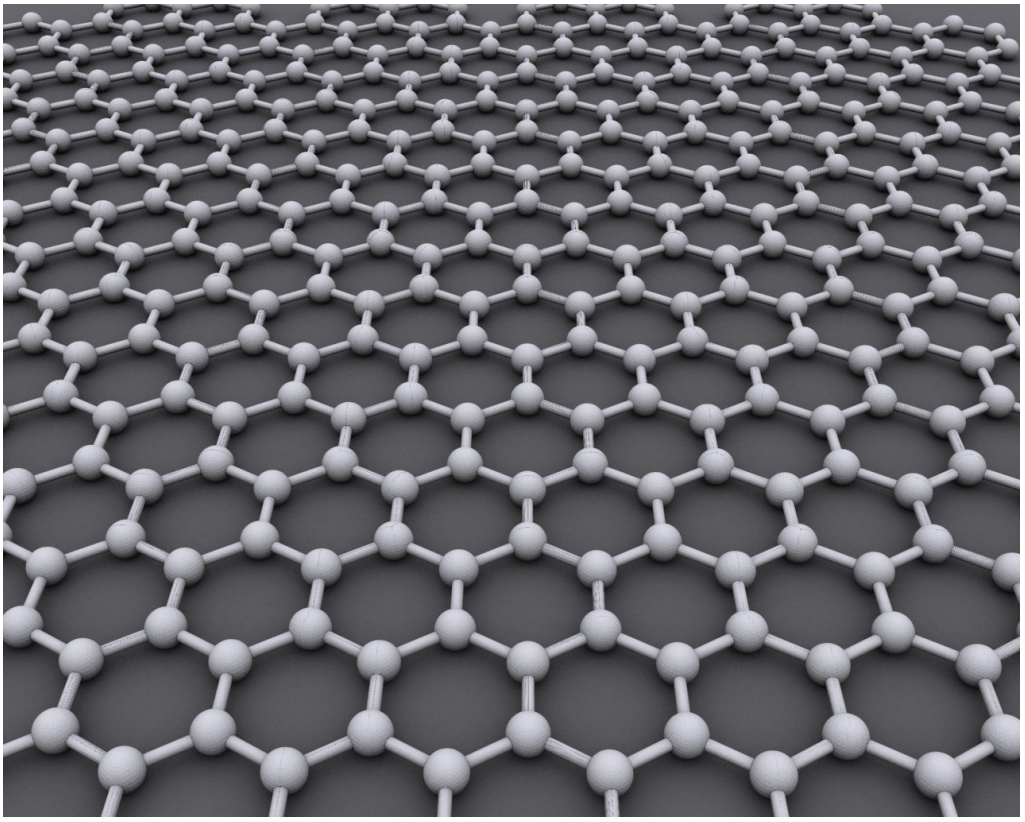


Figure 11. Schematic of the structure of graphene layer [45].

Although the theoretical studies of graphene started long ago, this material began to attract worldwide attention only after free-standing graphene had been prepared [46]. Graphene possesses numbers of unusual physical properties such as high electrical conductivity, high surface area and high mechanical strength etc. It is thus considered as a very promising material for supercapacitor applications.

Graphene sheets can be synthesized by lots of different methods, including mechanical cleavage of graphite, chemical exfoliation of graphite, epitaxial growth and chemical vapor deposition etc. [30]. El-Kady and co-workers reported recently a novel preparation route for producing graphene sheets [47]. Firstly, a layer of graphene oxide (GO) supported by flexible substrate is placed on a DVD

disk; secondly, the disk is transported into a computerized DVD disk drive and laser scribed therein; then the stacked GO sheets are immediately reduced into well-exfoliated graphene layers which are suitable for direct use in supercapacitor electrodes.

The specific capacitance of the graphene electrode can achieve quite high value. Kannappan et al. have reported fabrication of graphene based supercapacitors with high specific capacitance of 150.9 F g^{-1} at high cycling current density of 5 A g^{-1} in EBIMF 1 M ionic liquid electrolyte [48]. The laser-scribed graphene layer prepared by El-Kady et al. even achieved an extremely high capacitance of 276 F g^{-1} when the capacitor cell is operated with ionic liquid as electrolyte [47]. There is a clear trend that the energy density of graphene based supercapacitors is fast approaching that of conventional lithium ion batteries. However, a cost-effective and environmental friendly route for mass production of high quality free-standing graphene is up to now still not realized. Deeper and more thorough understanding of the physics and chemistry of graphene under various processing conditions is required.

3.4.3 Electrolyte

The electrolyte influences greatly the performance of a supercapacitor because both its energy density and power density are proportional to the square of cell operating voltage which is determined by the electrochemical stability window (ESW) of the electrolyte. Moreover, the properties of the selected electrolyte play also essential roles in the following aspects:

1. The electrical conductivity of the electrolyte determines the power output of the capacitor.
2. The behavior of electrolytic ionic adsorption in the porous structure of the active material influences greatly the double layer capacitance and as well the resistance of the cell.

3. The dielectric constant of the electrolyte is also a very important factor determining the double layer capacitance [49].

Therefore the selection of electrolyte is clearly of great importance.

The electrolytes employed in supercapacitor applications are generally divided into three different classes: aqueous electrolytes, organic electrolytes and ionic liquids.

The first aqueous electrolytes for supercapacitors were selected as H_2SO_4 and KOH because of their extensive use in the accumulator field. They have very good conductivity which enables high power output of the capacitor. However, due to the thermodynamic decomposition of water, the ESW of such acidic and alkaline solutions is normally under 1 V. This big disadvantage limits critically the energy density of the capacitor cell. Furthermore, H_2SO_4 and KOH are very corrosive in nature and can be quite dangerous for the cell components, especially the metallic current collectors. In a scientific laboratory, it is no problem to test the cells with noble metal current collectors like gold. But it is obviously economically impossible to use the same material in mass production of industrial scale. Therefore many researchers are working on neutral pH aqueous electrolytes. The group of Wu [50] has investigated three sulfides solution (Li_2SO_4, Na_2SO_4 and K_2SO_4) as electrolytes for supercapacitors. The rate capabilities follow the sequence of Li_2SO_4<Na_2SO_4< K_2SO_4 because the migration speeds of the hydrated ions in the bulk electrolyte and within the inner pores of AC electrode increase in the order of Li^+<Na^+<K^+. Therefore the K_2SO_4 solution is considered as a suitable candidate for high power capacitors. However, according to the results from Fic et al., Li_2SO_4 solution exhibits the widest ESW and thus supplies the cell the highest operating voltage of 2.2 V. The reason for this unusual high voltage is the strong hydration of Li^+ [51]. Thus the Li_2SO_4 solution is considered as a good choice for high energy capacitors.

Organic electrolytes are the most often used candidate in commercial supercapacitors. The most popular ones among them are tetraalkylammonium (R_4N^+) salts in acetonitrile (AN) or propylene carbonate (PC) [49]. With help of those electrolytes, 2.7 V of cell voltage can be realized. Jänes et al. have reported testing of mixture from four different BF_4^- salts in γ-butyrolactone (γ-BL) as supercapacitor electrolyte which is electrochemically stable up to 3 V [52]. Although higher operating voltage of the cell gives comparative advantage of organic electrolytes over aqueous electrolytes, they still have drawbacks like relatively high ESR, toxicity, high cost, vulnerability to moisture and so forth [49].
Ionic liquids (ILs) are presently attracting very much attention because of their special physical and chemical properties such as high ESW, high thermal stability, non-toxicity, variety of combination of choices of ions etc. ILs are room temperature molten salts which can be directly employed as supercapacitor electrolytes without the involvement of solvents [34]. Typical examples include EMITFSI (1-ethyl-3-methylimidazolium bis(trifluromethanesulfonyl)imide), PYR_{14}TFSI(N-butyl-N-methylpyrrolidinium bis(trifluromethanesulfonyl)imide) etc. By using such ILs as electrolytes, 3.5 – 3.7 V of cell voltage can be achieved and the capacitor cell is thus featuring high energy density [49]. However, ILs are typically very viscous liquids under room temperature and therefore have relatively low conductivity which leads to high ESR values. This property affects negatively the power density of the cell. But in the field of hybrid electric vehicle (HEV), capacitor modules work under elevated temperature so the problem of high ESR is not so much pronounced [49].

3.4.4 Separator

A separator is a layer of porous membrane sitting between the negative and the positive electrode, facilitating a good ion transport and at the same time electronic insulating. There have been numbers of various materials employed in

supercapacitors as separators, such as rubber, plastic, aquagel, glass fiber, resorcinol formaldehyde polymers, polyolefin films, etc. [53]. Recently, Yu and co-workers have tested the possibility of using eggshell membrane – a biological product – as separator in supercapacitor cells. The cell possesses low ESR and excellent cycling stability [53].

3.4.5 Current collector

The most current collectors presently employed in commercial supercapacitors are thin metal foils (Al or Cu).The foils can be used in many different ways: plain foils, etched foils, pre-coated foils etc. The goal of all of these treatment methods is to improve the interface contact between the metal foil and the active material. Portet and co-workers pre-coated the Al current collector with conductive carbonaceous material by sol-gel method [54]. The assembled cell with such current collector shows much smaller interface resistance in comparison to the cells with untreated foils.

Moreover, currently lots of researchers are working on nanomaterials which have the potential to be implemented as current collectors in supercapacitors. Zhou et al. have developed supercapacitors using super-aligned carbon nanotube sheets as current collectors. The prepared sheets are lightweight, highly conductive and flexible [55]. The group of Lee has prepared coaxial nanowires of polyaniline (PANI) and Indium tin oxide (ITO) by combination of chemical vapor deposition to grow the ITO nanowires and electropolymerization process to deposit the PANI. The rigid ITO nanowire supports make facile and uniform surface coating of PANI possible. In comparison to electropolymerized PANI film on planar substrates, PANI on ITO nanowire shows more excellent performances in aspects of specific capacitance, rate capability and cycling stability [56].

3.5 APPLICATION FIELDS OF SUPERCAPACITORS

Supercapacitors are nowadays widely used in both consumer and industry applications thanks to their characteristics like high power, excellent stability and long cycling life.

In industrial applications, Supercapacitors are playing essential roles in various fields. They are able to start vehicles in very cold weather when the most batteries would be frozen and capture large power from the regenerative braking systems. There are currently 61 Capabuses (Supercapacitor buses) operating on the streets of Shanghai (see Figure 12). The Capabuses are able to drive more than 10 km per single charge which takes only 90 s [57]. Furthermore, supercapacitors are also employed as the power source of the emergency gates in aircrafts due to their outstanding reliability. In wind parks, supercapacitors are used to regulate the output voltage of the wind mills in order to fit the requirement of the electric grid. In construction fields, supercapacitors help forklifts and cranes to lift heavy loads by supplying burst power. In data server centers, they are working in the function of Uninterruptible Power Supplies (UPS) which keep the power supply of the servers for short time and initiate the backup power systems like diesel generators or fuel cells [58].



Figure 12. Capabus (Supercapacitor bus) in Shanghai completely powered by supercapacitors [59].

In the field of consumer electronics, there are also several commercial products available. Blueshift has released a Bluetooth speaker which is powered by four Maxwell BCAP0350 supercapacitors [60]. Coleman has developed a cordless screwdriver powered by supercapacitors, it is able to handle 22 screws per one single charge of 90 s [61]. Furthermore, 5.11 Tactical has announced a flashlight "Light For Life UC3.400" which needs also only 90 s to charge and can provide light for 90 min [62]. However, a massive use of supercapacitors as the main power sources for consumer electronics has not been observed yet. Lithium ion

batteries are still holding the most market share due to their much higher energy density in comparison to supercapacitors.

4. Experimental

4.1 RAW MATERIALS

All the raw materials used in this work are listed in Table 2, the raw materials and activation methods for all six carbon materials are shown in

Table 3.

Table 2. Raw materials used in this dissertation.

Material	Abbreviation	Supplier	Category
YP-17D	YP	Kuraray Chemical Co.	Activated carbon
FC-SK1 P75	FC	CPL Carbon Link	Activated carbon
Cabot Black SC2	CB	Cabot Corporation	High capacitance Carbon black
HC-20BST	HC	Haycarb PLC	Activated carbon
	S0	confidential	Activated carbon
	SV	confidential	Activated carbon
Polytetrafluoroethylene	PTFE	3M	Binder
Denka Black	DB	DENKI KAGAKU KOGYO KABUSHIKI KAISHA	Conducting Carbon black
Electrodag EB-012	EB-012	Henkel	Adhesive agent

Table 3. Precursor materials and activation methods of six carbons.

	YP	FC	SV	S0	CB	HC
Precursor	Coconut	Coal	Coke*	Coke*	proprietary	Coconut shell
Activation method	Steam	Steam	KOH*	KOH*	No	Steam

*: Estimated

4.2 ELECTRODE PREPARATION

The electrodes used in this study were prepared by employing a novel dry preparation route which doesn't involve the use of any solvent (see Figure 13). In comparison to the traditional wet method, the new route avoids the contamination of solvent residue and provides high degree of compaction to the carbon electrodes. Furthermore, this method is expected to make a very good contact between carbon electrodes and the current collector. The details of the preparation are explained below.

Firstly, the active material (providing capacitance, YP, HC, S0, SV or FC) was dry-mixed with conductive agent (DB) and the binder (mechanically bind all components together, PTFE) by ball-milling. In the case of CB, the use of DB is not necessary so CB was mixed only with PTFE. The weight percentage of each component has been varied as described in the following chapters. After the ball-milling, the powder mixture was transferred into an agate mortar and compacted by a pestle. A piece of plastic film was then obtained from the mortar and further compacted in a calender until a free-standing film with a final thickness of about 100 μm is obtained.

Two kinds of etched aluminum foils (from JCC and MCT, respectively) were used as current collector and pre-treated with a commercial adhesive agent (EB-012) before use.

The calendered free-standing film was cut into pieces of 5×5 cm^2 and then hot-pressed on the current collector for three minutes using various pressures and temperatures.

In the end the final electrodes were obtained as three-layer structure consisting of carbon electrode composite, adhesive agent and Al foil.

Alternatively, several freestanding films have been attached to Aluminium foils by means of lamination. The lamination process has been performed by using different rolling forces while keeping the moving speed and processing temperature constant.

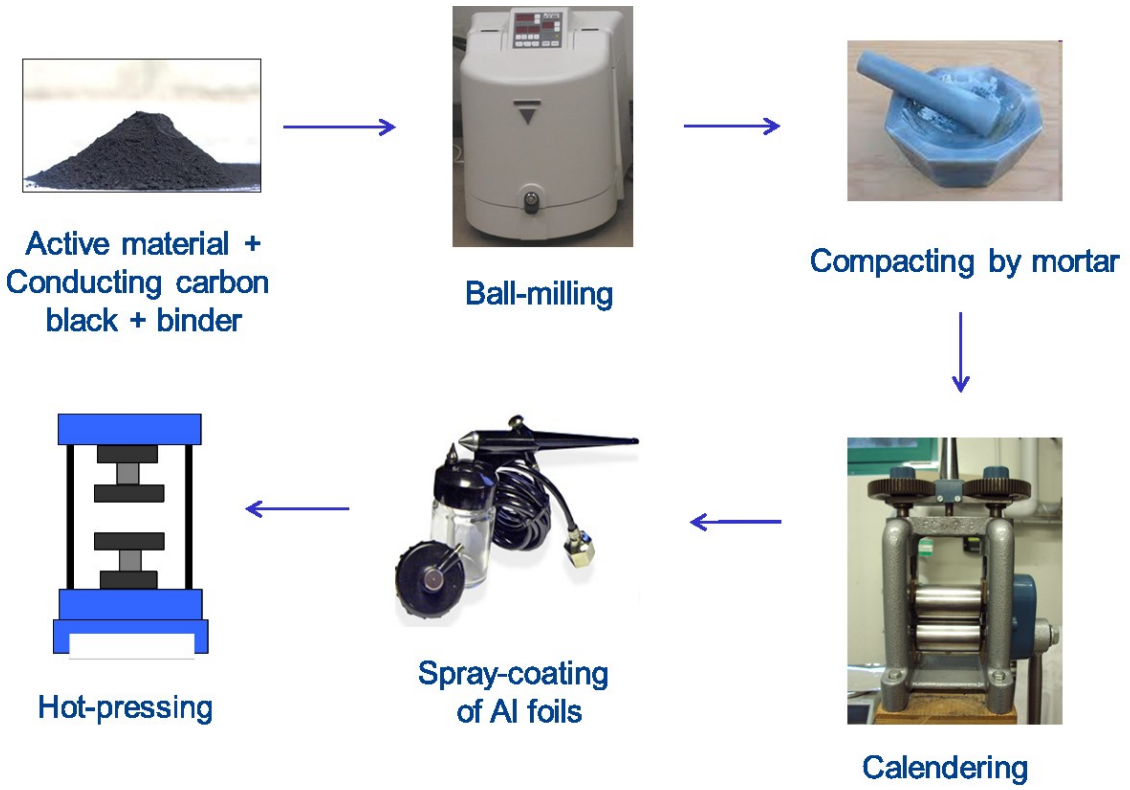


Figure 13. Schematic demonstration of the solvent-free electrode preparation procedure.

4.3 Cell assembly

Laboratory scale electrodes (ø=12 mm) were punched out from the finished 5×5 cm^2 films and dried overnight in vacuum oven (from Büchi) at 130 °C. The electrodes have been then hermetically transferred into an Ar-filled glovebox (H_2O and O_2<0.1 ppm, from MBraun). Swagelok® type cells (see Figure 14) have been employed for assembling the test capacitors which consist of two identical electrodes separated by three glass fiber separators (from GFA). For cell balancing experiments, carbon electrodes (85% YP-17D carbon, 5% Denka

black and 10% PTFE binder, prepared by the same procedure as the other electrodes) were used as quasi-reference electrode [63]. 1M tetraethylammonium tetrafluoroborate ($TEABF_4$) in acetonitrile (AN, from Honeywell) was used as electrolyte.

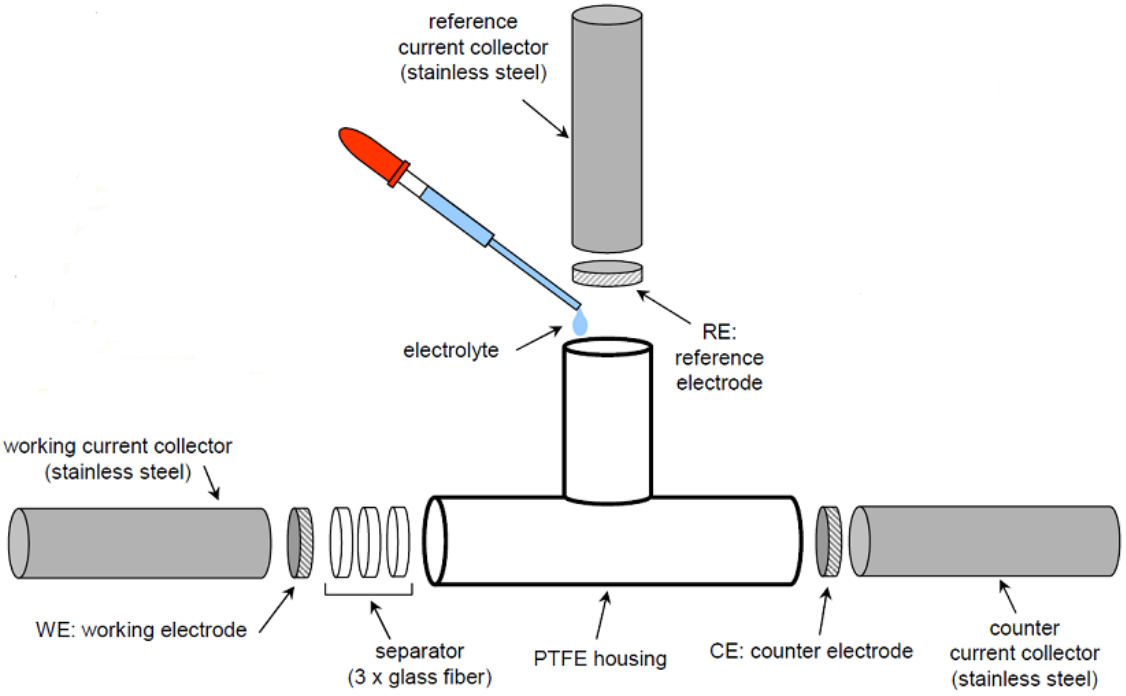


Figure 14. Sketch of a Swagelok cell (adapted from [64] with permission of the author).

4.4 Characterization methodologies

4.4.1 Gas sorption measurements and pore property analysis

The N_2 and CO_2 sorption measurements were conducted by an Autosorb Station (from Quantachrome Instruments). Isotherms of all the carbon powders and

electrodes have been obtained directly from the instrument. According to IUPAC definition (Figure 15), isotherms of porous materials are classified into six types. Type I and type IV are the two most important ones for study of carbon materials for EDLC application because they show classical micro- and mesoporous behavior, respectively.

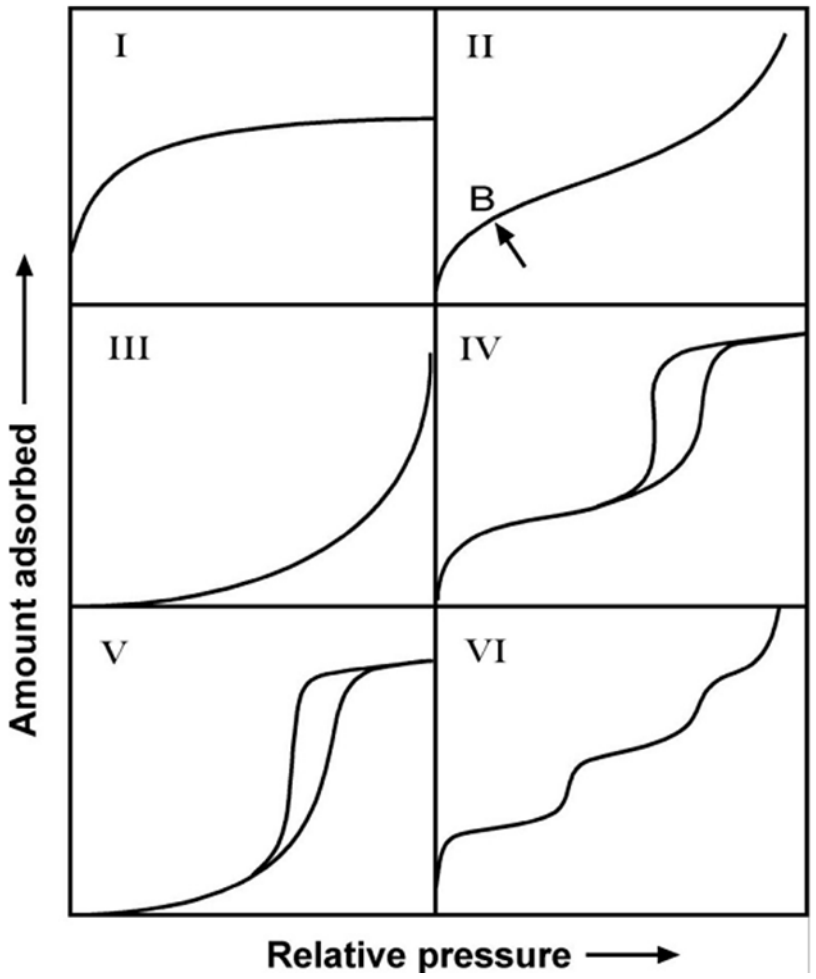


Figure 15. Six typical isotherms of porous materials [65].

Furthermore, IUPAC has also defined four different types of hysteresis loops for the type IV and type V isotherms (Figure 16). The shapes of hysteresis loops provide important information of fine structure of the pores.

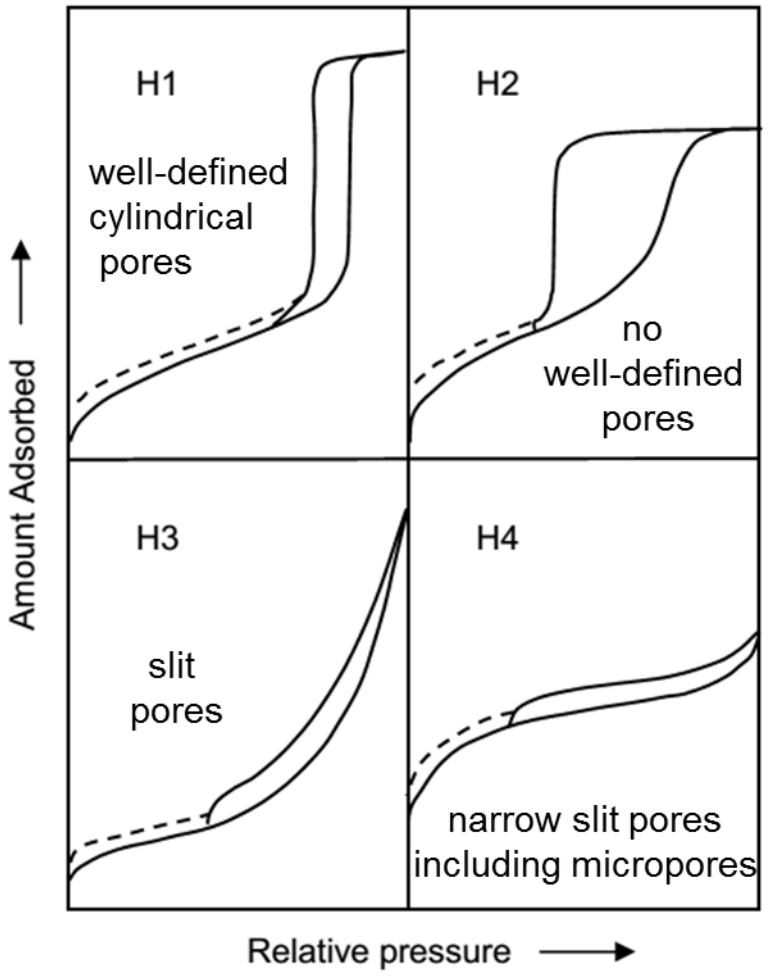


Figure 16. Four typical hysteresis patterns of isotherms of porous materials [65].

After the isotherms have been obtained from the experimental instrument, they were directly imported into a computer program AsiQWin (from Quantachrome Instruments). This software is able to perform various analyses on the raw data (isotherms) and many meaningful parameters of the characterized porous material can be extracted.

4.4.1.1. The multipoint BET method

The Brunauer-Emmett-Teller (BET) [66] method is the most widely used tool for the determination of the surface area of porous materials. It involves the use of the BET equation:

$$\frac{1}{W\left(\left(\frac{P_0}{P}\right)-1\right)} = \frac{1}{W_m C} + \frac{C-1}{W_m C}\left(\frac{P}{P_0}\right) \quad (3)$$

where, W is the weight of gas adsorbed at a relative pressure, P/P_0, and W_m is the weight of adsorbate constituting a monolayer. The term C is the BET C constant and is related to the energy of adsorption in the first adsorbed layer and consequently its value is an indication of the magnitude of the adsorbent/adsorbate interactions.

In order to solve the BET equation, one needs a linear plot of $1/[W(P_0/P)-1]$ versus P/P_0. For most porous materials using N_2 as adsorbate, the proper region of making the plot locates in the P/P_0 range of 0.05 to 0.35. At least three points in this region have to be selected to ensure a good linear fitting. After the fitting the weight of a monolayer of adsorbate W_m can be calculated from the slope and intercept of the BET plot.

Secondly, the total surface area of the porous material can be calculated from the equation:

$$S_t = \frac{W_m N A_{cs}}{M} \quad (4)$$

where N is Avogadro's number (6.0221415×10^{23} molecules/mol) and M is the molecular weight of the adsorbate. A_{cs} stands for the molecular cross-sectional area of the adsorbate molecule. For the hexagonal close-packed nitrogen monolayer at 77 K, the value of A_{cs} is 16.2 $Å^2$.

In the last step, the specific surface area of the material is obtained by dividing the total surface area S_t by the sample weight [67].

4.4.1.2. The Non-Local Density Functional Theory (NLDFT)

The classic BET theory is not able to give a realistic description of the filling of micropores, this leads to an underestimation of pore sizes. Therefore, another treatment called Non-Local Density Functional Theory (NLDFT) has been used to compute the DFT specific surface area (DFT SSA) and the pore size distribution (PSD) of all the samples [68][69].

The NLDFT method is able to correctly describe the local fluid structure near curved solid walls; adsorption isotherms in model pores are determined based on the intermolecular potentials of the fluid-fluid and solid-fluid interactions. The relation between isotherms determined by these microscopic approaches and the experimental isotherm on a porous solid can be interpreted in terms of a Generalized Adsorption Isotherm (GAI) equation:

$$\mathbf{N}\left(\frac{\mathbf{P}}{\mathbf{P_0}}\right) = \int_{\mathbf{W_{MIN}}}^{\mathbf{W_{MAX}}} \mathbf{N}\left(\frac{\mathbf{P}}{\mathbf{P_0}}, \mathbf{W}\right)\mathbf{f}(\mathbf{W})\mathbf{dW} \qquad (5)$$

where $N(P/P_0)$ represents the experimental adsorption isotherm data, W is the pore width, $N(P/P_0,W)$ stands for the isotherm on a single pore of width W and f(W) is the pore size distribution function.

The GAI equation reflects the assumption that the total isotherm consists of a number of individual "single pore" isotherms multiplied by their relative distribution, f(W), over a range of pore sizes. The set of $N(P/P_0,W)$ isotherms for a given system (adsorbate/adsorbent) can be obtained by the density functional theory. The pore size distribution is then derived by solving the GAI equation numerically via a fast non-negative least square algorithm [67].

4.4.1.3. The t-method

The t-method of de Boer has been employed in this study for the determination of micropore volume and surface area in the presence of mesopores. This technique involves the measurement of nitrogen adsorbed by the sample at

various low-pressure values (between p/p_0 = 0.2 and p/p_0 = 0.5). The procedure is the same as that employed in the BET surface area measurement, but it extends the pressure range to higher pressures to permit calculation of the external (mainly mesoporous) surface area of the material. A t-plot is a plot of the volume of gas adsorbed (V_{ads}^{STP}) versus t, the statistical thickness of an adsorbed film.

The t values are calculated as a function of the relative pressure using the de Boer equation:

$$\mathbf{t}(\text{Å}) = \left[\frac{\mathbf{13.99}}{\mathbf{\log\left(\frac{P_0}{P}\right)+0.034}}\right]^{\mathbf{1/2}} \quad (6)$$

A typical t-plot of a porous material which has both meso- and micropores is shown in Figure 17. The plot comprises of two parts representing the micro- (B) and mesopores (A) in the material.

The mesoporous surface area S_{meso} can be easily calculated from the equation:

$$\mathbf{S_{meso}} = \frac{\mathbf{V_{ads}^{STP}\times 15.47}}{\mathbf{t}(\text{Å})} \quad (7)$$

where the constant 15.47 represents the conversion of a gas volume to liquid volume and $\frac{V_{ads}^{STP}}{t(\text{Å})}$ is simply the slope of the part A. Furthermore, the microporous surface area can be simply obtained by $S_{micro} = S_{BET} - S_{meso}$ [67].

Moreover, the micropore volume can be calculated from the equation:

$$\mathbf{V_{micro}(cm^3) = I \times 0.001547} \quad (8)$$

where I is the intercept of the extrapolation from the curve B and 0.001547 enables the conversion between gas and liquid volume. Furthermore, the total volume of both meso- and micropores can be got from the last point (P/P_0=0.99) of the adsorption isotherm in high pressure regime. In the end, the mesoporous volume can be calculated as $V_{meso} = V_t - V_{micro}$ [67], [70].

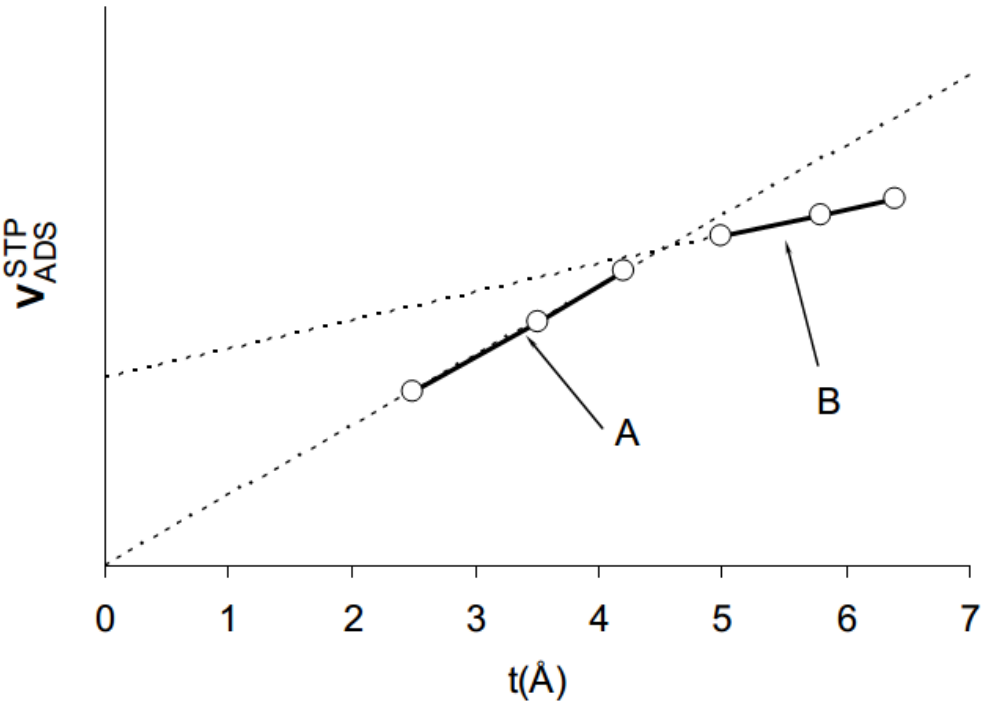


Figure 17. Typical t-plot of a porous material with presence of both meso- (A) and micropores (B) [67].

4.4.2 Scanning electron microscopy (SEM) and image analysis

Scanning Electron Microscopy (SEM) images of all samples were taken by a LEO 1530-VP-Gemini microscope (Carl-Zeiss).

In order to evaluate the macroporosity and particle packing of the electrodes the images were analyzed using ImageJ, a public domain, Java-based image processing software [71][72]. It has been widely used to display, edit, process and analyze 8-bit, 16-bit, 32-bit images. In this work, ImageJ was used to analyze the pore size of the composite activated carbon electrodes prepared at different conditions. The purpose was to observe the effect of temperature and pressure on the particle packing and morphology and thus to have a direct correlation with the electrochemical results.

The image processing steps are described in Figure 18. The SEM pictures have been firstly converted to binary images by selecting an appropriate threshold value. Then the area of the pores has been calculated using the "Analyze Particle" function in the ImageJ program menu by fitting the pores with ellipses. The total number of the analyzed pores taken from two individual SEM images for each sample is sufficient for exhibiting the differences in the pore structure (2500-5000 counts for samples) [73].

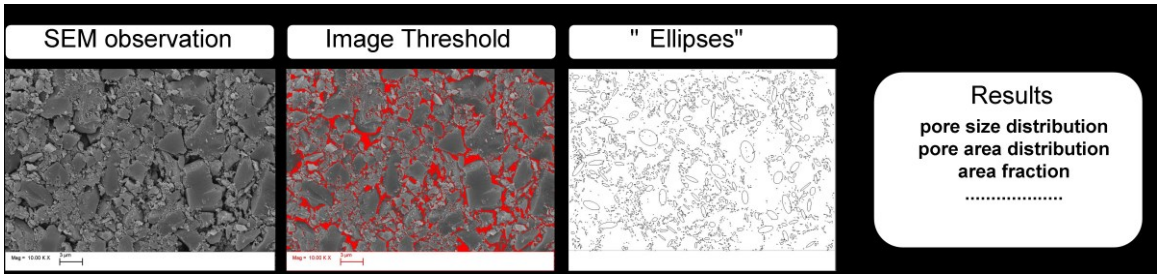


Figure 18. Image processing steps for characterization of the pores [73].

4.4.3 Electronic conductivity measurements

Electronic conductivity is an intrinsic material property which measures how much a material allows a flow of electric current through its volume. Its unit is often given as S cm^{-1}. Practically, it is usually obtained by taking the reciprocal value of the resistivity (Ω cm).

In this work, a self-constructed device powered with a Keithley 2400 Sourcemeter was employed for measuring resistance of the electrodes. The detailed experimental setup is shown in Figure 19. A test current has been generated and flowed through the electrodes. The corresponding voltage response generated between the upper and lower surface of the electrode was recorded. The external ring electrode was only used as guard to avoid parasitic current leakages. Conductivity values can be then calculated by the equation:

$$\frac{1}{\sigma} = \rho = R\frac{A}{\tau} \quad (9)$$

where σ is the conductivity, ρ stands for resistivity, R is the resistance, A is the area of the test electrodes and equals 3.14 cm^2, τ is the thickness of the electrodes.

Before each measurement, electrodes with radius of 18 mm were punched out from large pieces and properly dried. The same pressure (50 N cm^2) and electrification time (60 seconds) were applied to all samples. In order to avoid thermal drifts, during all experiments the offset-compensation function was enabled at the Keithley 2400 Sourcemeter. One can directly read the resistance values of the electrodes from the display of the sourcemeter.

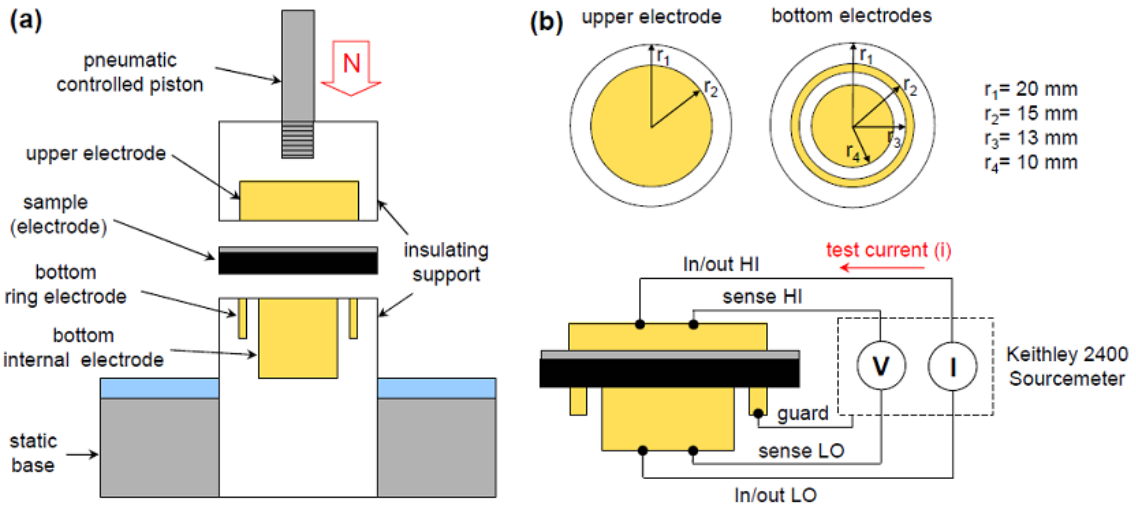


Figure 19. Experimental setup for measuring the volume electronic conductivity of electrodes. (a) Schematic of the device and (b) detailed view of the 4-wire sensing setup [64].

4.4.4 Electrochemical characterization

All Electrochemical measurements were performed by a VMP3 multichannel potentiostat (Bio-logic Science Instrument) equipped with an EC-Lab® software for instrument operation and data evaluation.

4.4.4.1 Galvanostatic cycling with potential limitation (GCPL)

Galvanostatic cycling (charging/discharging) is the most common electrochemical technique used for the characterization of electric energy storage devices. In such experiments, a constant current is applied between the working and the counter electrode (see Figure 20); the voltage of the full cell can be therefore either increased or decreased to a certain value. By inverting the flowing direction of the current, the cell voltage can be brought backwards to the initial status (see Figure 21).

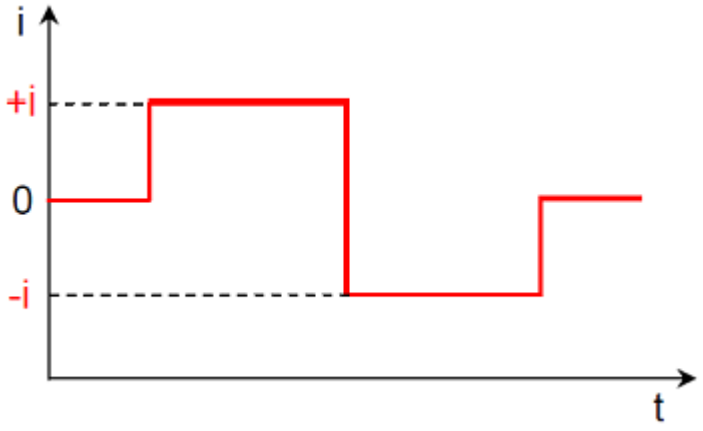


Figure 20. Schematic of current excitation in a GCPL measurement [64].

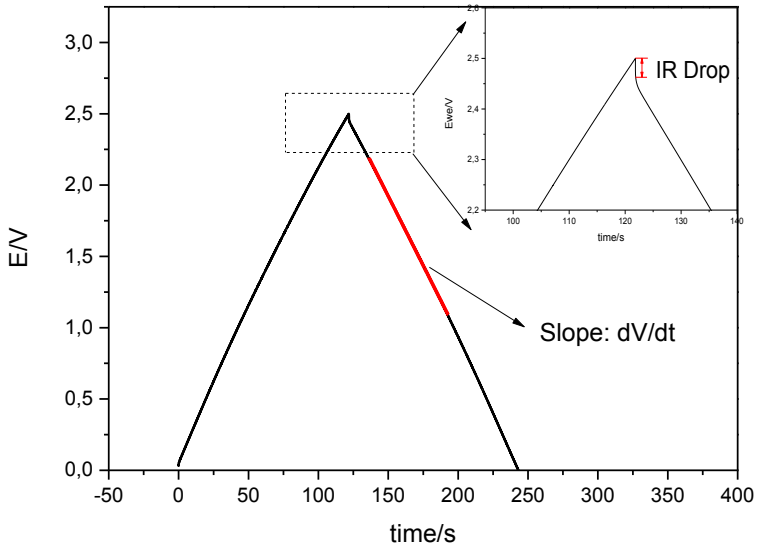


Figure 21. Typical charging-discharging curve of an EDLC cell.

Two important parameters (specific capacitance and IR-drop) of the cell can be extracted from the GCPL curve.

The cell capacitance, using a galvanostatic method, is normally deduced from the slope of the discharging curve (Figure 21) by using the equation below:

$$C = \frac{I}{dV/dt} \tag{10}$$

where *C* is the cell capacitance in Farad (F), *I* the discharge current in Ampere (A) and *dV/dt* is the slope of the discharging curve in Volt per second (V s^{-1}).

The following equation applies for a two-electrode system, assuming that the electrodes have the same weight:

$$C_{cathode} = C_{anode} = C \tag{11}$$

In this case, the measured cell capacitance is:

$$C_{cell} = \frac{1}{2} C \quad (12)$$

The specific capacitance (C_{spec}) in Farad per gram of active material (F g^{-1}) is related to the capacitance of the cell (C_{cell}) by:

$$C_{spec} = \frac{2 \cdot C_{cell}}{m_{AM}} \quad (13)$$

where m_{AM} represents the active material weight of each electrode.

IR-drop is a measure of the total resistance of the cell (depicted in Figure 21). One can easily compare the resistances of different capacitor cells by referring to their IR-drop values.

In this study, GCPL experiments have been performed with different current density (ranging from 125 mA g^{-1} to 8 A g^{-1}) and potential limitation (2.5 V, 3 V and 3.25V).

4.4.4.2 Cyclic voltammetry (CV)

Cyclic voltammetry is a potentiodynamic technique for studies of electrochemical systems and very useful in obtaining information about electrode redox reactions. As displayed in Figure 22, in a CV experiment the voltage applied is linearly varied versus time till a set potential is reached. Meanwhile the current response is recorded. Peaks of current are present where redox reactions take place.

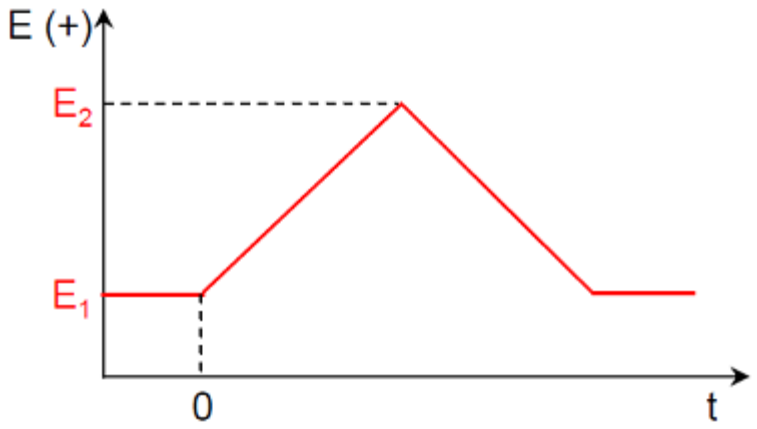


Figure 22. Schematic of voltage excitation in a CV measurement [64].

In Figure 23, a typical cyclic voltammogram of an EDLC is shown. Its quasi-rectangular shape indicates a main contribution from static charge storage.

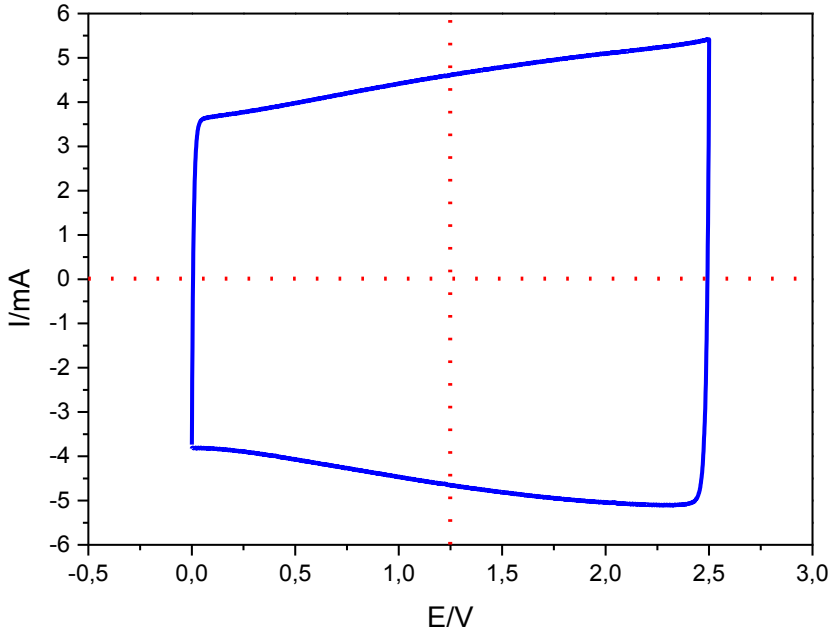


Figure 23. Typical cyclic voltammogram of an EDLC.

Furthermore, the specific capacitance of the tested active material can be calculated from $C_{spec} = \frac{I}{dV/dt \cdot m_{AM}}$ at the midpoint of the whole CV profile (1.25 V). However, the voltammogram shows rarely a perfectly rectangular pattern and thus a precise reading of the specific capacitance is not possible. Therefore in this dissertation it is always referred to the specific capacitance value derived from GCPL experiments.

In this study, CVs were performed at 10 mV s^{-1} scan rate in the potential range of 0 to 2.5 V if not differently specified.

4.4.4.3 Electrochemical impedance spectroscopy (EIS)

Electrochemical Impedance spectroscopy is a powerful technique for investigating interfaces (electrode-electrolyte, electrode-current collector etc.)

and of the processes occurring at them. Differently from galvanostatic and voltammetric methods, where the electrode is usually driven rather far from its equilibrium condition, in EIS an alternating signal (voltage or current) of very small amplitude is applied to the system.

First of all, a Frequency Response Analyzer (FRA) provides a sinusoidal signal to the potentiostat that can be expressed as:

$$E(t) = E_0 \sin(\omega t) \quad (14)$$

where ω is the angular frequency and E_0 is the signal amplitude. This is added to the working electrode potential and fed to the cell. Depending on the nature of the investigated system, the current response might result shifted in phase ($\emptyset$) and with different amplitude (I_0):

$$I(t) = I_0 sin(\omega t + \emptyset) \quad (15)$$

Furthermore, according to the Ohm's law, the impedance *Z* is then obtained as follows:

$$Z = \frac{E(t)}{I(t)} = \frac{E_0 sin(\omega t)}{I_0 sin(\omega t + \emptyset)} = Z_0 \frac{sin(\omega t)}{sin(\omega t + \emptyset)} \quad (16)$$

Using the complex numbers notation, *Z* can be described in a vector diagram as a function of its real (Z_{real}) and imaginary (Z_{im}) parts:

$$Z = Z_0(cos\emptyset - jsin\emptyset) = Z_{real} - jZ_{im} \quad (17)$$

where *j* indicates the imaginary unit ($j = \sqrt{-1}$). The plot of imaginary versus real components of the impedance for different values of frequency is the so-called Nyquist plot.

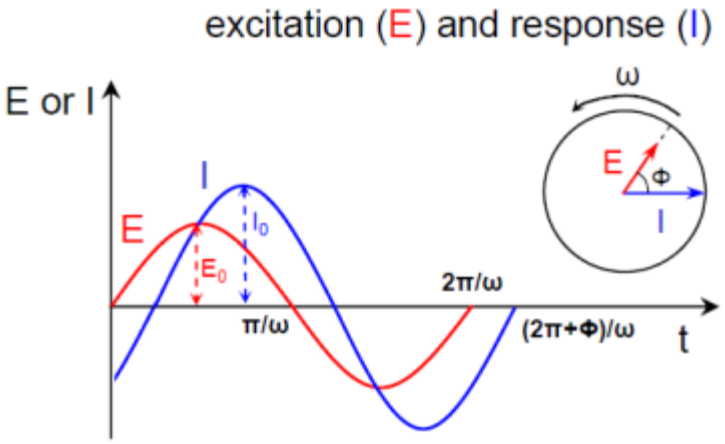


Figure 24. Sinusoidal excitation and response in an EIS experiment [64].

A typical Nyquist plot for an EDLC based on porous carbon shows from high to medium frequencies a typical diffusion region which reflects the resistance of the electrolyte through the electrode pores. The diffusion part is followed by a vertical line indicating a purely capacitive behavior (Figure 25).

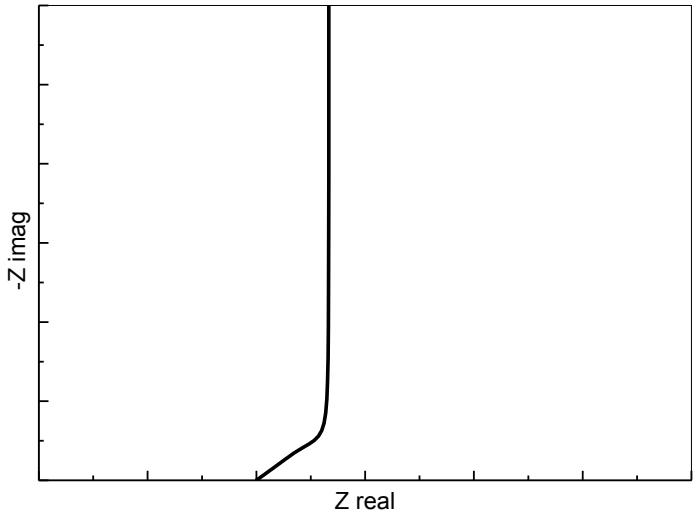


Figure 25. Typical Nyquist plot for a carbon/carbon EDLC.

However, experimentally, the Nyquist plot of a carbon electrode shows very often a semicircle at high frequencies which shifts the total resistance towards higher values as depicted in Figure 26. This semicircle is reported by several other groups as well [54][74][75].

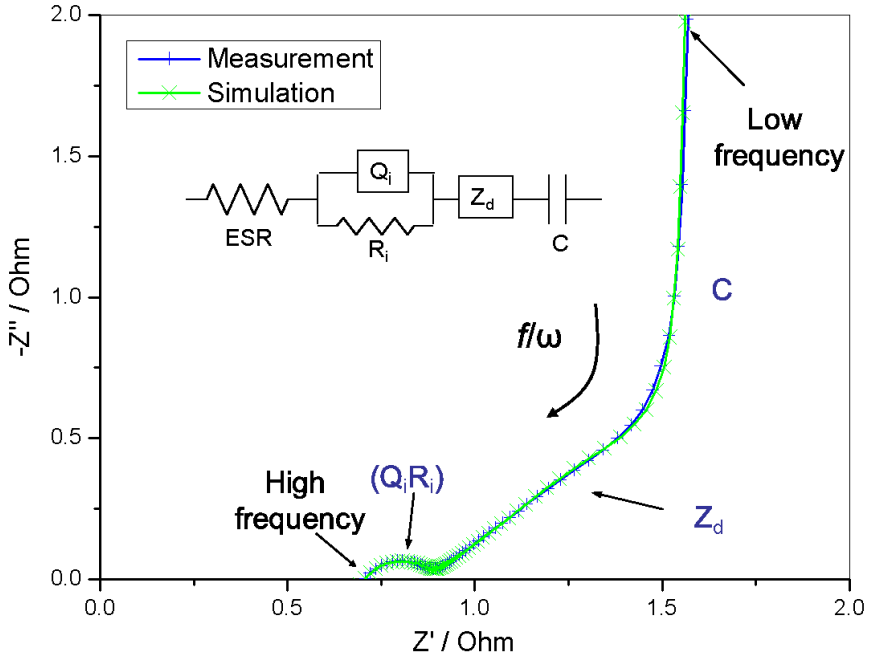


Figure 26. Experimental Nyquist plot and corresponding simulation. The inset shows the equivalent circuit used for the simulation.

There are various hypotheses that might explain the nature of this semicircle. In the case of activated carbons with functional groups operating in an aqueous electrolyte it can be correlated to the charge transfer corresponding to faradaic processes [75]. Moreover, it can be associated to the poor electronic conductivity among the particles (activated carbon/activated carbon and activated carbon/carbon black contacts). Furthermore, another possible explanation can be

the poor contact between the current collector and the composite electrode [54]. In general, the poor contact at the interface between electrode and current collector is a critical and persistent problem not only on the supercapacitor development but also on the Li-ion battery manufacturing. Recently, M. Gaberscek et al. investigated the influence of different current collectors on the kinetics of Li-ion battery electrodes [76]. Gabersceket al. found a direct correlation between the semicircle at high frequencies detected in the Nyquist plot and the interface between the current collector and the composite electrode. With this work we confirm that also in the case of carbon/carbon supercapacitors this semicircle can be associated to the poor contact between the current collector and the composite electrode (detailed discussion follows in further sections).

The equivalent circuit used for simulating the impedance spectra is shown in the inset of Figure 26. The circuit may be rewritten, using the Boukamp's notation [77], as $R_{el}(R_iQ_i)TQ_{dl}$ where R_{el} is the electrolyte resistance, (R_iQ_i) represents the resistance and the constant phase element associated to the semicircle, T is the finite-diffusion element and Q_{dl} is the constant phase element associated to the double layer capacitance. The commonly used equation for simulating the diffusion impedance of electrochemical double layer supercapacitors [78][74] is:

$$\boldsymbol{Z_w(\omega) = Z_0(J\omega)^{-1/2} coth\left[B(J\omega)^{-1/2}\right]} \quad (18)$$

Where Z_0 and B are the Warburg factors [74]. The results of the non-linear regression analysis showed that the Nyquist plots can be well simulated by using the equivalent circuit mentioned above (see simulated and measured curves in Figure 26). The "chi-squared" parameter (χ^2, i.e. the sum of the square of the differences between measured and simulated points) which is an indication of the quality of the fit has a value of smaller than 10^{-4}. In general, a value of 10^{-4} or less for indicates a reasonable to a good fit.

The simulation allowed us to extract the parameters of interest, which in this dissertation are essentially the resistance related to the semicircle and the resistance related to the diffusion.

Since the thickness of the electrode (which in this study ranges from 90 to 120 µm) is directly proportional to the diffusion resistance, the "diffusion resistivity" has been calculated as:

$$\boldsymbol{\rho_d = (R_d \times A)/L} \quad (19)$$

Where ρ_d is the diffusion resistivity, R_d is the diffusion resistance as calculated from the impedance simulation; A represents the geometric area of the electrode and L the thickness of the electrode.

Furthermore, an apparent diffusion coefficient of the electrodes can be calculated by following the equation [77]:

$$\boldsymbol{D = \frac{L^2}{B^2}} \quad (20)$$

The Electrochemical Impedance Spectroscopy (EIS) tests were carried out by applying a sinusoidal voltage of 5 mV at a bias of 0 V (fully discharged state) and the measuring frequency ranged from 100 kHz to 10 mHz. The resulting EIS spectra have been analyzed using the fitting program EQUIVCRT developed by Boukamp [77].

4.4.4.4 A standard test protocol

A standard test protocol has been composed by combining GCPL, CV and EIS techniques. It is used in plenty of measurements in this work. The detailed procedure is drawn below in Figure 27. As mentioned in previous sections, CV experiments are responsible to check the possible redox reactions; GCPL measurements serve for calculation of specific capacitance and IR-drop; EIS enables detailed investigation on the impedance from various sources of the cell.

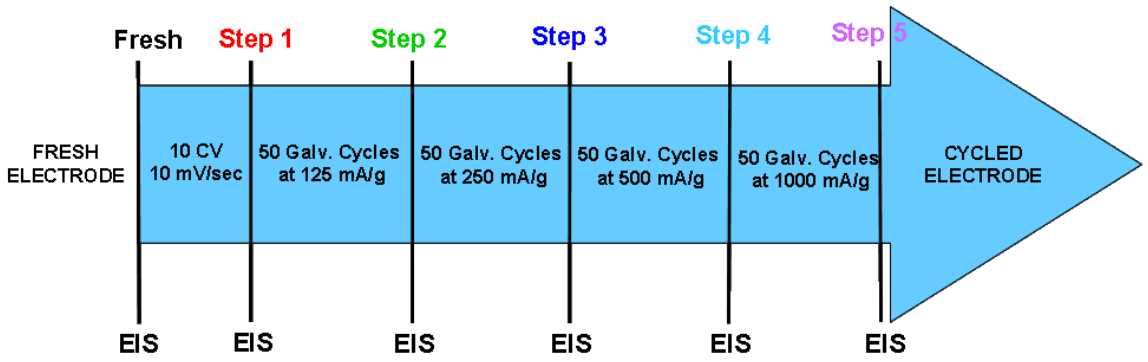


Figure 27. The standard test protocol used in this study.

5. Results and discussion part I: Effects of electrode preparation, recipe and mass ratio

5.1 Effects of electrode preparation techniques

As already described in the experimental part, the carbon electrodes used in this work have been prepared under different processing conditions. A very interesting point would be investigating the influences of the electrode preparation conditions to the physical and electrochemical properties of the carbon electrodes. For the physical properties, it is quite straightforward to anticipate that the porous structure of carbon electrodes might be altered. But how could the electrode preparation change the electrochemical properties of carbon electrodes?

Within the framework of this dissertation, the focus is to investigate the possible influences to the resistance of carbon electrodes. The resistance of a supercapacitor is the sum of various contributions such as the electrolyte resistance, the particle-particle resistance, the contact resistance between the active material and the current collector and the diffusion resistance of the electrolyte within the porous structure of the active material [79]. Schematically, the resistance sources of a supercapacitor can be depicted as in Figure 28. The intrinsic resistance of the electrolyte ($R_{electrolyte}$) and the diffusion resistance of the electrolyte into the porous structure of the activated carbon (R_{diff}) depend essentially on the specific features of the material used (electrolyte and activated carbon). On the other hand the boundary resistances at the interfaces carbon-carbon and carbon-current collector can be controlled during the electrode preparation. Every of these interfaces is associated to a boundary resistance and to the related constant phase element which are in parallel ($R_{boundary}$ and $Q_{boundary}$ in Figure 28). The electrode preparation processes have been studied in detail and described in following sections.

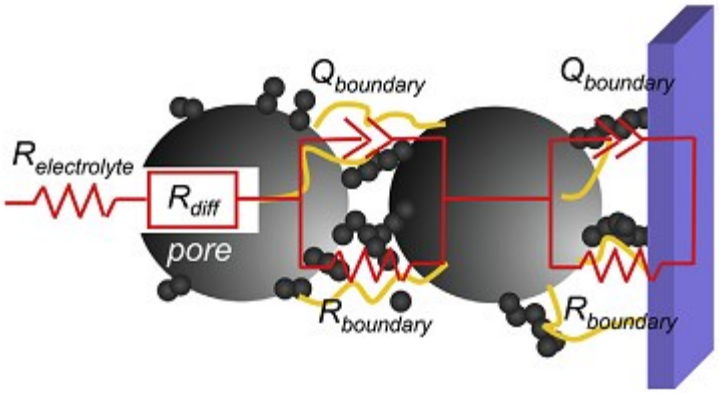


Figure 28. Resistance sources in an EDLC electrode [73].

5.1.1 General effects of the Hot-pressing method

The Hot-pressing preparation method includes several steps of compacting the electrodes (mortar compacting, calendering and hot-pressing). Therefore the prepared electrodes were tested by N_2 and CO_2 adsorption in order to unveil the possible change of the porous structure of the carbons.

The N_2 isotherms of both powders and electrodes made from six different carbons are drawn in Figure 29.

By comparing these isotherms, it is observed that the characteristic shapes of the two sets of curves are rather similar (The characteristics of all isotherms will be discussed later in chapter 6 in depth.). However, one noticeable difference should not be ignored. Almost all six carbons showed smaller adsorption volume at standard temperature and pressure (STP) after they have been processed and made as electrodes. This is a first sign showing that the electrode preparation may decrease the porosity of carbon materials.

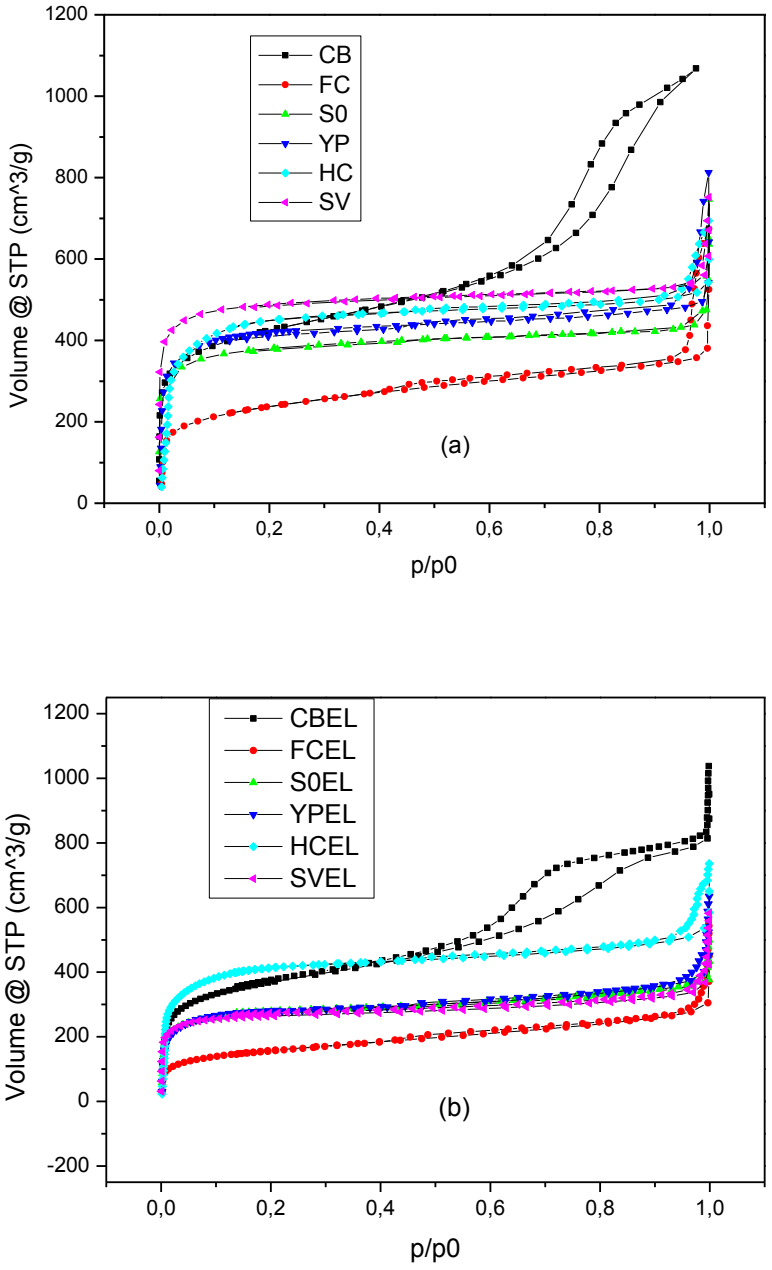


Figure 29. N_2 adsorption and desorption isotherms of powders (a) and electrodes (b) of six carbonaceous materials.

Furthermore, the specific surface area of all six carbons has been computed by both BET and NLDFT models (see Table 4). It can be clearly observed that no matter which model has been used, the surface areas of all six carbons decreased after they had been made into electrodes. The electrode preparation has surely closed plenty of pores which lead to considerable decrease of surface area. The possible influencing factors may include the processing pressure and the additives (conducting agent, binder) used in the electrode preparation.

Table 4. Comparison of the specific surface area data from both pure carbon powders and ready electrodes by employing the BET and NLDFT models.

	S_{bet} ($m^2\ g^{-1}$)	S_{bet} EL ($m^2\ g^{-1}$)	S_{nldft} ($m^2 g^{-1}$)	S_{nldft} EL ($m^2\ g^{-1}$)
FC	864	574	517	349
YP	1596	1086	938	615
CB	1550	1339	989	831
S0	1433	1058	955	621
SV	1889	1041	1248	638
HC	1705	1555	861	856

Moreover, pore size distribution patterns of powders and electrodes made from all the carbons have been obtained from N_2 and CO_2 isotherms (see Figure 30). It is interestingly observed that the most peaks of all carbons have got much closer to each other in comparison with the ones obtained from pure carbon powders, especially for the case of carbon “HC” which was showing a unique high peak.

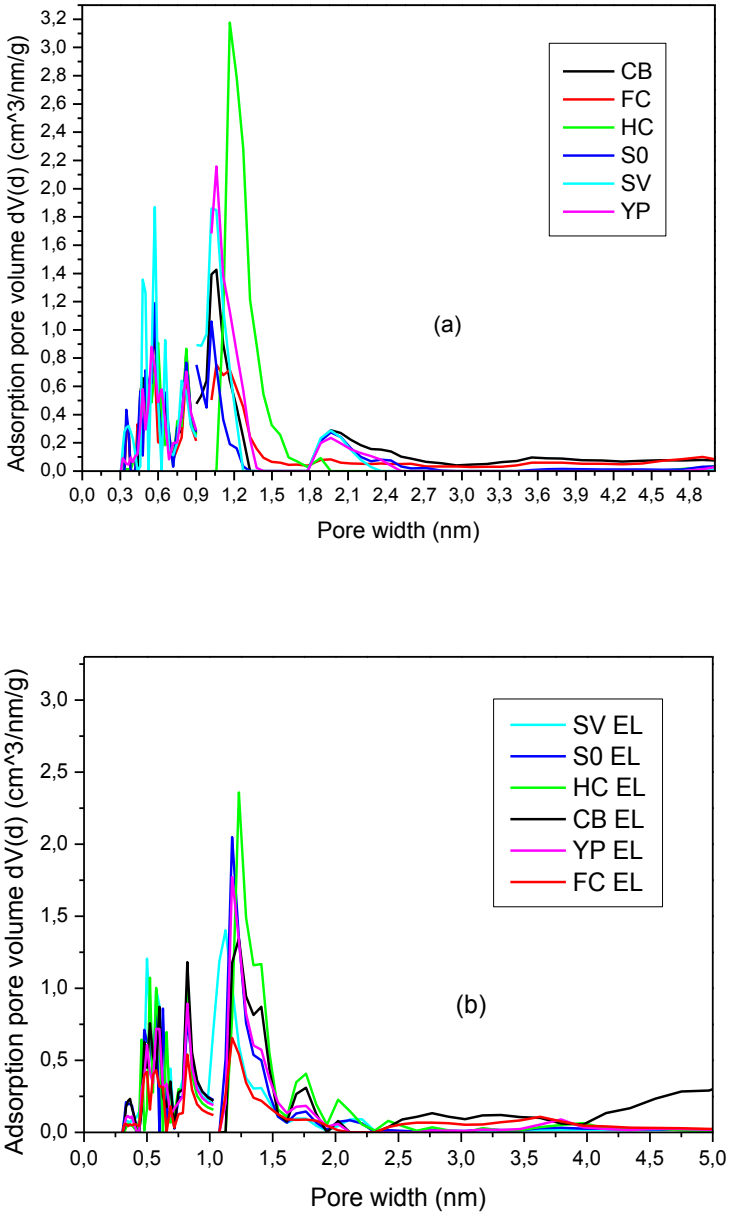


Figure 30. Pore size distribution patterns of powders (a) and electrodes (b) from six carbonaceous materials obtained by both N_2 and CO_2 adsorption measurements. The model used for computation was based on NLDFT.

Table 5. Microporous surface area and microporous volume fraction of six carbonaceous materials (powder form and electrode form).

	S_{micro} ($m^2\ g^{-1}$)	S_{micro} EL ($m^2\ g^{-1}$)	V_{micro} ($cm^3\ g^{-1}$)	V_{micro} EL ($cm^3\ g^{-1}$)
FC	505	277	0.215	0.116
YP	1454	939	0.578	0.37
CB	913	675	0.383	0.2838
S0	1269	898	0.522	0.3541
SV	1753	920	0.7	0.3566
HC	1572	1360	0.646	0.5575

In Table 5, the microporous surface area and microporous volume fraction of six carbonaceous materials (both powder form and electrode form) are summarized. A clear trend can be observed. The microporous fraction of all six carbons have been decreased after the electrode preparation process, both surface and volume fractions. This is probably attributed to the high pressure condition

applied during the electrode preparation. Moreover, the conductive carbon and polymer binder may have blocked some pores.

Table 6. Mesoporous surface area and mesoporous volume fraction of six carbonaceous materials (powder form and electrode form).

	S_{meso} ($m^2 g^{-1}$)	S_{meso} EL ($m^2 g^{-1}$)	V_{meso} ($cm^3 g^{-1}$)	V_{meso} EL ($cm^3 g^{-1}$)
FC	359	297	0.597	0.5812
YP	142	147	0.313	0.6112
CB	637	664	1.269	1.1872
S0	164	160	0.633	0.317
SV	136	121	0.462	0.4122
HC	133	195	0.281	0.4485

Furthermore, the corresponding surface and volume mesopores fraction of all six carbon materials (both powder and electrode form) are shown in Table 6 and

very interesting phenomena can be observed. The mesopores fraction of various carbons was very much differently influenced by the electrode preparation; it can decrease and also increase. The first case is rather easy to understand because this should come from the same reason as the case for micropores. However, it requires some deeper consideration to explain why the mesoporous portion can be increased by the electrode preparation process. We have proposed one hypothesis for this rather “abnormal” observation: Plenty of micropores can be strongly compressed by the electrode preparation leading to fracture of pore walls so that many previous micropores joined together and formed new mesopores (possible mechanism see Figure 31).

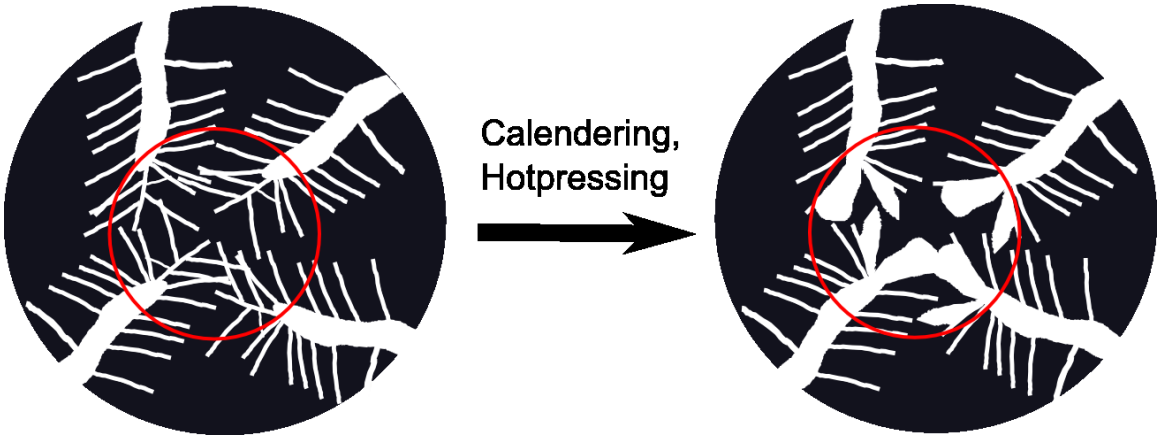


Figure 31. Schematic of a process in which micropores join together to form mesopores, only the transition process inside the red circle is depicted for simplicity.

Moreover, the relation between diffusion resistivity (obtained from EIS analysis) and external surface proportion (mainly mesoporous) from six carbon materials in form of electrode has been drawn in Figure 32. Higher external surface proportion leads to lower diffusion resistivity. More detailed discussion can be found in chapter 6.

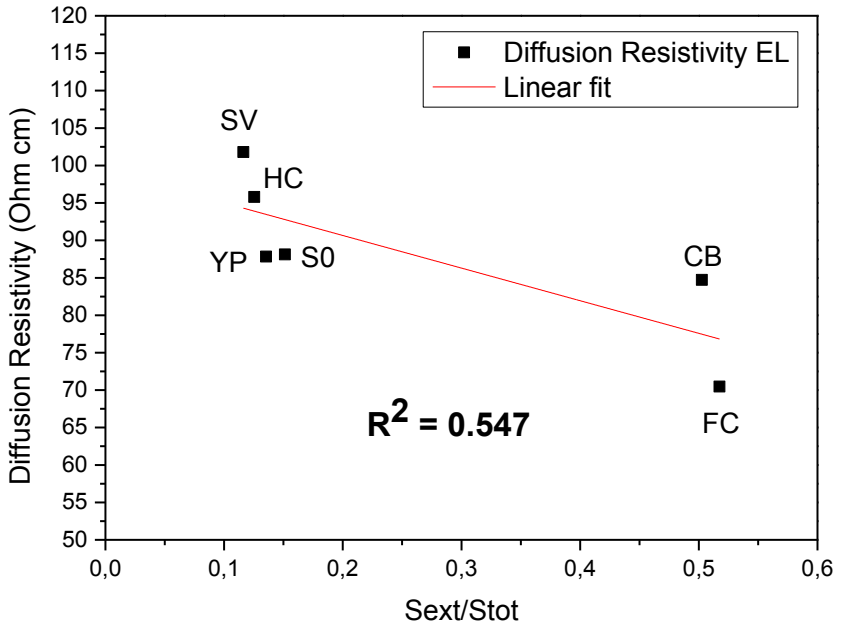


Figure 32. Relationship between diffusion resistivity and external surface proportion of electrodes made from six carbon materials.

Additionally, the relation between diffusion resistivity and mesoporous volume proportion from six carbon materials in form of electrode has been drawn in Figure 33. The same trend has observed as shown in Figure 32.

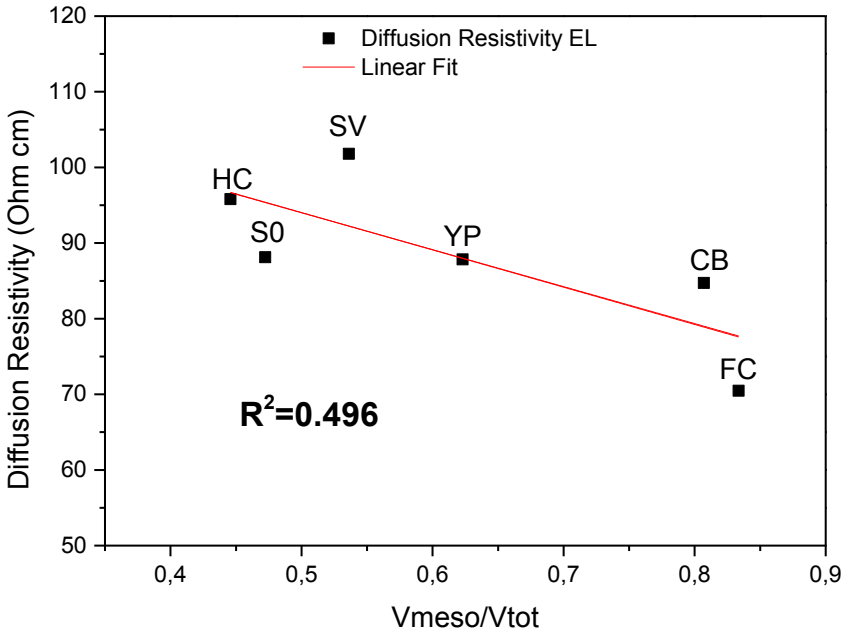


Figure 33. Relationship between diffusion resistivity and mesoporous volume proportion of electrodes made from six carbon materials.

5.1.2 Hot-pressing effect – varying pressure

After the general effect of the hot-pressing electrode preparation method has been investigated, detailed analysis has been also performed to study the pressure and temperature effects during the processing procedure. For all the studies in following sections, Kuraray YP-17D has been used as the sole active material for all electrodes.

We started firstly with pressure effect. For this purpose, electrodes have been laminated onto the aluminum current collector by using the same temperature (160°C) and applying 10, 30 and 50 bar, respectively. As shown in Figure 34 the voltammogram shape is retained for all the investigated electrodes. This suggests that changing pressure during the electrode compaction has little influence on the micro structure of the activated carbon.

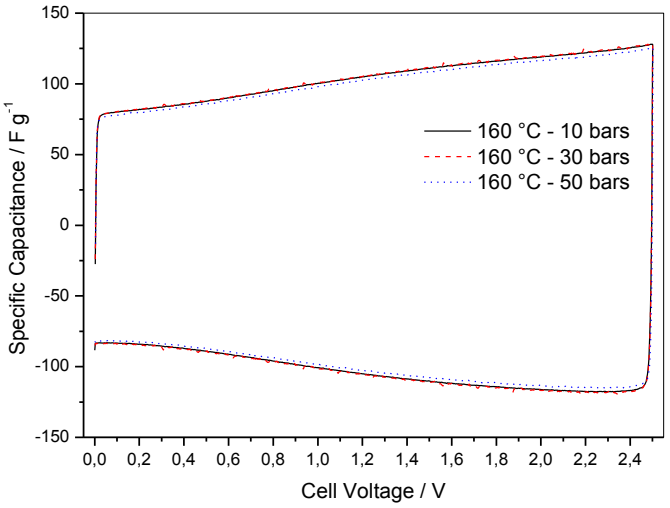


Figure 34. Specific capacitance versus cell voltage of carbon electrodes prepared at various pressures. The data are obtained from CV at 10 mV s^{-1} by dividing the specific current by the scan rate. Electrolyte: $TEABF_4$ in Acetonitrile.

The capacitance values are confirmed by the galvanostatic cycles performed at 1 A g^{-1} (Figure 35 a). The electrodes deliver very similar capacitance values: 104, 105 and 103 F g^{-1} for electrodes pressed at 10, 30 and 50 bar, respectively. The magnification of the galvanostatic cycle at more positive potentials allows estimating the IR-drop of the cell. As depicted in Figure 35 b the ohmic drop is strongly dependent on the pressure used for preparing the electrodes: the lower the pressure the higher is the ohmic drop. However, the calculation of the IR-drop gives only an indication of the total resistance of the cell, but does not allow an understanding of the specific contributions of the various electrode components to the overall cell resistance. A deeper understanding can be obtained by analyzing the EIS data. Figure 36 shows the Nyquist plots of the electrodes treated at various pressures. When the electrode is pressed at 10 bar a significant semicircle at high frequencies is present. By raising the pressure, the diameter of this semicircle decreases. At 50 bar the semicircle almost disappears and the related Nyquist plot is close to the ideal behavior of a porous electrode. As it was already discussed in the characterization methodologies section, the linear decrease of the semicircle with the pressure can be correlated either to an improvement of the contact at the interface aluminum/carbon electrode or to a better internal particle-particle contact. The latter can be achieved, if the electrode material is properly compacted. However, if two electrodes are compacted using the same conditions (50 bar and 160°C) but attached onto different current collectors – i.e., Al grid or Al foil – the resulting Nyquist plots show significant differences in the semicircle diameter (Figure 37). This means that the semicircle at high frequencies can be correlated to the interface electrode/current collector rather than to the particle-particle contact. The different lengths of the 45° slopes in Figure 37 are simply due to the

differences in the electrode thickness and it is not correlated to the current collector type.

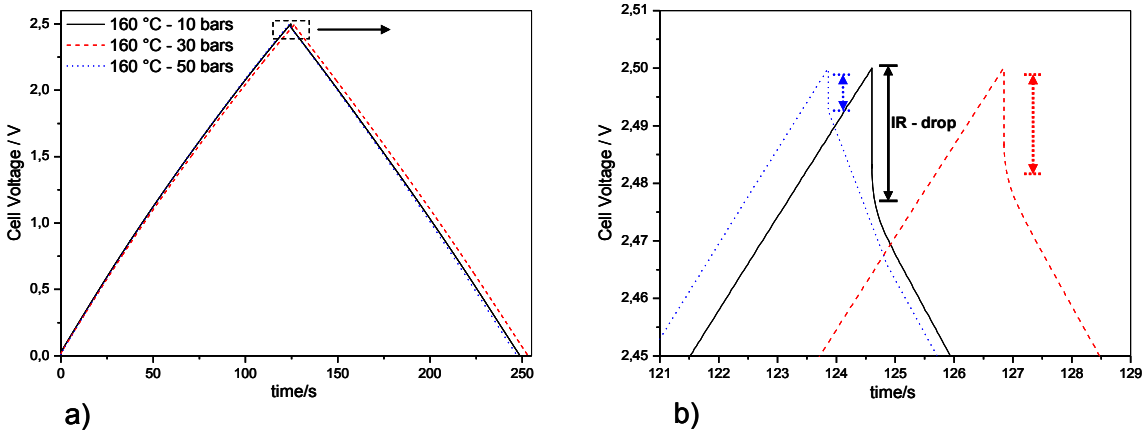


Figure 35. (a) Galvanostatic cycle at 1 A g^{-1} of carbon electrodes pressed on a treated Al foil at 160 °C and at 10, 30, and 50 bar. (b) Magnification of the curves at more positive potentials. Electrolyte: $TEABF_4$ in Acetonitrile.

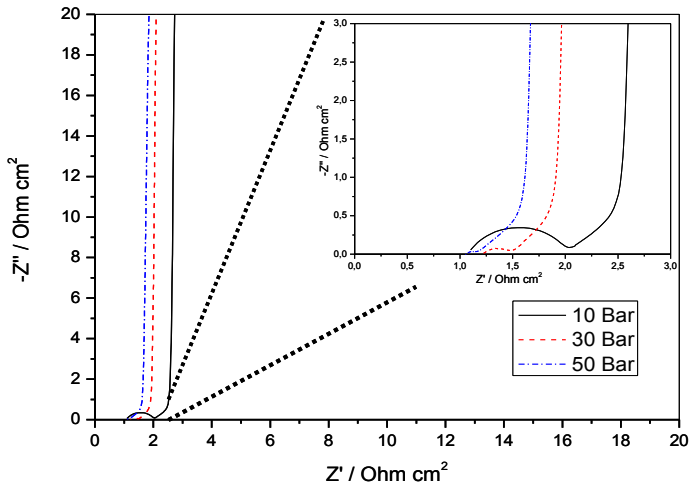


Figure 36. Nyquist plots of cells assembled with electrodes pressed on a treated Al foil at 160°C and at 10, 30, and 50 bar. Electrolyte: $TEABF_4$ in Acetonitrile. The inset shows the Nyquist plots magnification.

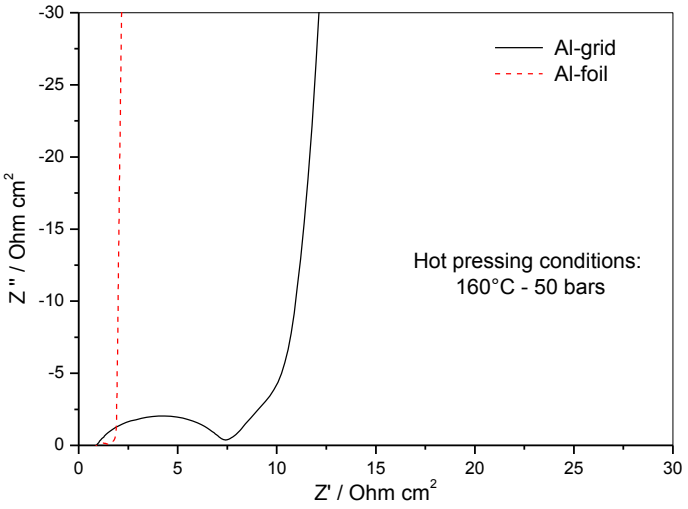


Figure 37. Impedance spectra of electrodes pressed using the same conditions (160 °C and 50 bar) but onto different current collectors.

From the results of Figure 36 it is clear that the best conditions for attaching the electrode to the current collector (in this case etched aluminum foil) are 50 bar and 160 °C. However, it is also important to consider the effect of the pressure on the electrode porosity and particle packing. As a first approach the electrode bulk densities have been calculated. The density is slightly increasing with the applied pressure. In fact, the calculated values are 0.697, 0.715 and 0.719 g cm^{-3} for the electrode pressed at 10, 30 and 50 bar, respectively. In order to investigate the electrode morphology and porosity the SEM images have been analyzed by using the ImageJ software. Figure 38 shows the original and the corresponding converted images (after applying a threshold) of the three electrodes under investigation.

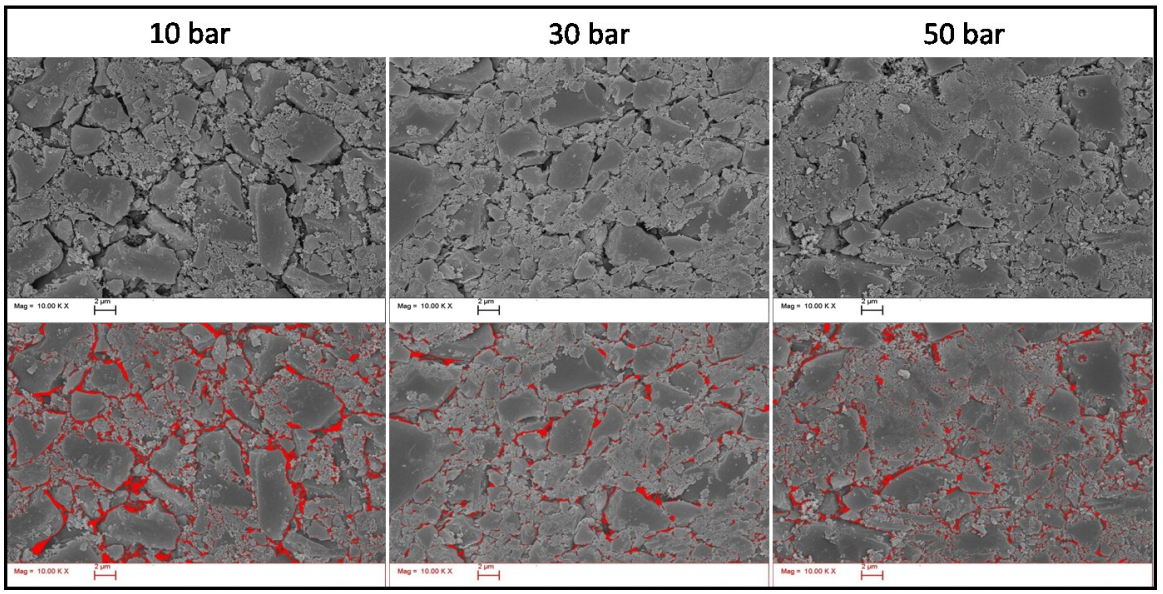


Figure 38. Original and with ImageJ-converted micrographs of the electrodes pressed at 160 °C and different pressures.

The resulting histogram (Figure 39) shows that the macro-pore area significantly reduces with the pressure. The average pore area is 0.018 μm^2 and 0.01 μm^2 for the electrode pressed at 10 and 50 bar, respectively.

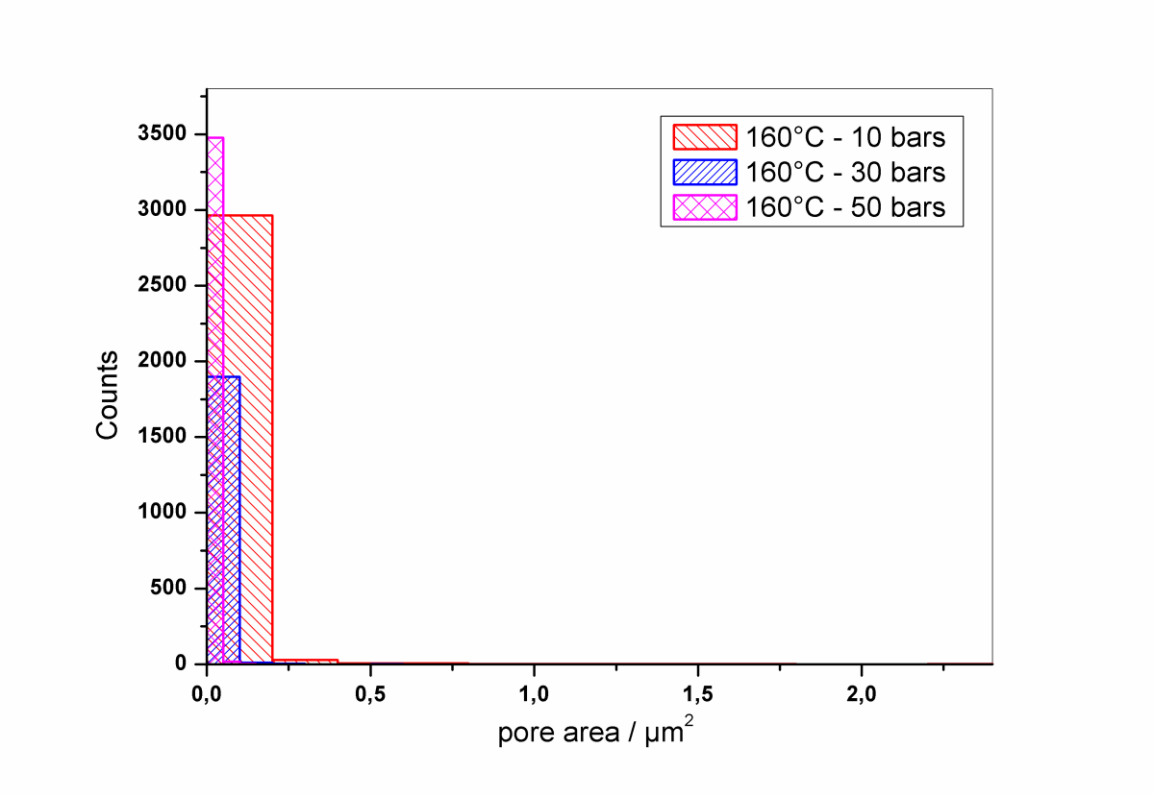


Figure 39. Pores area calculated by using ImageJ analysis of the electrodes of Figure 38.

More information about the electrode morphology can be obtained from the images at higher magnification (Figure 40). As it is evident, excessive pressure causes change in the binder morphology. While at 10 bar the PTFE binder retains its original spherical shape, at 50 bar the binder particles are much more compacted as shown in the dashed areas.

Therefore, even if 50 bar are very effective on reducing the contact resistance between the electrode and the current collector (see the disappearing of the semicircle at high frequencies in the Nyquist plot of Figure 36), applying such a high pressure can also have a negative effect on the binder packing density and

on the electrode porosity. One solution is to treat the electrode at higher temperatures while maintaining the pressure as low as possible.

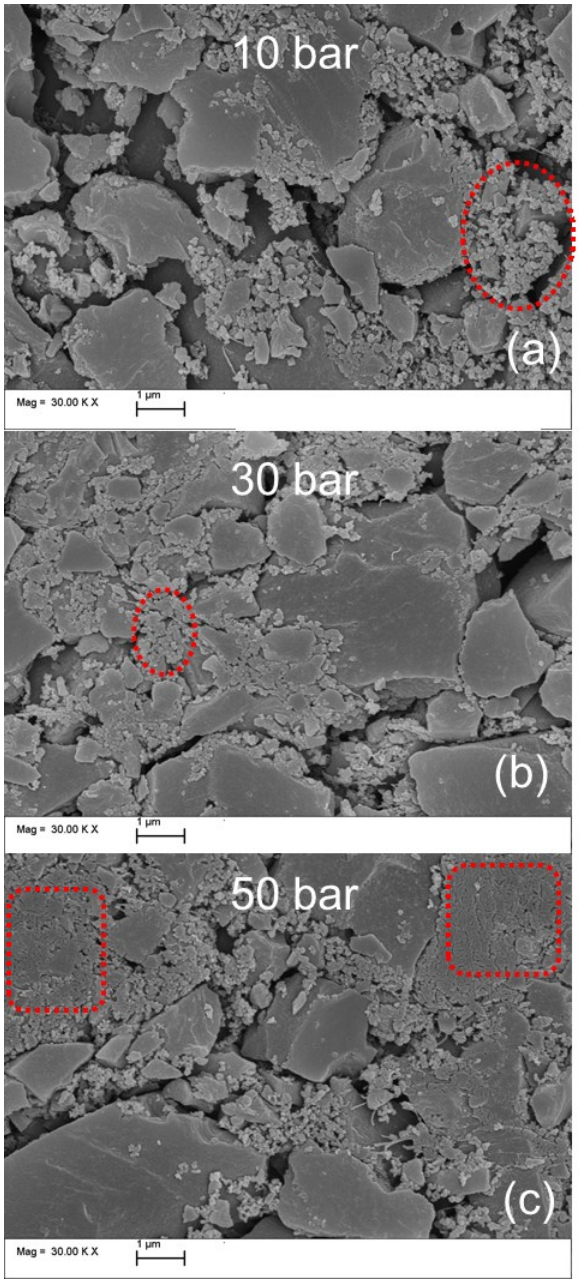


Figure 40. SEM images at higher magnification of carbon electrodes pressed at 160 °C and at various pressures. The areas marked with dashed line indicate the binder.

5.1.3 Hot-pressing effect – varying temperature

The temperature plays also an important role on the electrode preparation. As it is shown in the Nyquist plot of Figure 41, at 200 °C a pressure of 10 bar is already enough to reach a good electrode adhesion (disappearing of the semicircle). This means, when using higher temperatures it is not anymore necessary to subject the electrode to such high pressures. In this way the electrode macroporosity can be easily retained.

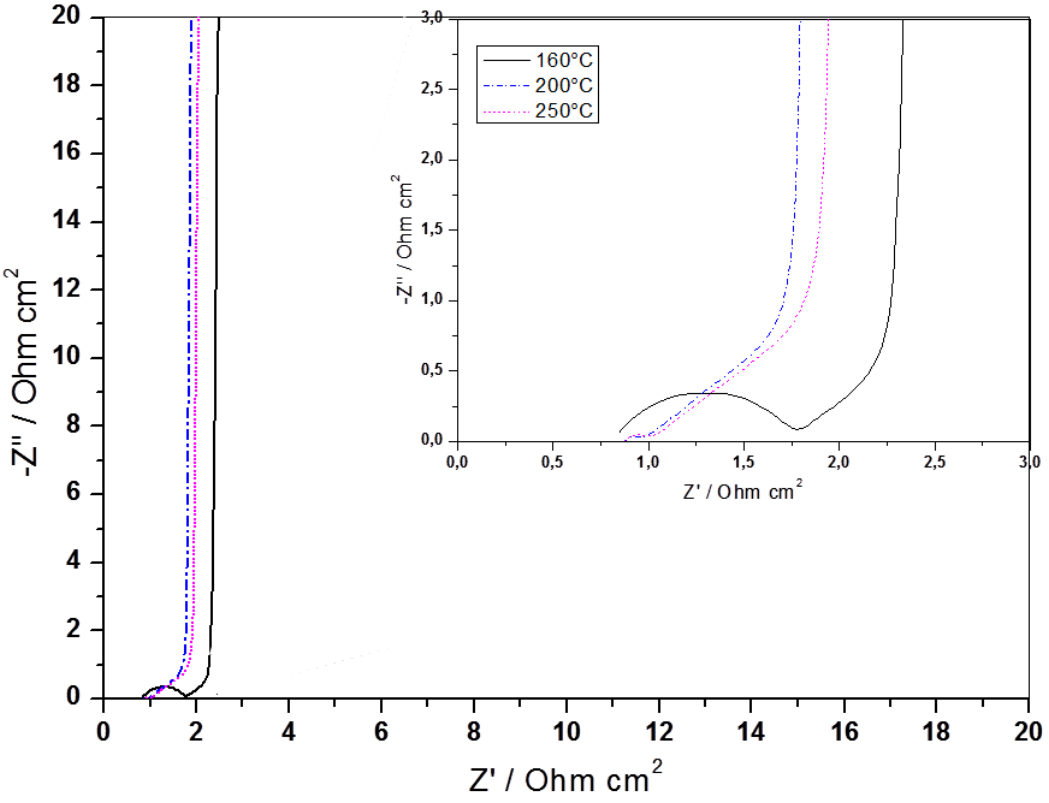


Figure 41. Nyquist plots of cells assembled with electrodes pressed on a treated Al foil at 10 bar and at different temperatures. Electrolyte: TEABF4 in Acetonitrile. The inset shows the Nyquist plots magnification.

In fact, no relevant morphological differences can be observed among electrodes treated at different temperatures (Figure 42). The electrode porosity as calculated from the image analysis is very similar for the three electrodes. The average pore area is 0.018, 0.015 and 0.015 μm^2 for the electrodes pressed at 10 bar and 160, 200 and 250 °C, respectively.

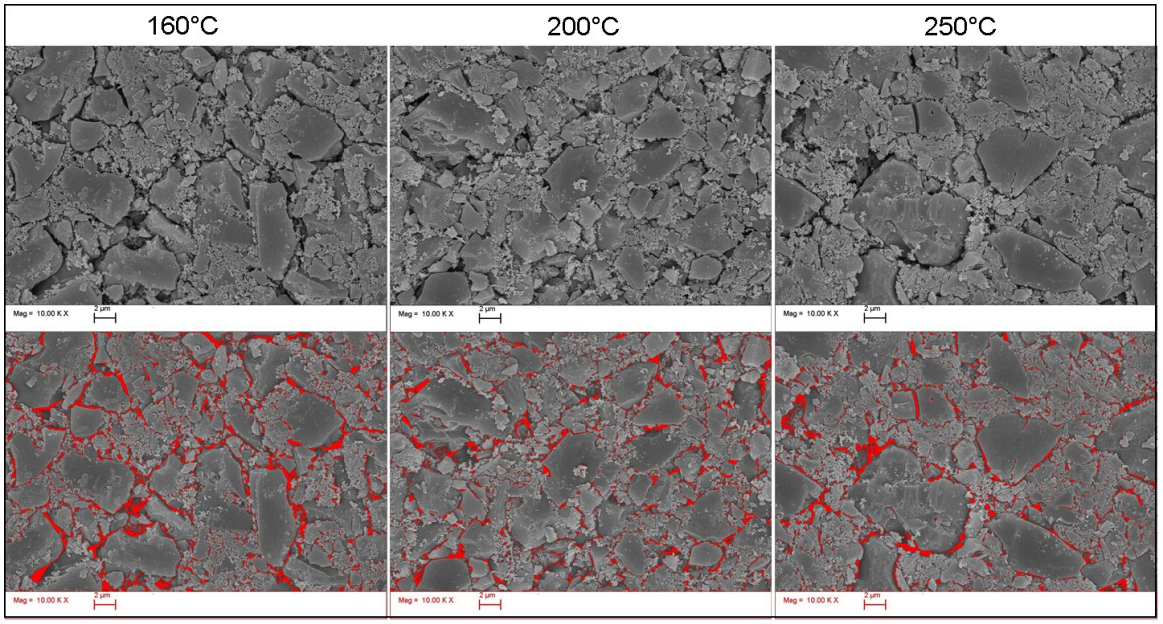


Figure 42.Original and with ImageJ-converted micrographs after threshold of electrodes pressed at 10 bar and different temperatures.

The data obtained from the image analysis have been compared with the diffusion parameters obtained from the EIS analysis. As already explained in Section 4.4.4.3, the diffusion resistivity instead of the diffusion resistance has been calculated in order to avoid the influence of the electrode thicknesses. Figure 43 reports these results for all the electrodes investigated in this work. A very good correlation can be observed between the pore dimension, as calculated from ImageJ analysis (Figure 43 a) and the diffusion resistivity of the electrolyte through the electrode pores as calculated from the fit of the EIS data

(Figure 43 b). The two graphs are in a good agreement: the electrode pressed at 50 bar shows smaller macro-pores and higher diffusion resistivity. Therefore, the diffusion impedance (Z_d) is not only dependent on the micro-structure of the porous carbon used but is also influenced by the electrode macro-porosity and can be controlled during the electrode preparation. The macro-pores serve as electrolyte pathway and can influence the electrode kinetics.

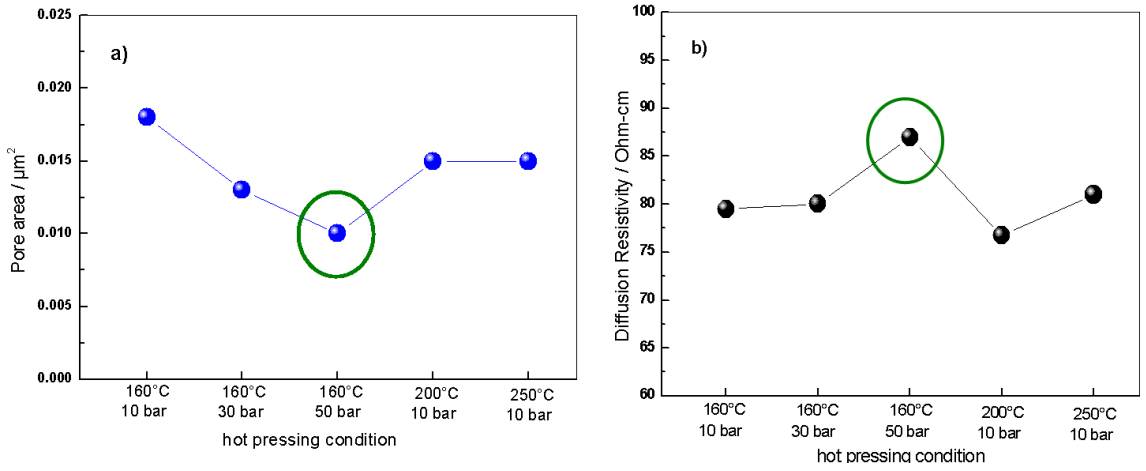


Figure 43. (a) Pore area average calculated by SEM images using ImageJ software and (b) Diffusion resistivity as calculated from the EIS simulation.

5.1.4 Laminating effect – varying rolling force

Electrodes prepared by the optimized hot-pressing process showed outstanding electrochemical performances. However, this discontinuous process does not allow an up-scaling for industrial production. Therefore another machine -laminator- has been employed as a substitute for the hot-press in order to prepare much larger electrodes through a continuous manufacturing process.

The most important operating parameter of the laminator is the rolling force. Different as the case of hot-press, the electrodes are passing through two rolls of the laminator and thus are subjected to dynamic linear force instead of static area force. This makes a direct conversion of the already optimized pressure value for the hot-press into a force for the laminator almost impossible. The unit of force used in the laminator is kilogram force (kgf), by definition 1 kgf = 9.8 newton. In following paragraphs the effects of varying rolling force on the electrochemical properties of electrodes are discussed.

The contribution of Equivalent Series Resistance (ESR) could derive from the electrolyte resistance, the intrinsic resistance of the active material, and the contact resistance at the interface of active material/current collector [73][54][80]. As it has been already done with the hot-press, the main goal of this part of work is also to decrease as much as possible the interface resistance between active material and current collector. In the following section, the EIS patterns of both fresh and aged carbon electrodes which have been prepared under different conditions (laminated and also hot-pressed) are compared. The hot-pressing condition was 50 bar and 160 °C.

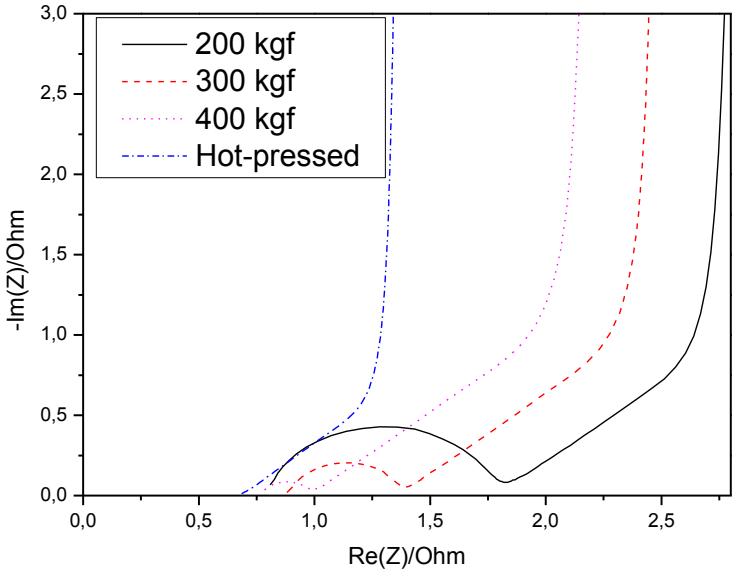


Figure 44. Nyquist plots (fresh electrodes) of supercapacitor cells laminated with different forces in comparison with the one processed by hot-press.

In Figure 44, one can clearly observe that with increasing lamination forces, the size of the semicircle (which can be correlated with the Al/electrode contact) of the fresh assembled capacitor cell sinks. However, the electrodes prepared by using the hot-press show the lowest contact resistance among all samples. One must take into consideration that the laminator is not able to provide enough force to attach the active material and the current collector very well together as the hot-press does.

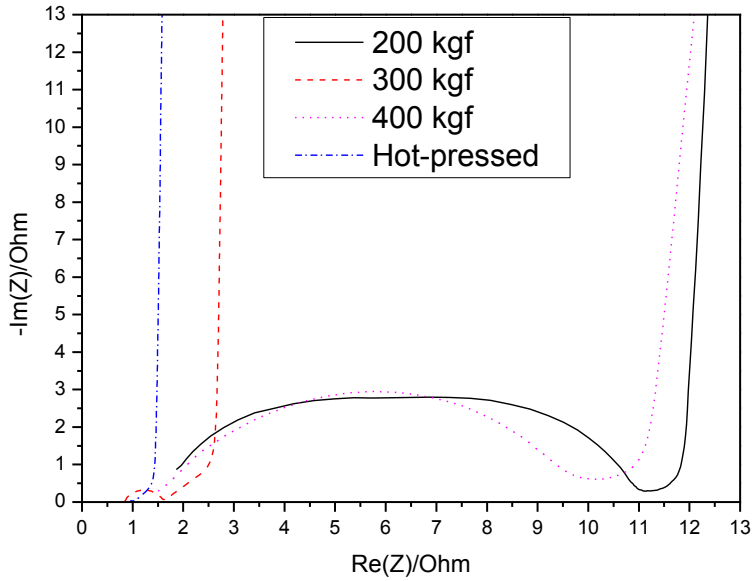


Figure 45. Nyquist plots (after 200 cycles) of supercapacitor cells laminated with different forces in comparison with the one processed by hot-press.

However, by comparing the Nyquist plots (Figure 45) of aged electrodes (after 200 cycles, cycling condition: 50 cycles at 0.125 A g^{-1}, 50 cycles at 0.25 A g^{-1}, 50 cycles at 0.5 A g^{-1} and 50 cycles at 1 A g^{-1}) one can conclude that the optimized force of the lamination process should be around 300 kgf; too little pressure does not properly help to improve the interface contact and too high force induces internal stress between the active material layer and Al foil so that they lose contact with each other during cycling. Once again, the hot-pressed electrodes show the best performance. However, the total resistance value of the electrodes laminated at 300 kgf is not much higher than that of the hot-pressed sample. This indicates that the lamination technique is promising in preparing supercapacitor electrodes on a large scale and also maintains a proper contact between the active material layer and the current collector foil.

Furthermore, the carbon electrodes have been also tested by cyclic voltammetry to find the influence of electrode processing conditions. The cyclic voltammograms of all four samples (laminated and hot-pressed) are shown in Figure 46. The shapes of all voltammograms are very similar to each other, exhibiting quasi-rectangular pattern.

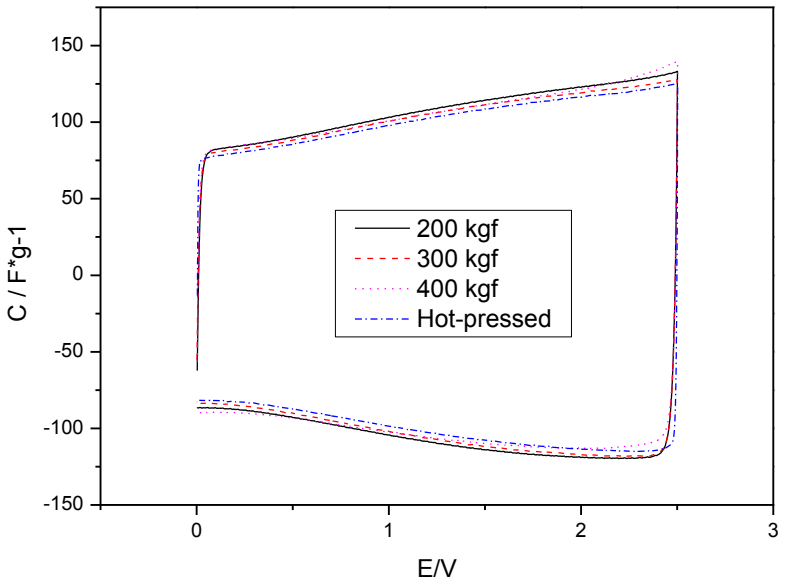


Figure 46. Gravimetric capacitance of supercapacitor cells laminated with different forces in comparison with the one processed by hot-press (Scan rate 10 mV s^{-1}).

The gravimetric specific capacitance of all electrodes can be calculated from the CVs. The exact values are taken from the mid-point of the potential range (at 1.25 V) and summarized in Table 7. From the values one can conclude that all the electrodes, independent of the processing methods, shows analogous

gravimetric specific capacitances. This is a proof showing that the micro structure of the activated carbon has not been much influenced by alternating the force.

Table 7. Gravimetric specific capacitances of supercapacitor electrodes laminated with different forces in comparison with the one processed by hot-press (calculated from CV).

	200 kgf	300 kgf	400 kgf	Hot-pressed
Specific capacitance (F g^{-1})	109	106	106	103

Moreover, the “IR-drop” values have been obtained from GCPL experiments and depicted in Figure 47. It shows clearly that the resistances of all electrodes follow the sequence of 200 kgf > 400 kgf > 300 kgf > hot-pressed sample which is perfectly consistent with the results got from the EIS measurements (Figure 45).

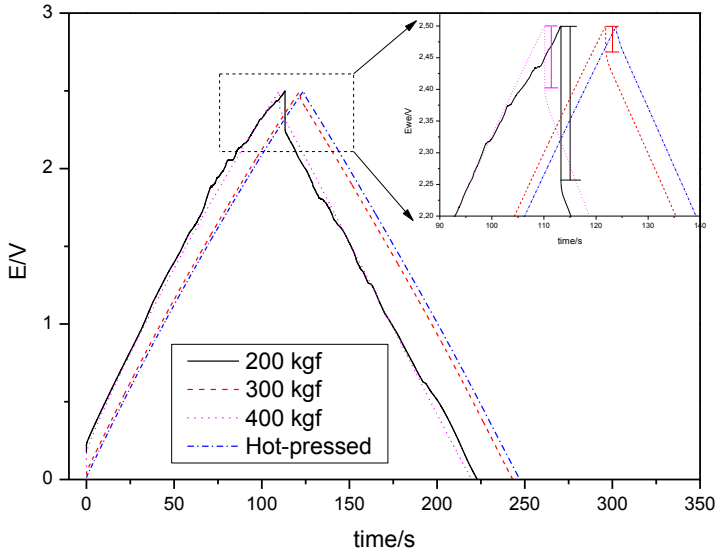


Figure 47. Galvanostatic cycling curves of supercapacitor cells laminated with different forces in comparison with the one processed by hot-press (Cycling condition: 1 A g^{-1}).

Furthermore, the gravimetric specific capacitances of all electrodes can be obtained from slopes of the discharging curves in the GCPL plots. Again similar values are got from all samples. These results are in line with the ones from CV measurements.

Table 8. Gravimetric specific capacitances of supercapacitor electrodes laminated with different forces in comparison with the one processed by hot-press (calculated from GCPL).

	200 kgf	300 kgf	400 kgf	Hot-pressed
Specific capacitance ($F\ g^{-1}$)	99	102	98	101

In order to further investigate the effects of rolling force on the micro structure of carbon electrodes, ImageJ was again employed to analyze the SEM photos of them.

The pictures were first converted to binary image by the same method described in previous sections, the area of pores were marked with red color (see Figure 48). The fraction of the pores and the average pore sizes were then calculated by using the ImageJ program.

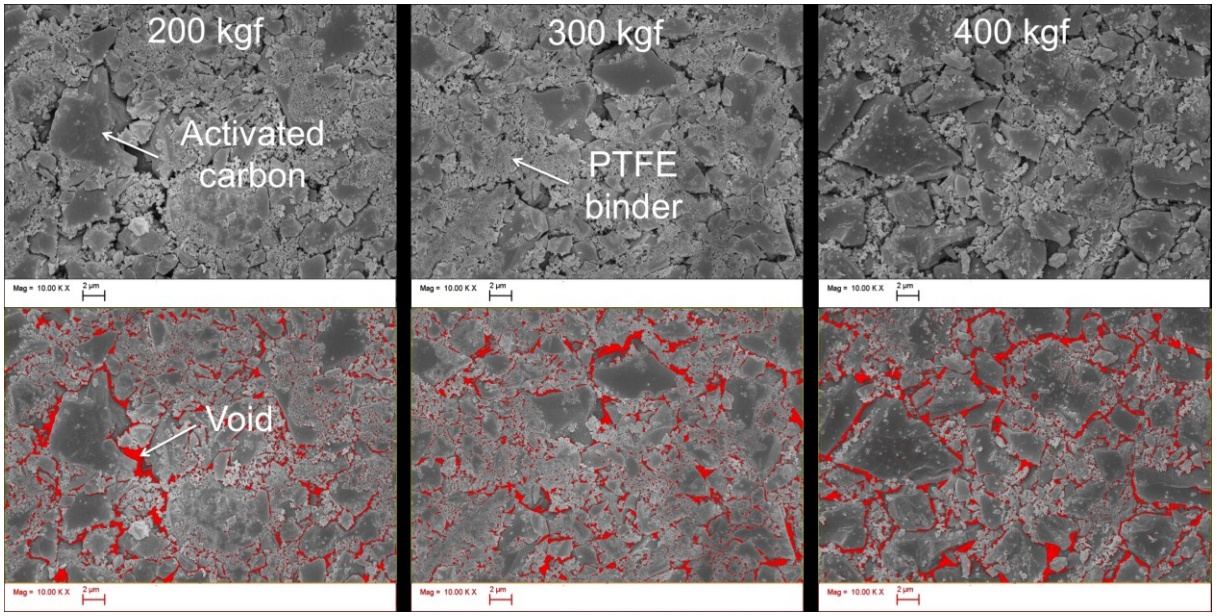


Figure 48. Scanning Electron Microscopy (SEM) images and the analysis thereof from supercapacitor electrodes laminated with different forces.

From both Figure 48 and Table 9 one can observe and conclude that the SEM image analysis showed very little differences among all three samples. This fact confirms again that varying the rolling force of the laminator has little influence on the microstructure of active material.

Table 9. Pore fraction and average pore size values of supercapacitor electrodes laminated with different forces.

	200 kgf	300 kgf	400 kgf
Pore fraction (%)	6.6	7.3	6.9
Average pore size (nm)	16	15	19

5.2 Effects of electrode recipe

As it has already been discussed in previous chapters, selection of active materials and electrode preparation methods play essential roles on determination of the electrochemical performances of the electrodes. Moreover, the optimization of the electrode recipe is also very important and has been studied in this work. Generally an EDLC electrode is composed by the active material (i.e. porous carbon), a conductive agent (conductive carbon) and a binder (e.g. PTFE or PVdF). The function of the active material is to store charges and provide capacitance for the capacitor; the role of the conductive agent is to increase the electrical conductivity of the cell and the polymer binder is mainly responsible to maintain the mechanical stability of the whole compound electrode.

First of all, the percentage of carbon black in the electrode recipe has been varied.

It is widely recognized in literature that the function of carbon conductive agent is to improve the conductivity and to decrease the resistivity of the electrode because it provides better particle-to-particle contact and establish faster electron pathway [81][82][83]. However, there is not much literature which studied in depth the effect of changing carbon black percentage. In this dissertation, electrodes with the same activated carbon YP-17D and five different carbon black concentrations have been prepared, ranging from 0% to 10%. The electrodes have been tested by employing the standard test protocol which has been described in the experimental chapter.

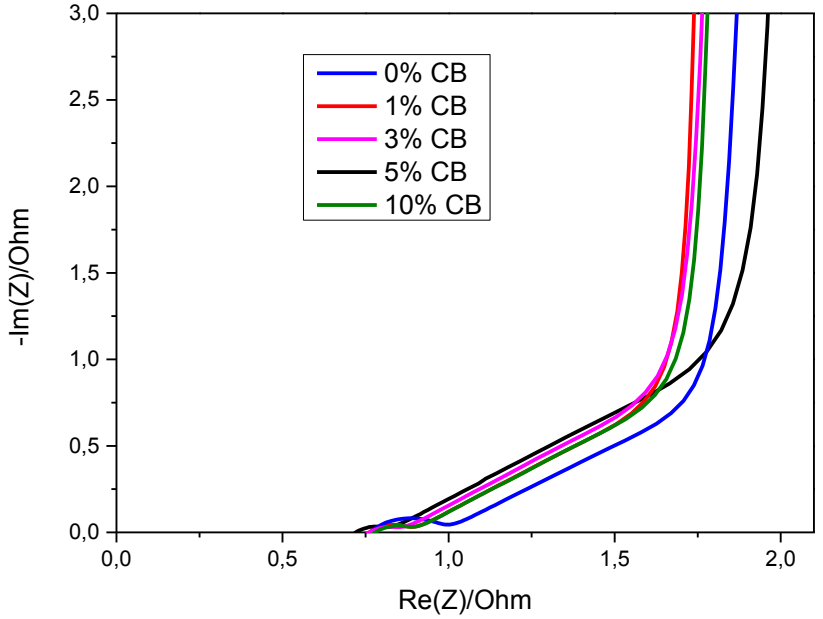


Figure 49. Nyquist plots of fresh carbon electrodes with different carbon black content.

The values of interface contact resistance can be extracted from the semicircles of impedance spectra (see Figure 49). They are basically the subjection of semicircles on the X-axis.

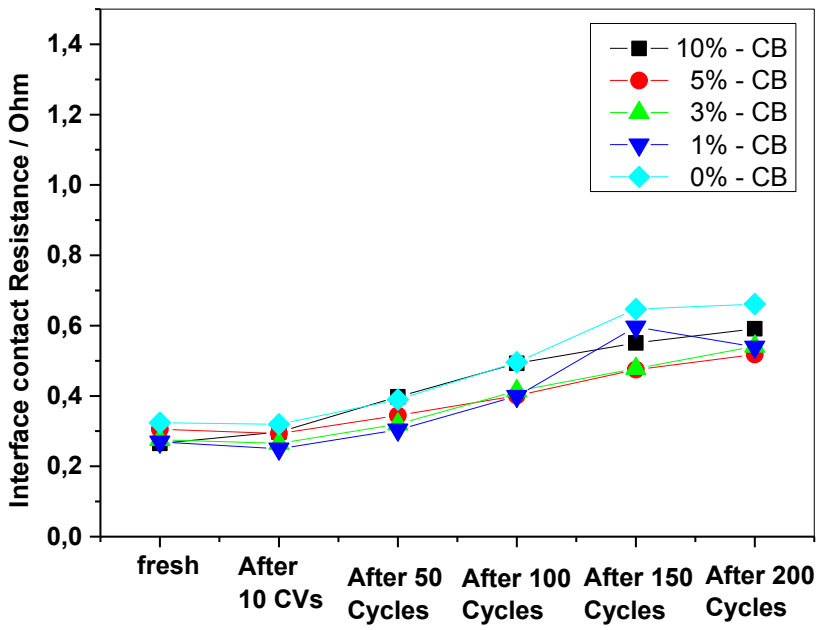


Figure 50. Development of interface contact resistance of carbon electrodes containing different percentage of carbon blacks during electrochemical testing.

Interface contact resistance values have been obtained from the fit of the impedance spectra reported in Figure 49 for all samples with various carbon black contents and were drawn in Figure 50 together with their evolution during the electrochemical tests.

Surprisingly, all the samples show very similar behavior, no matter how much percent of carbon black has been added in the electrodes. Even the sample without any carbon black exhibits not much higher resistance in comparison to other samples. What can be also observed is that all samples have experienced increase of resistance during the test procedure. This is quite normal as cycling of the cells has led to gradual contact loss between carbon particles and the Al current collector.

Moreover, the apparent diffusion coefficient of all samples with different carbon black contents has been obtained from the method described in the experimental chapter. Once again no obvious difference could be observed among all samples. These steady values show that cycling of the cells did not influence much the diffusion capability of the porous carbon.

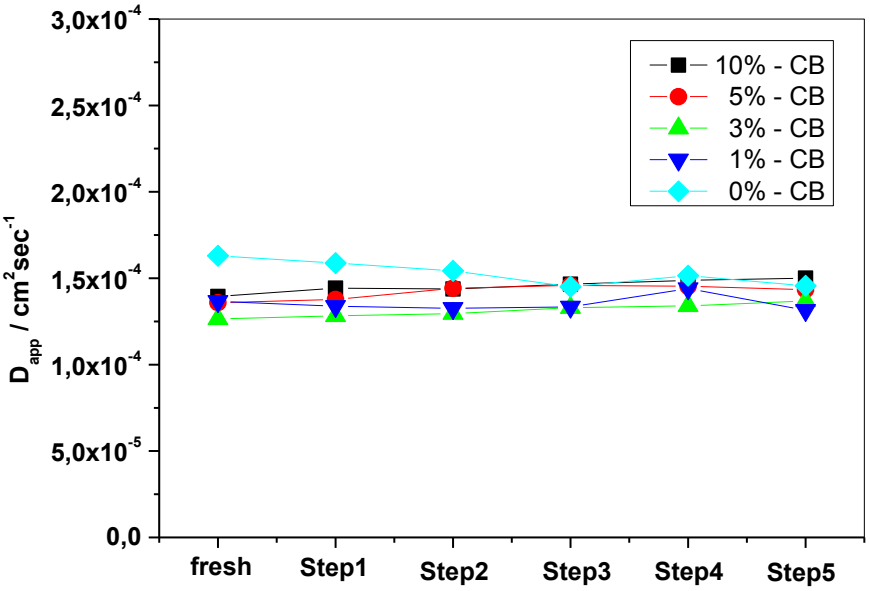


Figure 51. Development of apparent diffusion resistance of carbon electrodes containing different percentage of carbon blacks during electrochemical testing.

A hypothesis has been proposed for explaining the anomalous phenomenon that content of carbon black influenced little contact resistance of the electrodes.

As it has been already shown, the electrodes characterized in this thesis were all prepared by a dry method and strongly compacted by the calender and the hot-press machine. Thus it is considered that this high degree of compaction may lead to very good interparticle and also particle-Al foil contact which provides the electrodes very low contact resistance. Shown below in Figure 52 are the SEM images of both uncompacted mixture (activated carbon, carbon black and binder) and highly compacted free-standing-electrode. One observes clearly a huge difference of compaction degree. In fact, the density of free-standing-electrodes is around 39% higher than that of uncompacted mixture. Furthermore, in literature there are also results supporting this proposed hypothesis. For instance, Sánchez-González et al. have investigated the electrical conductivity of carbon blacks under compression and they have found an increase of conductivity with increase of the density [84]. It seems that with the dry preparation method developed by our group, a good electrical conductivity of electrodes can be achieved without adding carbon black as conductive agent. However, carbon black should still play important role when the electrodes are prepared by the traditional wet method.

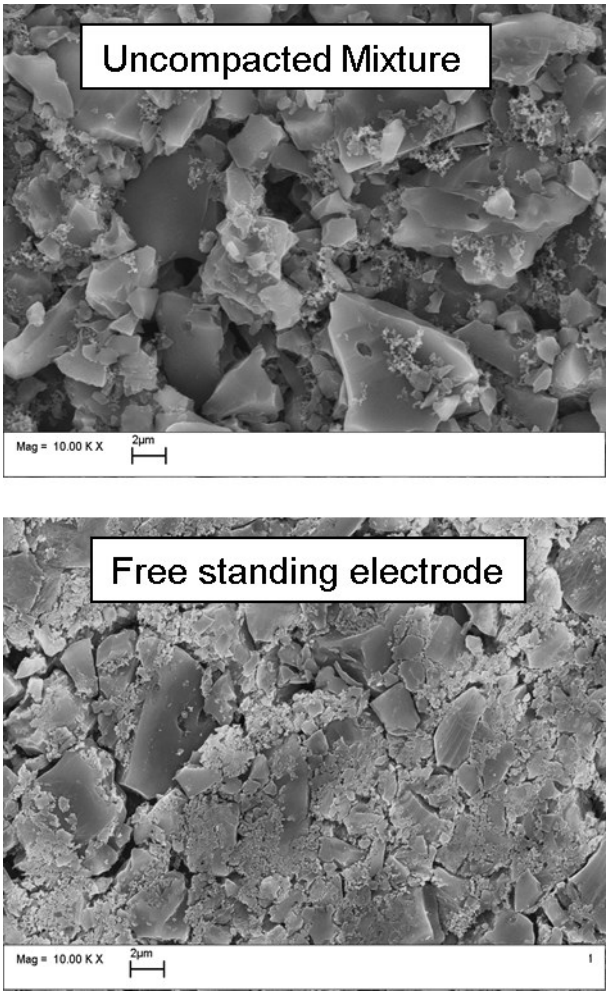


Figure 52. SEM pictures of uncompacted mixture (activated carbon, carbon black and binder) and free standing electrode.

The binder contributes significantly to the mechanical stability of the electrodes, higher binder content brings more stable electrodes. However, due to its electrochemically inert nature, too high binder content influences negatively the specific capacitance of the whole electrode. Therefore the percentage of binder should be kept as low as possible.

In this study, the PTFE binder content has been varied between 5% and 20% in order to investigate the effect on the electrochemical performance of the electrodes. The apparent diffusion coefficients of carbon electrodes with three different binder contents have been illustrated in Figure 53. It can be clearly observed that the binder content influences greatly the diffusion behavior of the electrolyte through the porous structure of electrodes by modifying the morphology of meso- and macropores. Generally less binder content enables higher diffusion coefficient and thus better diffusion behavior. When the two samples with 10% and 5% binder content are compared with each other, it is observed that at the beginning of the test protocol, the two samples showed rather very similar behavior. However, after 10 cycles of CV and 50 times of cycling at 125 mA g^{-1}, the sample with 5% binder content experienced an activation process which provided the electrode increasing apparent diffusion coefficient. Nevertheless, the mechanism of this activation process remains up to now unclear.

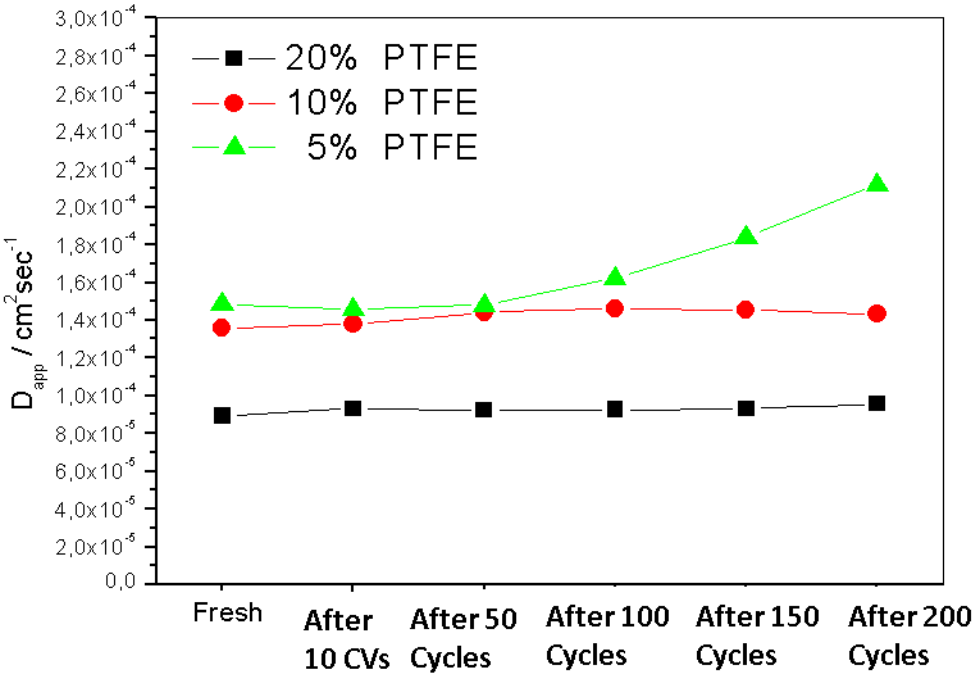


Figure 53.Development of apparent diffusion coefficient of carbon electrodes containing different percentage of PTFE binder during electrochemical testing.

Furthermore, the SEM pictures of all three samples (with 5%, 10% and 20% binder) have been shown in Figure 54. It is quite obvious that the higher binder content the electrode has, the more it looks to be compacted. Or in other words, whose macropores look smaller.

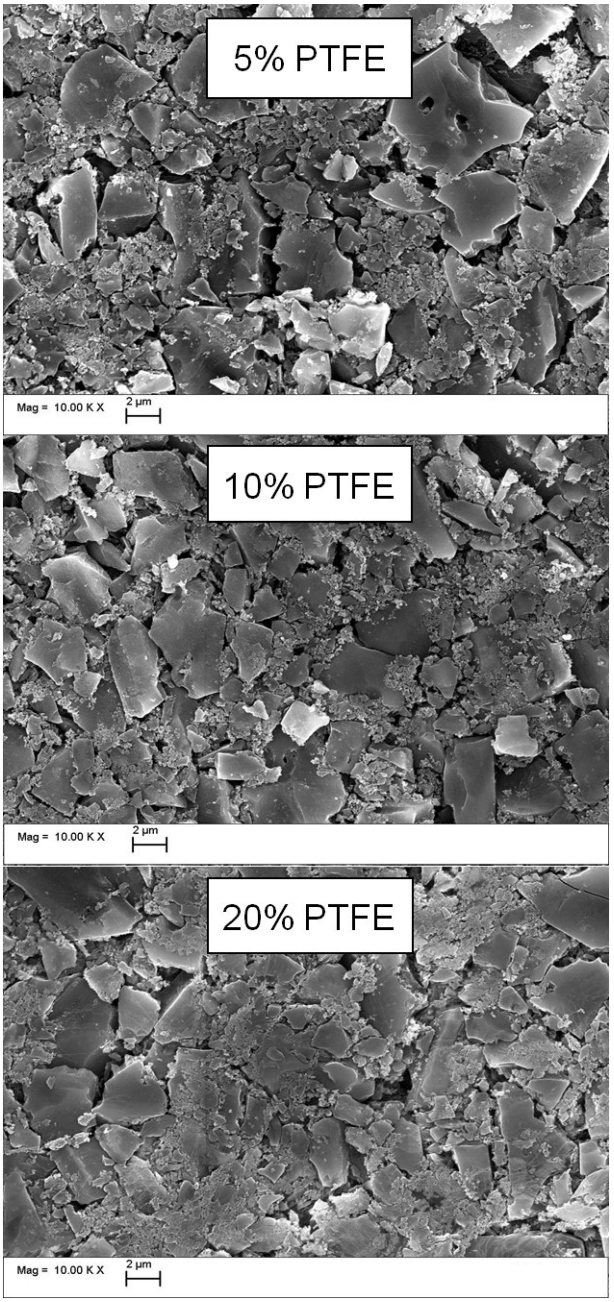


Figure 54. SEM images of EDLC electrodes with three different PTFE binder content.

Furthermore, the surface pore fraction of carbon electrodes can be calculated by using the software ImageJ. The results for all three samples have been shown in Figure 55. There is again a clear trend: more PTFE binder covers more macropores on the electrode surface. A good surface porosity, which is essential for electrolyte diffusion, can be achieved by lowering the binder content in the electrode recipe.

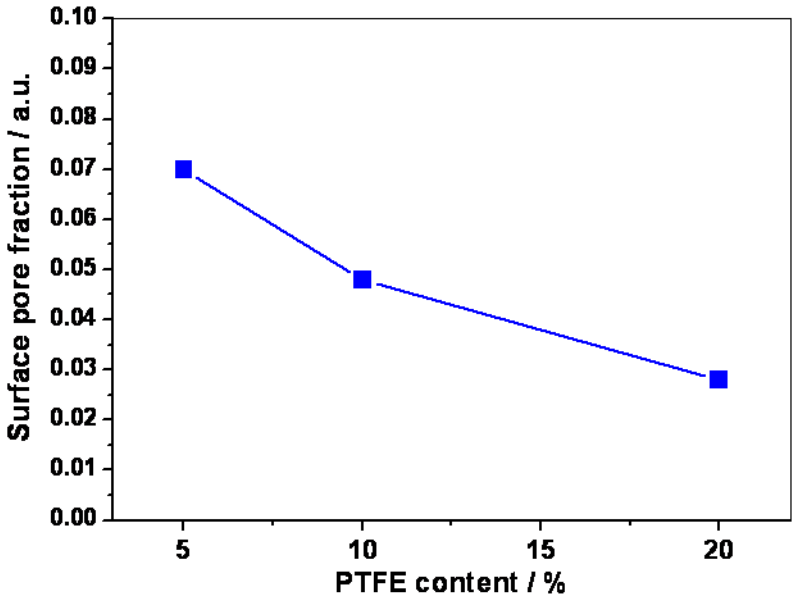


Figure 55. Relationship of surface pore fraction and PTFE binder content of the carbon electrodes (obtained from SEM photos analysis by ImageJ).

5.3 EFFECTS OF ELECTRODE MASS RATIO

The amount of electrical energy stored in a capacitor can be calculated from the formula $E = ½ CV^2$ in which the capacitance is determined by the electrode material employed and the voltage depends essentially on the stability window of the electrolyte. EDLCs based on symmetric electrode configuration (same mass loading for both positive and negative electrode) are already worldwide commercially available. However, due to the fact that electrolyte cations have different sizes as anions, they behave very differently when adsorbed in the porous structure of the anode and cathode, respectively. This leads to insufficient utilization (detailed explanation see following paragraphs). Therefore EDLCs with asymmetric configuration (different mass loading for positive and negative electrode) have been assembled and characterized in this dissertation.

All experiments related to mass balancing in this work have been performed with $TEABF_4$/AN as electrolyte. The TEA^+ cation has larger size as the BF_4^- anion, thus fewer ions are adsorbed on the negative electrode than that on the positive electrode and therefore the negative electrode is limiting the performance of the whole cell [85] [86].

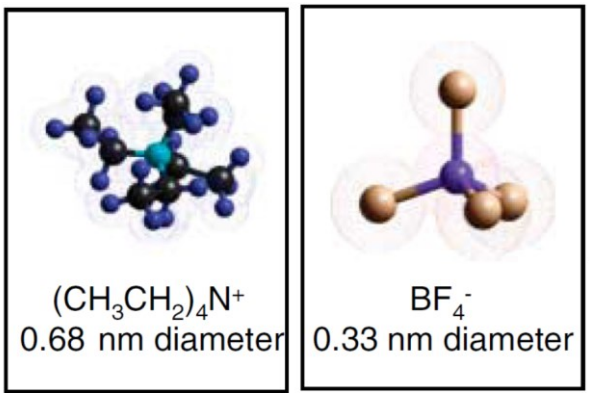


Figure 56. Schematic of TEA^+ and BF_4^- ions [86].

Furthermore, the mid-point of the electrochemical stability window (ESW) of the electrolyte is very often not found at the potential of the discharged carbon electrode. As it is shown in Figure 57, the ESW is not fully utilized in the case of symmetric EDLCs [87]. With proper balancing of the mass ratio between positive and negative electrode, full utilization of the electrolyte ESW could be possible (Figure 57b).

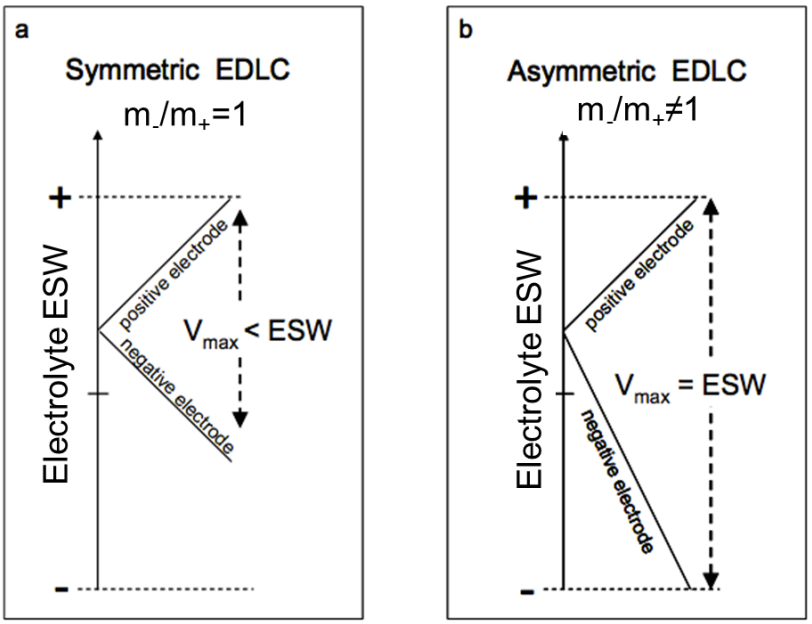


Figure 57. Comparison of symmetric and asymmetric EDLCs: difference on the width of electrochemical stability windows [87].

In order to find the proper mass ratio between the positive and the negative electrodes, the following equation has been employed based on charge neutrality between both electrodes:

$$C_+ \times \Delta E_+ \times m_+ = C_- \times \Delta E_- \times m_- \quad (21)$$

where C_+ and C_- are the gravimetric specific capacitance of the positive and negative electrodes; ΔE_+ and ΔE_- stand for the respective operating voltage window of the positive and negative electrodes; m_+ and m_- are weight of the positive and negative electrodes.

In order to separate the capacitance contribution from the positive and negative electrodes, activated carbon-based electrodes have been employed as quasi-reference electrode (QRE) [63], its potential is roughly 3 V vs. Li/Li^+.

First of all, symmetric cells have been assembled and tested by CV technique in order to obtain the values of C_+ and C_-. Below shown in Figure 58 is a "butter fly" pattern of the CVs from both the positive and negative electrodes. The both electrodes have identical mass loading, the values of ΔE_+ and ΔE_- are 1.164 V and 1.336 V, respectively. Therefore by employing equation 16, the value of C_+ /C_- can be obtained as 1.148. This number confirms the statement made above; the negative electrode is limiting the capacitance of the whole cell.

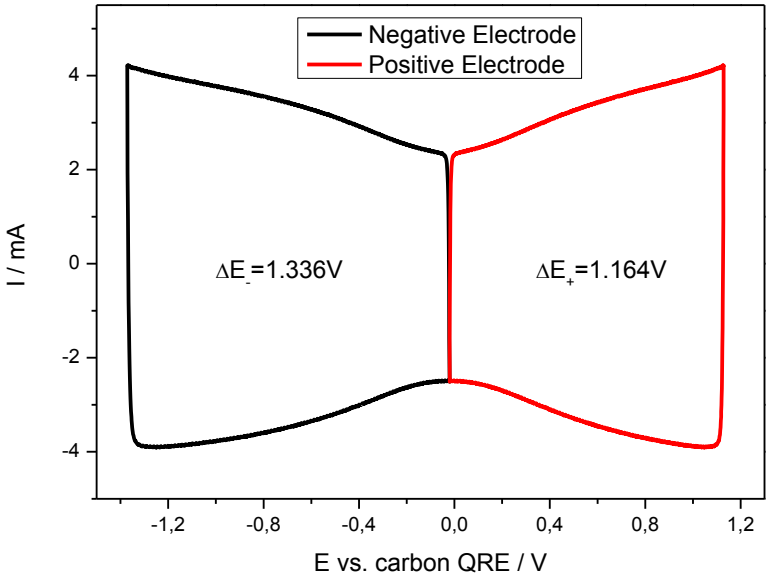


Figure 58. Individual contributions of both electrodes in a symmetric cell in the conventional potential range (2.5 V).

Secondly, the ESW of the applied electrolyte has to be precisely determined. This can be done by the following steps:

Numbers of capacitor half cells have been tested by CV technique in different scanning ranges (see Figure 59). Oxidative and reductive peaks have been observed in high potential ranges (both positive and negative) which indicated that redox reactions (decomposition of electrolyte, oxidation of electrodes etc.) had happened during cycling of the cells. In order to guarantee excellent cycling stability, the operating potential window of the capacitor cell has to locate within safe regime where redox reactions are minimized.

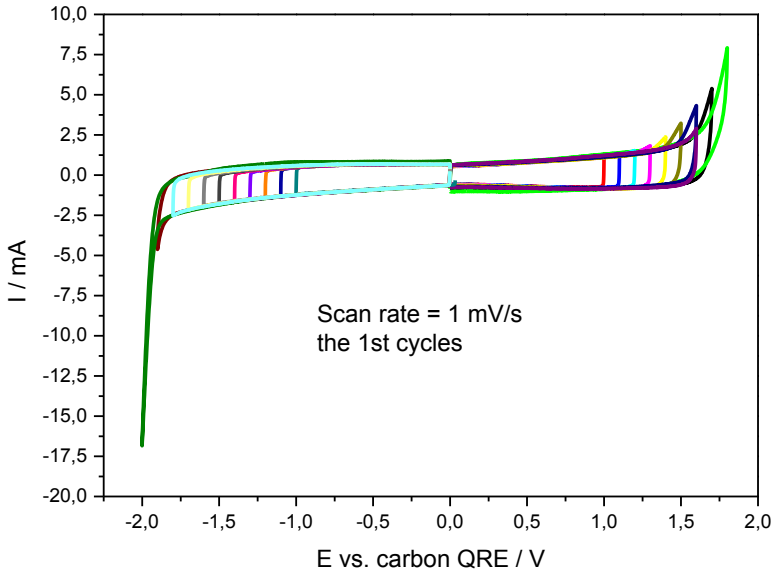
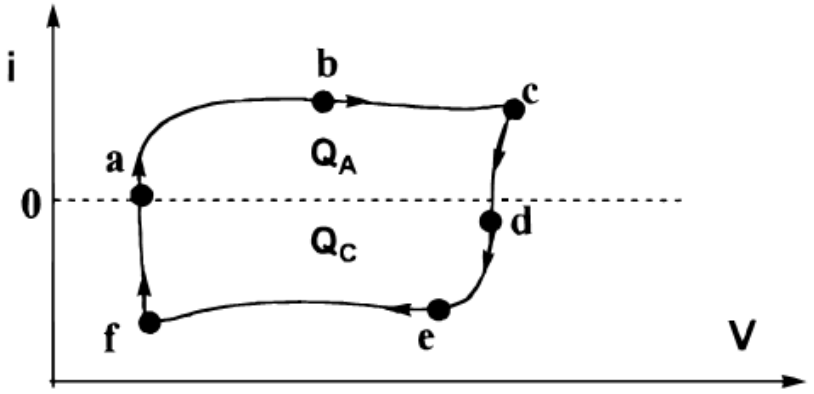


Figure 59. Determination of the electrolyte ESW in half cell.

Looking back to the literature, the group of Jow has introduced the concept of faradaic fraction R which is calculated by the equation in Figure 60 [99][100]. Q_A and Q_C can be calculated simply by integrating the current over time. For the cathodic territory, one just needs to exchange the positions of Q_A and Q_C in the formula. Faradaic fraction R is a measure of the capacitance contribution from faradaic reaction vs. that from non-faradaic process. The bigger R is, the higher percentage of the whole capacitance is from faradaic reaction. Jow and co-workers used R as criterion of determining the electrochemical stability window of the electrolyte and have chosen R=0.1 as the limit (n is the potential limit in Volt).



$$R = \frac{|Q_F|}{|Q_{NF}|} = \frac{|Q_A|}{|Q_C|} \quad -1.0$$

Figure 60. Schematic of calculation method for faradaic fraction in anodic territory [88].

A graph of faradaic fraction vs. potential has been obtained from the CV experiments and shown in Figure 61. According to Jow's theory, the cell is not stable at all in all potential ranges. This means that it is even not possible to assemble a capacitor cell with 2.0 V of operating voltage according to Jow's

theory. This statement, however, is against common sense. Therefore another criterion has to be applied in order to figure out a proper working potential range for the capacitor cells.

The group of Kötz has proposed another criterion for determination of the ESW of an electrolyte. By comparing the change of R of two successive points, they consider the change in slope should not be above 0.0005 dR/dV [90]. Depicted in Figure 61, the value of $\Delta_{n+1} - \Delta_n$ should be smaller than 0.005. However, after calculating the corresponding $\Delta_{n+1} - \Delta_n$ values of cells run at various potentials (shown in Table 10), it is still not possible to identify a proper working range of the electrolyte. As the constant 0.005 is strongly dependent on many factors like electrode preparation and cell assembly etc., it has been chosen arbitrarily by the authors [90]. In the case of this dissertation, instead of 0.005, 0.05 is considered as an appropriate limitation.

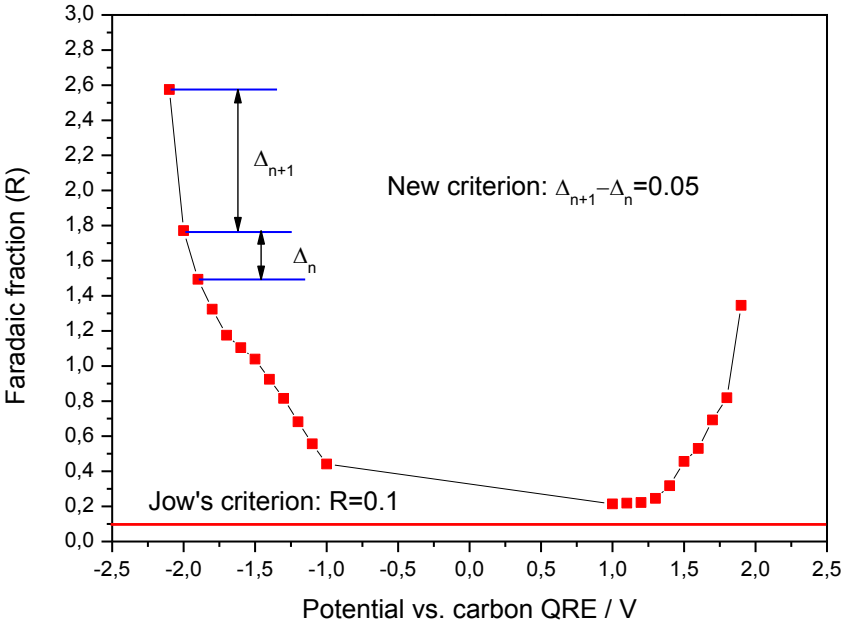


Figure 61. Faradaic fraction under various potentials and two different criteria of determining ESW of an electrolyte.

Table 10. Faradaic fraction (R), Δ_n and $\Delta_{n+1} - \Delta_n$ at different potentials.

Potential vs. carbon / V	Faradaic fraction (R)	Δ_n	$\Delta_{n+1} - \Delta_n$
1.8	0.81858	0.12641	0.4008
1.7	0.69217	0.16204	-0.03563
1.6	0.53013	0.07399	0.08805
1.5	0.45614	0.1384	-0.06441
1.4	0.31774	0.07192	0.06648
1.3	**0.24582**	**0.0234**	**0.04852**
1.2	0.22242	0.004	0.0194
1.1	0.21842	0.00464	-0.00064
1	0.21378		
-1	0.44107		
-1.1	0.55658	0.11551	0.01009
-1.2	0.68218	0.1256	0.00739
-1.3	0.81517	0.13299	-0.02381
-1.4	0.92435	0.10918	0.00544
-1.5	1.03897	0.11462	-0.04982
-1.6	1.10377	0.0648	0.00679
-1.7	**1.17536**	**0.07159**	**0.07693**
-1.8	1.32388	0.14852	0.02131
-1.9	1.49371	0.16983	0.10757
-2	1.77111	0.2774	0.52658

By following the criterion of $\Delta_{n+1} - \Delta_n = 0.05$ as limitation, test cells with five different mass ratios have been assembled and tested by GCPL technique with current density of 1 A/g for 1500 cycles. Full cell voltages are 3 V and 3.25 V, respectively. Different mass ratios lead to different potential limit values during cycling and also different faradaic fractions in both positive and negative regime.

A new concept called “Total faradaic fraction” has been introduced in this dissertation and was defined simply as the sum of both positive and negative faradaic fractions.

Figure 62 shows the plot of capacitance loss versus cycling number for capacitor cells in five different configurations. All cells exhibit relatively high capacitance losses (~10 to 20%) after only 1500 cycles which should be rather light load for EDLCs. However, one has to consider that all the test cells assembled in this study used the simple Swagelok type cell which is surely not comparable to the commercial ones using pouch or cylindrical cell configurations. Faradaic reactions happened during the cycling tests and the extent of capacitance loss should be correlated with the total faradaic fraction values of individual cell configurations.

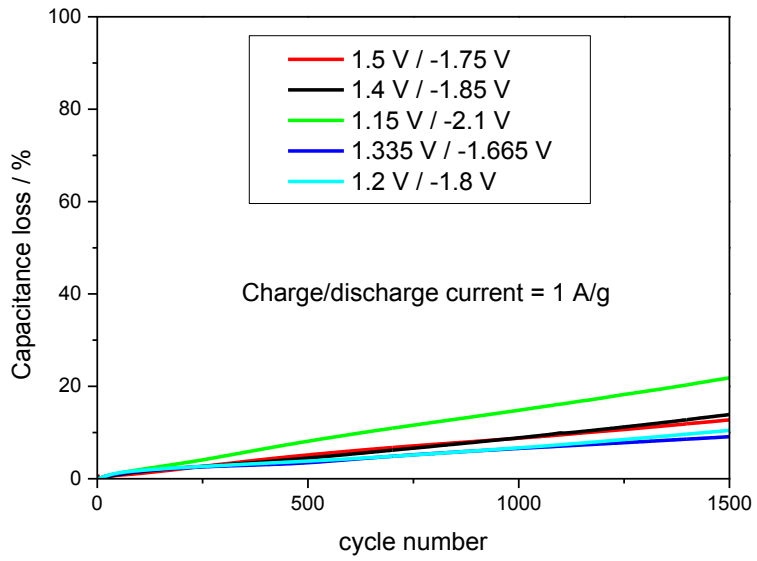


Figure 62. Capacitance losses of EDLCs with different operating voltages after 1500 cycles.

In Figure 63, the Relationship between total faradaic fraction and capacitance loss after cycling has been plotted. It is clearly observed that the cells which have higher total faradaic fractions show also higher capacitance losses after cycling. This result is very logical because higher faradaic fraction indicates stronger redox reactions at the interface electrode-electrolyte and this contributes negatively on the total capacitance of the cell.

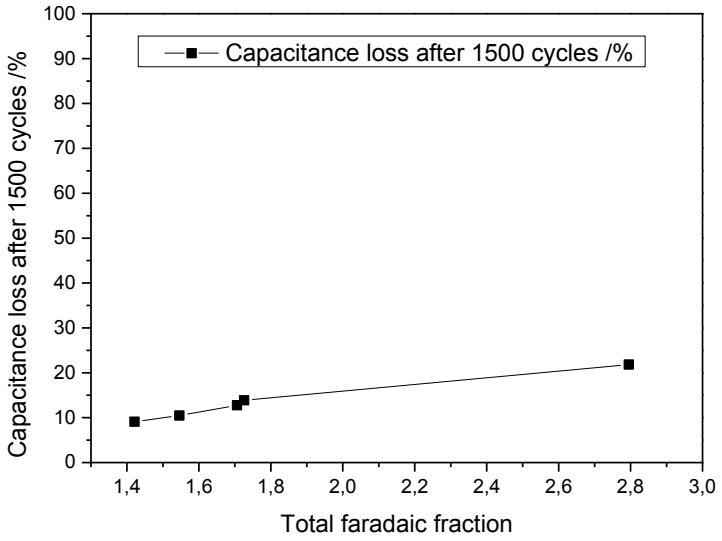


Figure 63. Relationship between total faradaic fraction and capacitance loss after cycling.

In order to get an overview, Table 11 summarizes all the relevant results and data discussed in this section. One could obtain clear idea about the influence of positive/negative electrodes mass ratios on the electrochemical stability of capacitor cells. If one wants to assemble a capacitor with relatively low capacitance loss after long term cycling, configuration A is the most suitable option.

Table 11. Summary of the experimental results from investigation of the relation between mass ratio and capacitance loss.

Configuration	**A**	B	C	D	E
Mass ratio m_+/m_-	**1.086**	1.307	1.016	1.151	1.591
Positive potential limit (V vs. Carbon)	**1.335**	1.200	1.500	1.400	1.150
Negative potential limit (V vs. Carbon)	**-1.665**	-1.800	-1.750	-1.850	-2.100
Total cell voltage (V)	**3**	3	3.25	3.25	3.25
Positive faradaic fraction	**0.271**	0.222	0.456	0.317	0.22
Negative faradaic fraction	**1.150**	1.324	1.250	1.409	2.575
Total faradaic fraction	**1.421**	1.546	1.706	1.726	2.795
Capacitance loss after 1500 cycles (%)	**9.102**	10.464	12.749	13.886	21.846

6. Results and discussion part II: Effects of electrode active materials

Within the framework of this dissertation, six carbonaceous materials have been tested as active components for EDLC electrodes. SEM pictures are shown in Figure 64. Except the high capacitance carbon black CB, all the other five activated carbons exhibit similar morphology and particle size. The carbon CB has much smaller particle size and the particles tend to join together and form aggregates.

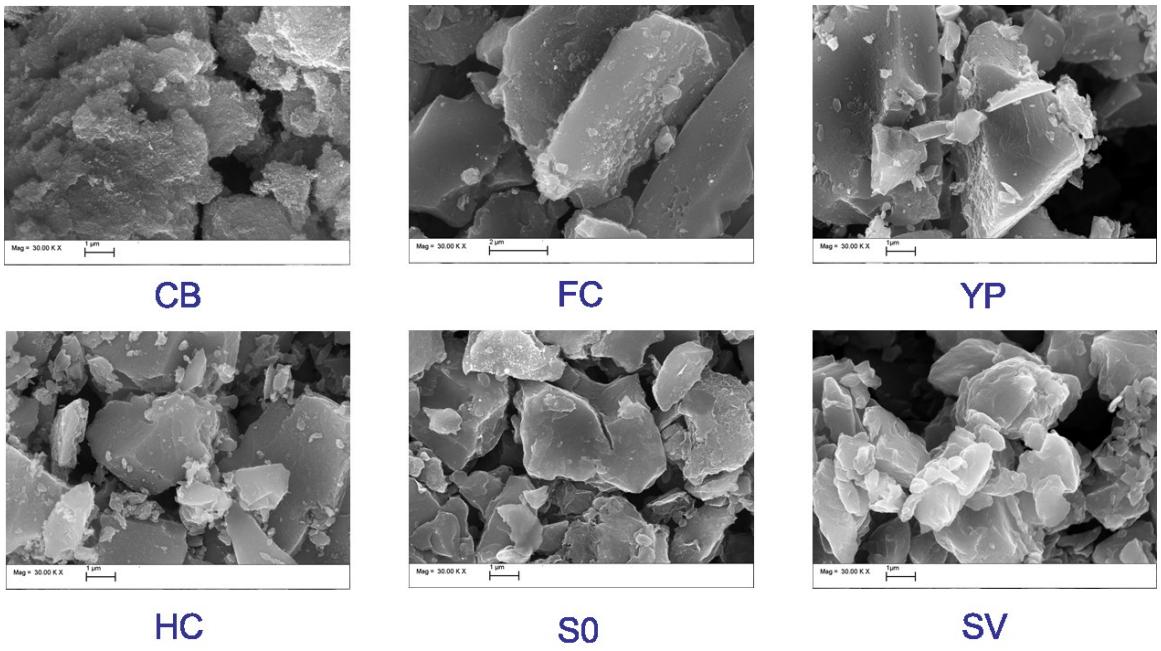


Figure 64. SEM photos of six carbon materials.

All six carbons have been firstly characterized by N_2 and CO_2 adsorption technique. Then the electrodes made from them were electrochemically tested in order to find reasonable correlations between the physical properties of the

porous carbons and the electrochemical performances of the corresponding electrodes.

6.1 PHYSICAL PROPERTIES AFFECTING HIGH ENERGY PERFORMANCE

Referring to the formula $E = 1/2CV^2$, the energy density of the electrode is proportional to the specific capacitance of the active material which is generally believed to be determined by the porous properties of the carbons (e.g. specific surface area, pore size distribution). Therefore the carbons have been firstly characterized by gas adsorption measurements.

Figure 65 shows the comparison among the N_2 adsorption and desorption isotherms of six carbonaceous materials. According to the IUPAC classification, the carbon CB shows typical Type IV isotherm behavior and this is an indication of its mesoporous nature. The carbon FC exhibits a hybrid shape of Type I and Type IV which is sign of coexistence of meso- and micropores. The rest four carbons (S0, YP, HC and SV) all show typical Type I behavior due to their dominating proportion of micropores.

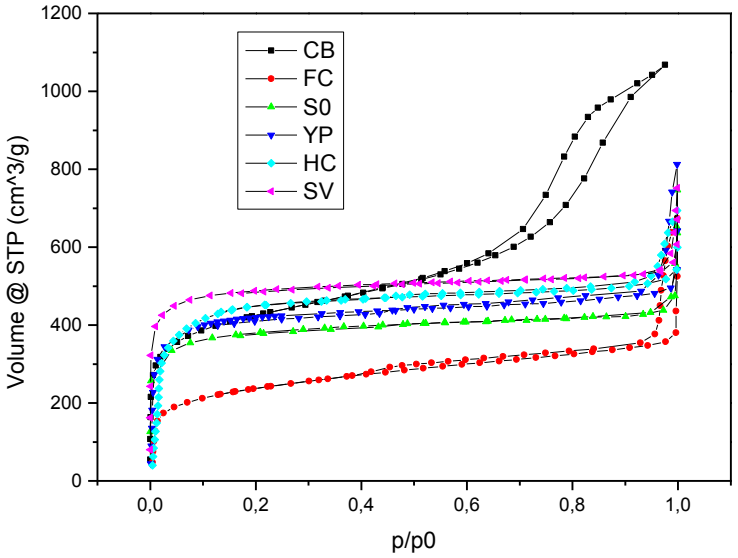


Figure 65. N_2 adsorption and desorption isotherms of six carbonaceous materials.

From the adsorption and desorption isotherms of the carbons, the BET SSA and the DFT SSA have been calculated by using the BET and the NLDFT model, respectively. And the corresponding gravimetric and volumetric capacitance values of the carbon electrodes have been computed from the GCPL measurements (measurement profile shown in Figure 66, the specific capacitances are calculated from the slope of discharging curves).

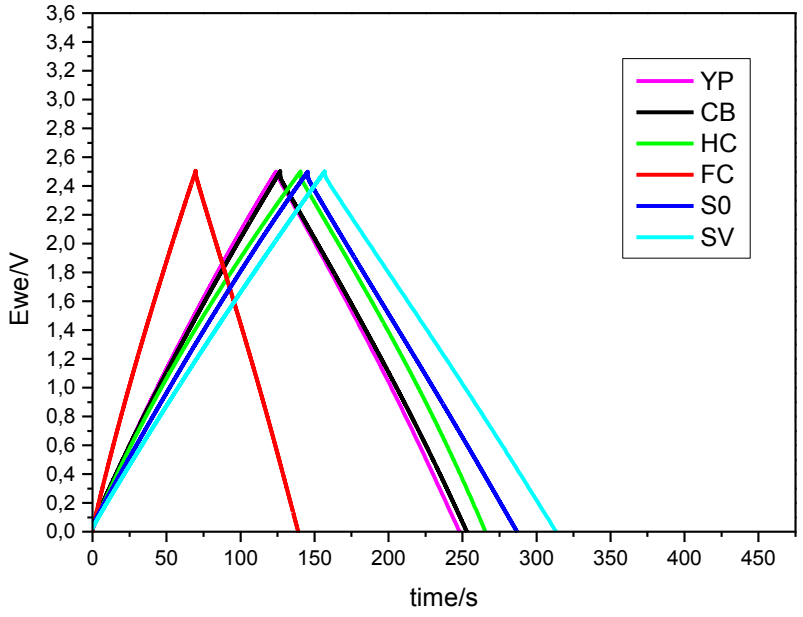


Figure 66. Charging/discharging curves of capacitor cells based on six carbonaceous materials. Cycling current density = 1 A g^{-1}.

The results of specific capacitances are summarized below in Table 12.

Table 12. Specific gravimetric and volumetric capacitance of the six carbon electrodes derived from GCPL measurements (Cycling range: 0-2.5 V, current density = 1 A g^{-1}).

Carbon	FC	YP	CB	HC	S0	SV
C_g (F g^{-1})	59	103	108	112	118	130
C_v (F cm^{-3})	38	60	68	79	85	84

As it is widely recognized, the SSA value of a carbon is relevant to its specific capacitance, no matter which model is employed for the computation [91][92][93]. The group of Kötz has tested 10 carbonaceous materials including activated carbons, carbon blacks and activated novoloid fibers. The carbon samples possess various SSA values and different specific capacitances. The authors have drawn graphs of SSA vs. C_g and tried to find the correlation between them. They have observed two phenomena [93]:

1. The BET SSA values of all the carbons are generally higher than the DFT SSA values of those carbons (Figure 67).
2. For both BET and DFT models, the specific capacitance of the carbons increase with the SSA before it reaches a certain value (about 1500 m^2 g^{-1} for BET SSA and 1200 m^2 g^{-1} for DFT SSA). After this point the capacitance fluctuates rather gently despite of considerable variation of SSA values (Figure 67).

The first phenomenon has been also confirmed from other research groups, they concluded that using the BET model for high surface carbon material leads to overestimation of the SSA [94][95].

About the second phenomenon the authors suggested a possible reason related to the space constriction of charge accommodation inside the pores. Large specific surface area leads to narrow pore walls, when the wall width becomes too thin, the ions inside two adjacent pores repel each other and this makes it more and more difficult for new ions who want to diffuse into the pores. As an end effect the specific capacitance of a carbon reaches a plateau ignoring the increasing specific surface area values [93].

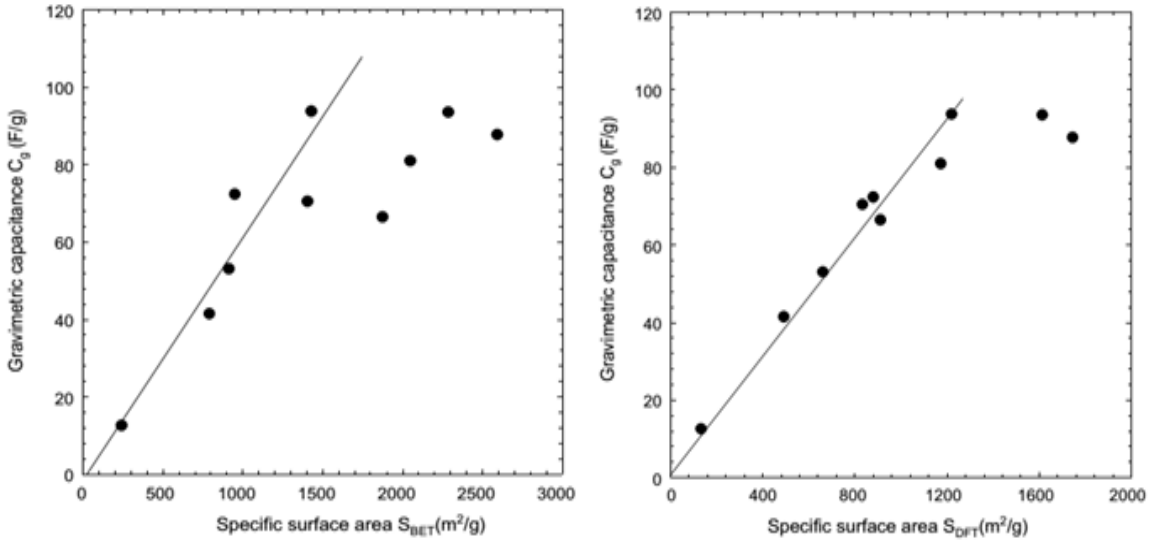


Figure 67. Relationship between specific surface area of carbon and gravimetric capacitance of electrode [93].

In this dissertation, the BET SSA and DFT SSA values of six carbonaceous materials have been obtained and plotted against their gravimetric capacitance values (see Figure 68 and Figure 69). Very similar trends as in the results from Kötz's group have been observed. The BET SSA values of all carbons are bigger than their DFT SSA values; increasing specific surface area values lead to increasing specific capacitance values. However, a plateau in the high SSA

region is not present in our case. This may probably be due to the lack of ultra-high SSA carbons within the framework of this study. Furthermore, the carbons tested in this study show generally higher gravimetric capacitance than the ones characterized by the Kötz's group. This phenomenon is considered to be an effect from the pore size distribution (PSD) of the tested carbons. However, as the results from Kötz's group do not include the PSD data, this statement is still remaining hypothetical.

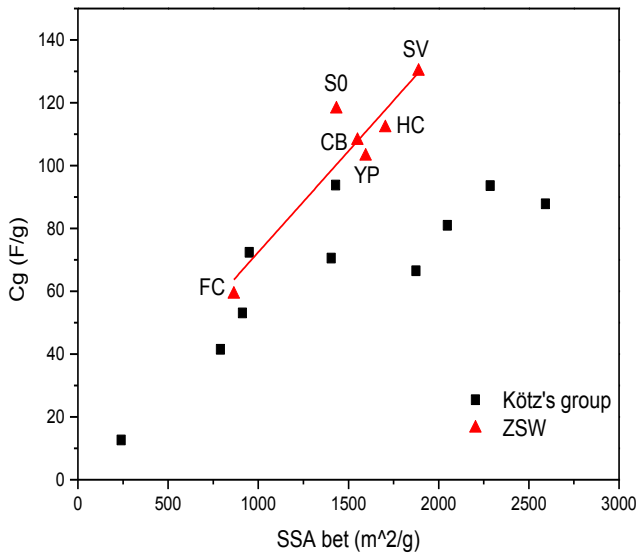


Figure 68. Relationship between BET SSA and gravimetric capacitance of the carbonaceous materials tested at ZSW and Kötz's group [93].

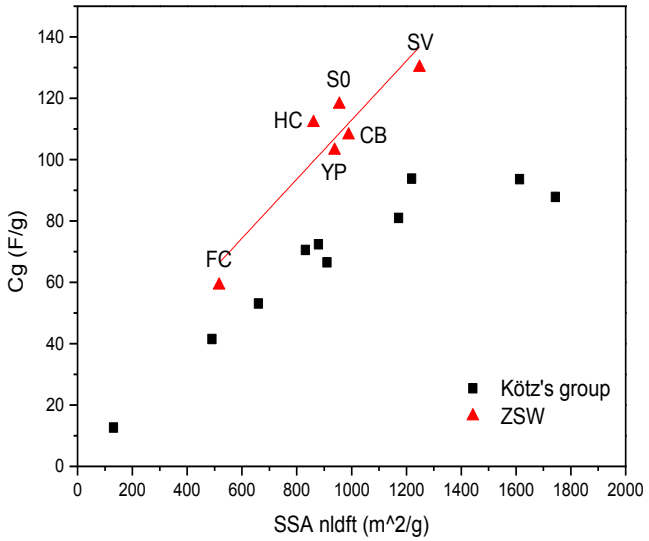


Figure 69. Relationship between DFT SSA and gravimetric capacitance of the carbonaceous materials tested at ZSW and Kötz's group [93].

The pores of carbon materials are generally divided into three categories: micropores (< 2 nm), mesopores (2 – 50 nm) and macropores (> 50 nm). Several research groups have reported that the pore size distribution of a carbon material plays essential role on determining the specific capacitance. In the case of meso- and macropores, the PSD of a carbon does not have so much impact because the pores are generally much bigger than both the naked electrolyte ions and the solvated electrolyte ions which can diffuse freely into the pores and be adsorbed on the pore walls. However, in the microporous regime, the situation can be much more complicated. Before 2006, it was considered that the solvated ions that have larger size than the pores were not able to enter the pores. Removal of the solvation shells and naked ions insertion into the smallest pores were considered to be negligible [96]. The carbon manufacturers were at that time mainly working on optimization of the pores that have sizes larger than 1 nm.

This might be the reason why the carbons tested in this study have generally higher specific capacitance than the ones characterized by Kötz's group.
However, in 2006 the groups of Gogotsi and Béguin have performed systematic study on various carbonaceous materials with different pore size distribution in common aqueous and organic electrolytes [97][36]. They have found out that it is possible for electrolyte ions to enter small pores with strongly distorted or even partially removed solvation shells. As consequence, a greatly increase of specific capacitance can be observed due to decreased distance between the ion center and the pore wall (see Figure 70, referring to the formula $C = \varepsilon_0 \varepsilon_r \frac{A}{d}$) [97].

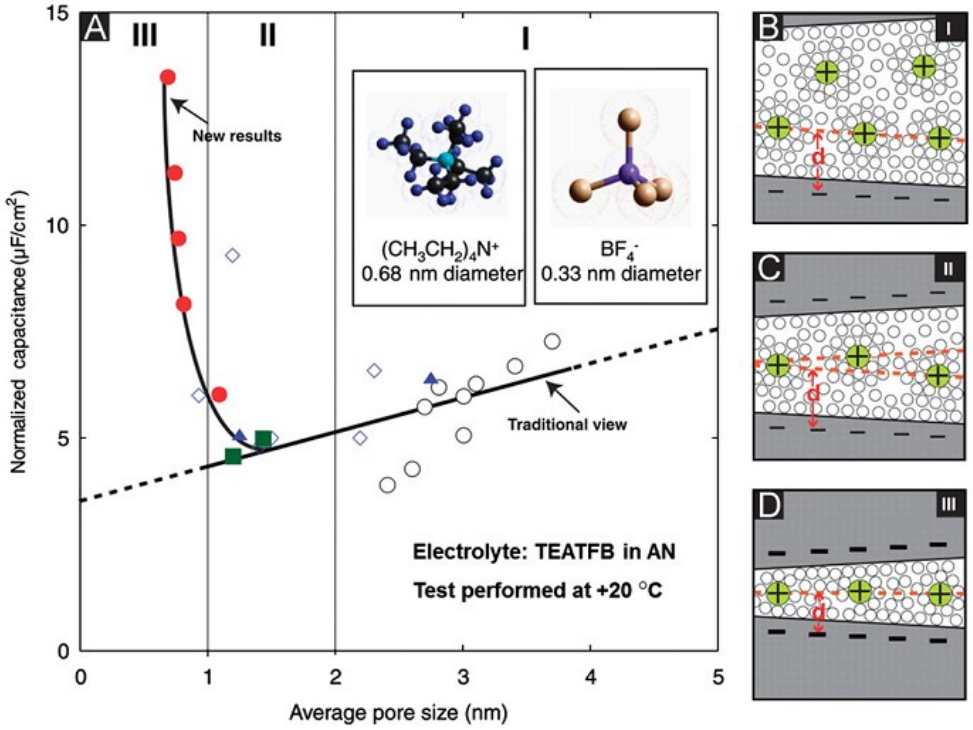


Figure 70. Effect of pore size on the area specific capacitance for the carbons in $TEABF_4$-based electrolyte, adapted from [97]: (A) The normalized capacitance increases in sub-nm pores; (B to D) schematic illustration of solvated ions in pores with distance between adjacent pore walls (B) > 2 nm, (C) 1 nm - 2 nm, and (D) < 1 nm.

Moreover, after further deeper investigation from several research groups, it was concluded when the pore size distribution of the carbons matches the size of the naked and solvated electrolyte ions, a maximum specific capacitance can be achieved [98][99][100][101].

In this study, gas adsorption measurements on all six carbons have been performed with both N_2 and CO_2 gases in order to achieve optimal accuracy for the PSD patterns. It has been observed that almost all six carbons show PSD in some narrow regions with certain pore width values which can be found in Figure

71 as 0.35 nm, 0.6 nm, 0.8 nm, 1.05 – 1.2 nm and 2 nm. The results are not surprising at all. Because the sizes of the mostly used electrolyte ions and the solvated configuration of them locate exactly in vicinity (see Table 13). Starting from around 2 nm, the pores are already able to accommodate freely the most naked as well as solvated ions.

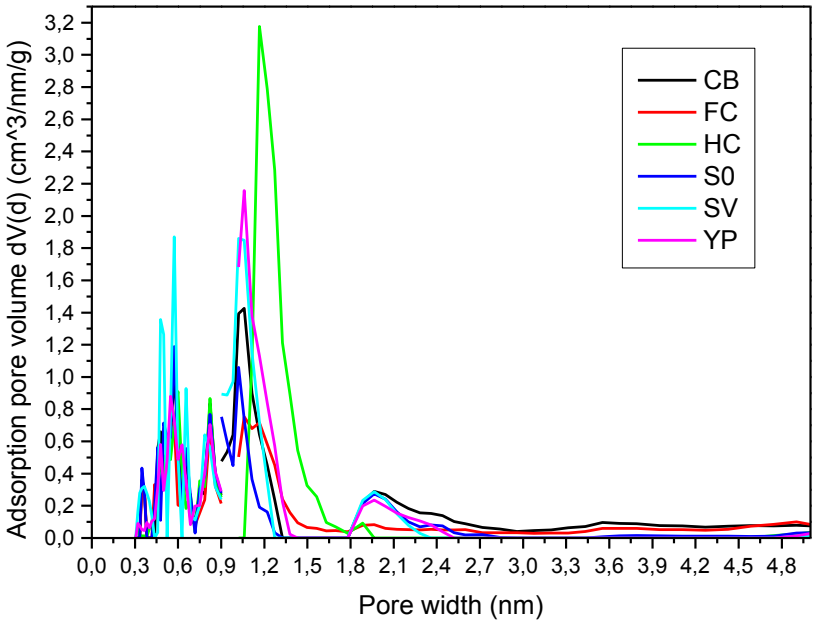


Figure 71. Pore size distribution patterns of six carbonaceous materials obtained from both N_2 and CO_2 adsorption measurements. The model used for computation was based on NLDFT.

Table 13. Comparison between the pore sizes of the carbon materials tested in this study and the sizes of the most commonly used ions [97][101].

Pore size (nm)	0.35	0.6	0.8	1.05 – 1.2
Ion Size (nm)	0.33 (BF_4^-)	0.68 (TEA^+)	0.7 – 0.8 (Ionic liquids like EMI^+ and $TFSI^-$)	~ 1 (Solvated ions of BF_4^- and TEA^+)

Furthermore, it was also possible to separate the capacitance contribution from microporous surfaces and external (meso- and macroporous) surfaces. Hang Shi has proposed in 1995 a simple model to describe the individual capacitance contribution from the above mentioned two types of surfaces [102]:

$$C = C_{micro} \times S_{micro} + C_{ext} \times S_{ext} \quad (22)$$

This formula can be easily transformed into:

$$\frac{C}{S_{ext}} = C_{micro} \times \frac{S_{micro}}{S_{ext}} + C_{ext} \quad (23)$$

By employing this formula and plotting $\frac{C}{S_{ext}}$ against $\frac{S_{micro}}{S_{ext}}$, C_{micro} and C_{ext} can be deducted from linear regression. This is a well-recognized method and has been used widely by plenty of research groups. Ito et al. have prepared cypress charcoals with different conditions and tested them as active materials for EDLCs. They have found out that the capacitance contribution from external surfaces was bigger than that from microporous surfaces [103]. Furthermore, Wang et al. have characterized EDLCs which employed phenol resin carbon spheres prepared under different conditions as electrode active materials. What they have observed was similar as the results from Ito et al.'s study [104].

In this study, the S_{micro} and S_{ext} values have been calculated by help of the T-method and a plot of $\frac{C}{S_{ext}}$ versus $\frac{S_{micro}}{S_{ext}}$ has been drawn in Figure 72 [70]. A

good linear fit can be obtained with R^2 = 0.963 which indicated above-average fitting quality. The values of C_{micro} and C_{ext} have been obtained from the intercept and slope of the linear fit as 0.0667 F m^{-2} and 0.0903 F m^{-2}. It is logical that C_{ext} is higher than C_{micro} because the electrolyte ions can easier get adsorbed on external surfaces in comparison to microporous surfaces [103][104].

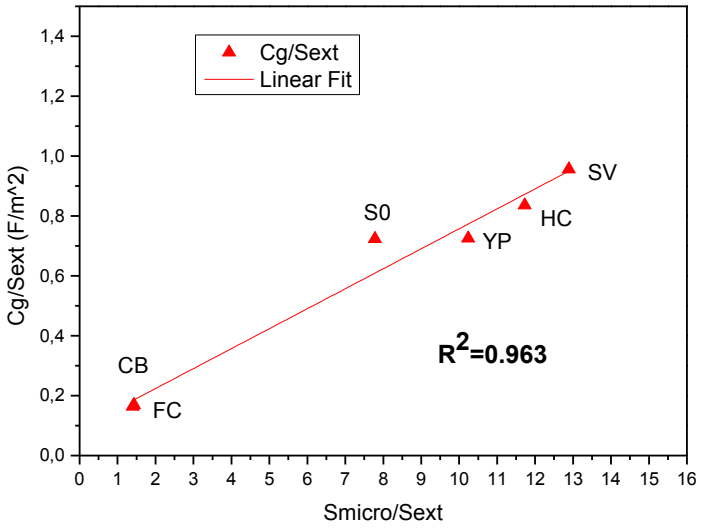


Figure 72. Linear fit of $\frac{C}{S_{ext}}$ versus $\frac{S_{micro}}{S_{ext}}$ for various carbonaceous materials.

In summary, we could conclude that the carbon SV and S0 have respectively the highest gravimetric and volumetric specific capacitance and are suitable for high energy applications.

6.2 PHYSICAL PROPERTIES AFFECTING HIGH POWER PERFORMANCE

Recall the formula $P_{max} = V^2/4R$, the power density of a supercapacitor is affected by its operating voltage and the impedance of the cell. The operating voltage is normally determined by the stability of the electrolyte and is not the focus of this part of study. However, the impedance of the cell is mainly controlled by the electrode active material and has been studied in depth.

6.2.1 Electrical conductivity and resistivity of carbon electrodes

Electrical conductivity of a carbon electrode influences greatly its power performance. In order to achieve high power output, the conductivity has to be as high as possible. For porous carbon materials, the sp^2 hybrid carbon sites are mainly responsible for electronic transport properties [105]. The more sp^2 carbon sites the material has, the higher conductivity it shows. In this study, the electrical conductivity of six porous carbonaceous materials including five activated carbons and one high capacitance carbon black have been measured (results shown below in Table 14).

The electrode made from high capacitance carbon black CB shows dominantly the highest conductivity due to the small particle size and excellent inter-particle contact of this material [84]. On the other hand, the electrodes from five activated carbons exhibit electrical conductivity in similar range; among them, the electrode from carbon YP has the lowest conductivity and also the highest resistivity. As the electrical conductivity of an activated carbon is determined by numbers of factors such as the particle size, the porosity, the surface functionality and even impurities etc., it was not possible to identify in detail the factors which lead to the close differences on conductivity among all five activated carbons. However, the experimental results from impedance spectroscopy verified the data obtained from electrical conductivity measurements (Figure 73).

Table 14. Electrical resistivity and conductivity of electrodes prepared from six different carbons.

Carbon	YP	HC	FC	SV	S0	CB
Resistivity (Ω cm)	8344	2668	2333	2024	1022	18.73
Conductivity (S cm^{-1})	1.2×10^{-4}	3.75×10^{-4}	4.29×10^{-4}	4.94×10^{-4}	9.78×10^{-4}	5.34×10^{-2}

In the Nyquist plot of a capacitor cell, the semicircle comes from inter-particle contact and particle-current collector contact (see Figure 26). In Figure 73, the electrode from carbon YP is the one who shows the biggest semicircle. This result echoes with its poor electrical conductivity obtained from the resistance measurement. Furthermore, the electrode made from carbon HC has the second biggest semicircle in Nyquist plots and also the second poorest conductivity.
Finally, it can be concluded that the electrode prepared by using carbon CB has the highest electrical conductivity and is suitable for high power applications.

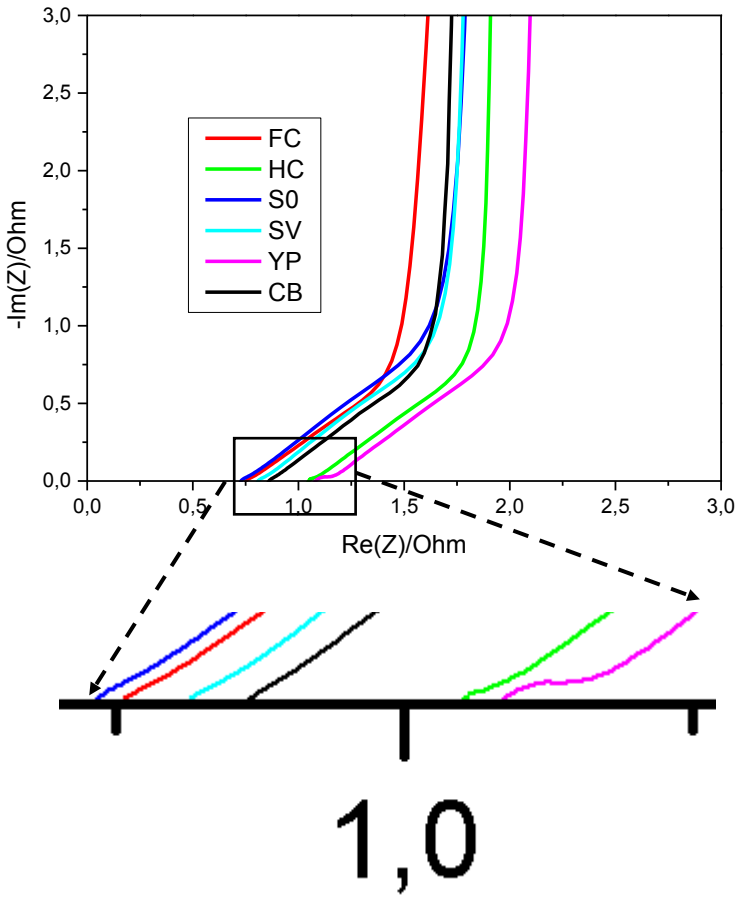


Figure 73. Nyquist plots of fresh capacitor cells using different carbon materials and a zoom-in of the semicircles.

6.2.2 Effects of mesoporous structure of carbon materials

Besides electrical conductivity, the diffusion capability of a carbon material is even more important for the high power performance of an EDLC. It is widely recognized that the mesopores in carbon materials play essential role on influencing the electrolyte diffusion behavior [42]. Therefore it has been also tried to find correlation between mesoporous fraction and diffusion resistivity. As already explained in the experimental chapter, the diffusion resistivity of capacitor

electrodes has been calculated from the electrochemical impedance spectra. The surface mesoporous fraction (external surface consists mainly of mesoporous surfaces, the macroporous part is negligible) has been obtained from the T-method.

It can be observed from Figure 74 that generally the carbons that have higher mesoporous surface fraction show lower diffusion resistivity. This is in consistence with the results obtained from most researchers.

Furthermore, a plot of diffusion resistivity versus mesoporous volume proportion has been drawn in Figure 75. The mesoporous volume proportion of the carbons has been obtained from the T-method and the last adsorption point on their isotherms.

The same trend as in Figure 74 could be observed. Higher mesoporous volume proportion of a carbon leads to lower diffusion resistivity of the electrode.

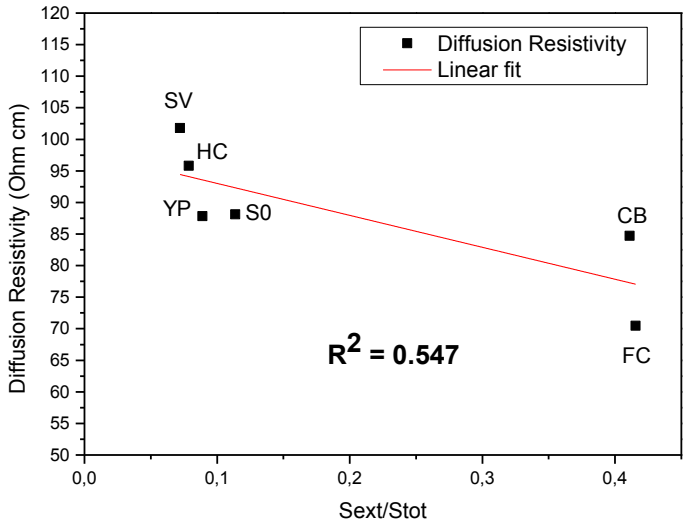


Figure 74.Relationship between diffusion resistivity and external surface proportion of six carbon materials.

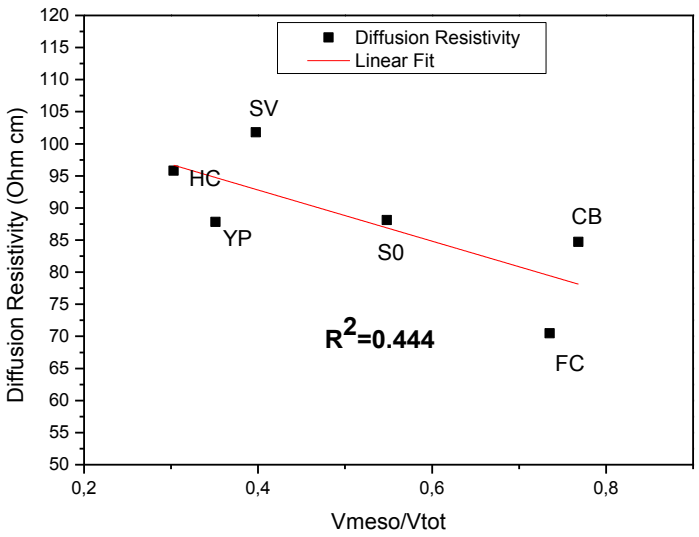


Figure 75. Relationship between diffusion resistivity and mesoporous volume proportion of six carbon materials.

Many research groups have reported decrease of the cell specific capacitance upon increasing cycling current rate [104] [106] [103].

In this dissertation, capacitor cells made from six different carbon materials have been cycled between 1 A g^{-1} to 8 A g^{-1}. A Ragone plot (energy density vs. power density) can be drawn based on the experimental results of the charge/discharge measurements (Figure 76). The energy density has been calculated by the equation:

$$\mathbf{E_m = \frac{I \cdot \int V dt}{m}} \qquad (24)$$

where I is the discharging current, V is the discharging voltage, t stands for the discharging time and m is the mass of the active material.

The power density is simply obtained as $P_m = \frac{E_m}{t_{discharge}}$.

All capacitor cells show excellent rate capability, their energy density decreased only limited amount (see Table 15) when the discharging power has been increased for 8 times. Among all of them, the cell based on CB material shows the highest energy retention with elevated power output. Therefore this carbon is considered to be a good option for high power applications.

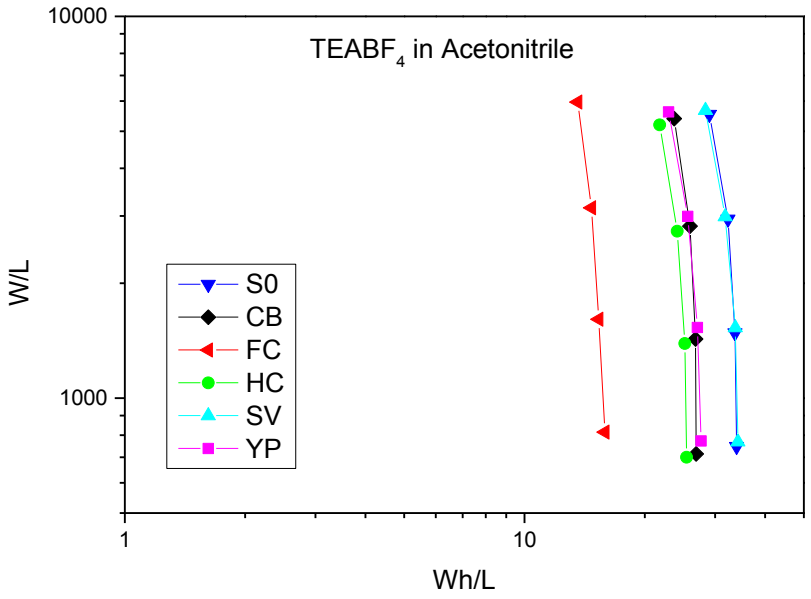


Figure 76. Ragone plots (energy density vs. power density) of EDLC cells made from six carbon materials.

Table 15. Energy retention of EDLC cells prepared from six carbonaceous materials.

Carbon	SV	YP	S0	FC	HC	CB
Energy retention (%) $E_{8A/g}/ E_{1A/g}$	82.91	82.94	85.49	85.51	85.69	88.08

Besides cycling the capacitor cells at various specific current, one could also analyze the EIS curves in order to compare the high frequency performances among all the electrodes.

The group of Chen has investigated three carbons with different mesopore fractions. They have employed EIS techniques and found out that at 1 Hz of testing frequency, the carbons that have higher mesopore fractions showed also higher specific capacitance values [107]. This result could be easily obtained by plotting C' against Frequency by help from the formula $C' = \frac{-Im(Z)}{\omega \cdot |Z|^2}$, in which C' is the real capacitance, $Im(Z)$ is the imaginary part of the impedance, ω is the angular frequency and $|Z|$ stands for the modulus of the impedance. However, we consider it as unfair to compare the absolute values of specific capacitance of the carbons at a certain high frequency. This is because in low-frequency regime the carbons have considerably heterogeneous capacitance values, but in high frequency regime the cells all show very similar specific capacitance which makes it actually very difficult to scientifically distinguish the six carbons. Therefore a new concept called "$C'retention$" was proposed and defined as

$$C'\,retention = \frac{C' @ 1Hz}{C' @ 0.01Hz} \quad (25)$$

With the help of this concept, it was possible to realistically assess the high power performance of the six carbons.

The plot of C' vs. frequency was drawn in Figure 77. The specific capacitance values of the carbons follow similar sequences as what were obtained from

galvanostatic cycling experiments. From this graph, the values of $C'retention$ have been easily calculated and plotted against the mesoporous volume proportion of the six carbon materials in Figure 78.

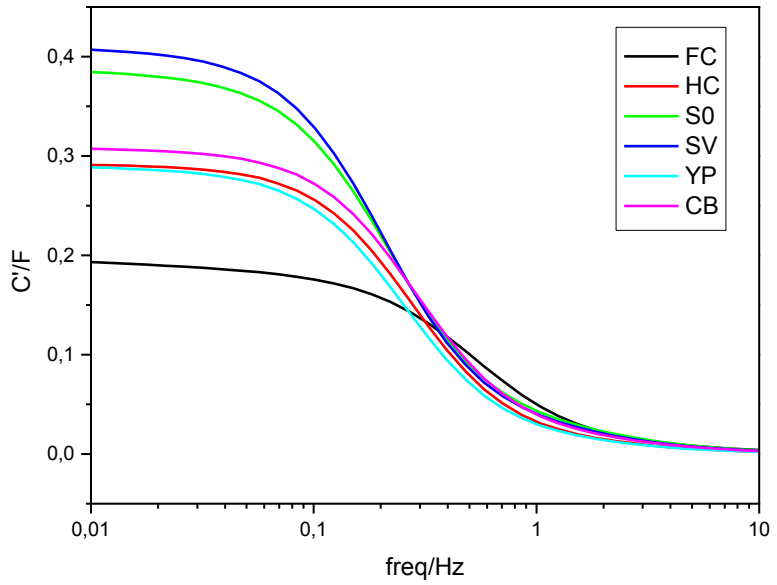


Figure 77. Plot of specific capacitance versus testing frequency, derived from EIS measurements.

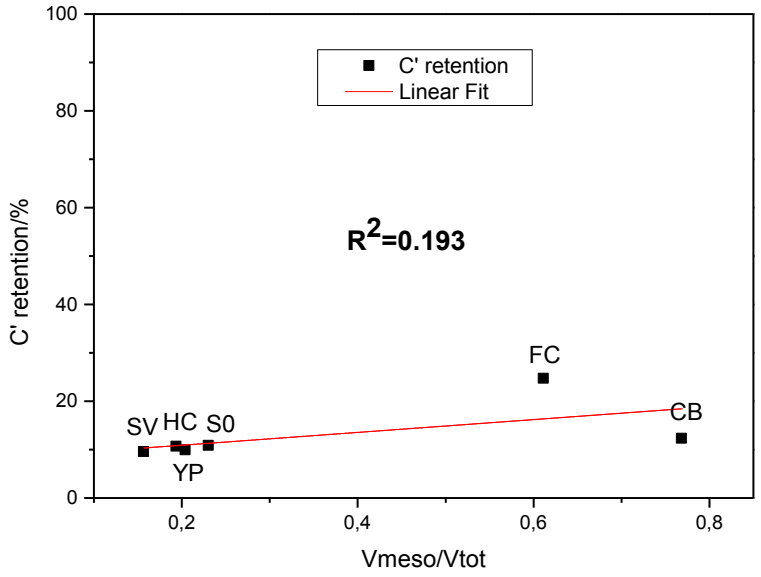


Figure 78. Plot of C' retention against mesoporous volume fraction of six carbon powders.

Although the fitting factor R^2 obtained was relatively small, a clear trend could still be observed. Higher mesoporous volume fraction leads to higher $C'retention$ of the capacitor cells. This result was exactly as what has been expected and the possible reason is explained below.

When the capacitor cells were tested by EIS with increasing frequency, it became more and more difficult for the pores to accommodate the fast moving electrolyte ions. For mesopores which have pore size bigger than 2 nm, the situation is not that critical as that for micropores, especially the pores which have size smaller than 1 nm. If the adsorbed ions inside the pores became less and less, the capacitance of the cell would correspondingly experience gradual descent.

Moreover, a plot of C' retention against mesoporous volume fraction of all electrodes is shown in Figure 79. It is quite similar as the plot obtained for the pure carbon powder and the linear fitting has better quality than the results obtained with the pure powder. This is obviously an indication stating that the physical characterization results of ready electrodes can be well correlated with the results from electrochemical tests. In the case of carbon powders, the correlation is not that strong. Generally we come to the conclusion that higher mesoporous fraction leads to better capacitance retention of the cell under high frequency tests.

In the end, by considering the results from conductivity measurements and electrochemical measurements, the carbon CB is considered to be the most suitable candidate for high power applications.

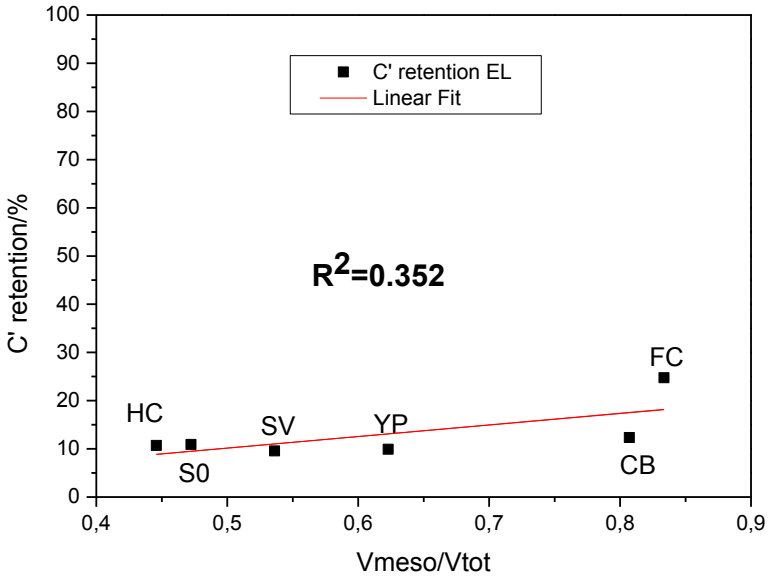


Figure 79. Plot of C' retention against mesoporous volume fraction of electrodes made from six carbon materials.

7. Conclusion and outlook

7.1 Conclusion

At the beginning of this dissertation, two main goals have been proposed as the main tasks. They can be summarized as electrode preparation and selection of active materials for EDLCs in different application fields. After deep investigation on these topics, the main results are concluded in following paragraphs.

7.1.1 Improvement of electrode preparation

Within the framework of this dissertation, the key point of investigation was controlling and limiting the resistance sources by optimizing the electrode preparation process.

By employing electrochemical impedance spectroscopy, it was possible to separate the contribution of various impedance sources. This dissertation has concentrated on decreasing the interface contact resistance (interparticle and particle-Al current collector) and the diffusion resistance.

There are several methods available to lower the interface contact resistance of the carbon electrodes. First of all, the resistance can be adjusted during the electrode preparation. The choice of the processing condition is of fundamental importance for achieving low contact resistance.

For typical lab scale, a hot-pressing procedure has been employed to provide proper interface contact to the electrodes. Two processing parameters of the hot-press method (temperature and pressure) have been properly modulated. Good adhesion between carbon electrode and Al foil has been reached by using a temperature of 160°C and pressing the electrode at 50 bar.

For larger scale (~40 times bigger than the lab scale) a lamination process has been used to improve the interface contact. The rolling force of the laminator has been considered as the most important parameter and optimized as 300 kgf. The

large electrode prepared by this method exhibits only slightly higher ESR value as that of the hot-pressed electrode.

Secondly, in the electrode recipe one can add conductive agent (e.g. carbon black) to provide more electron pathways and lower the contact resistance. However, the completely dry method developed in this work provides really optimized interparticle contact for electrodes and the addition of carbon black becomes rather unnecessary.

Moreover, the diffusion resistance of electrolyte inside the porous structure of carbons can be decreased by three techniques: optimizing electrode preparation techniques, adjusting the electrode recipe and selecting proper active materials with optimized pore size distribution.

In case of the hot-pressing process, the SEM image analysis revealed that the electrode porosity and thus the electrolyte diffusion are reduced if the electrode is treated at very high pressure. This drawback can be easily solved by increasing the working temperature up to 200 °C and consequently decreasing the pressure to 10 bar. These conditions are sufficient for reaching a good electrode adhesion and at the same time maintaining good electrode porosity.

In case of the lamination process, similar SEM image analysis has shown that the rolling force of the laminator is not strong enough to alter the microstructure and morphology of the carbon electrodes. Therefore one does not have to find an optimized value of the rolling force in order to maintain proper porosity of the electrodes.

Furthermore, the electrode preparation recipe plays also significant role on influencing porosity of the electrodes. Normally in EDLC electrodes, two additives (conductive agent and binder) are employed to improve the performance. Results from this thesis showed that the carbon black content influenced little the diffusion capability of the porous electrodes. On the other hand, the PTFE binder content is really important to facilitate a good electrolyte transport in the pores of

the electrodes. 5% of PTFE binder content has been found to be an optimized value.

In the end, the effects of electrode mass ratio have been studied as well. A ratio of m_+/m_- =1.086 has been proved to be the best choice to ensure a relatively good long term cycling stability. Cells assembled by following this ratio lost 9.1% of their original capacitance after 1500 charging/discharging cycles at 1 A g^{-1} with 3 V cell operating voltage.

7.1.2 Selection of proper carbons as EDLC active material for various applications

Six different carbonaceous materials have been physically and electrochemically characterized and compared with each other.

First of all, N_2 and CO_2 gas adsorption tests have been performed on all six carbons as powder and as electrodes in order to obtain information about specific surface area, pore size distribution and micro- and mesopore fraction. Furthermore, the electrodes have been also electrically and electrochemically characterized by resistivity measurement, cyclic voltammetry, electrochemical impedance spectroscopy and galvanostatic cycling tests. After analysis of the experimental results, good correlation between physical and electrochemical properties of the carbon materials has been found. Generally higher specific surface area brings higher specific capacitance under the condition that the carbon has proper pore size distribution which means the micropores should be distributed exactly at the sizes where the electrolyte ions also sit. Within the framework of this dissertation, the carbon SV has the highest gravimetric specific capacitance of 130 F g^{-1} and the carbon S0 has the highest volumetric specific capacitance of 85 F cm^{-3}.

Furthermore, the properties of the carbons greatly influence also the power density. The mesopores have been proved to be of essential meaning for the

electrolyte transport. The higher mesopores fraction the carbon has, the lower its diffusion resistivity is and the better the diffusion behavior is. Consequently, the better its power performance is. In this work, the carbons CB and FC have the highest mesopores portion. However, considering that the carbon CB has the highest electrical conductivity, it can be considered to be the best candidate for high power application.

In summary, the research results from this dissertation have provided important contribution for optimization of both energy and power performances of electrochemical double layer capacitors.

7.2 Outlook

As mentioned before, electrochemical stability of the employed electrolyte is the main influencing factor on operating voltage of the capacitor cell which plays decisive role on determining its energy density. In next works, one could try electrolytes like ionic liquids which are electrochemically more stable than most organic electrolytes in order to build an EDLC with high operating voltage and consequently high energy density.

Furthermore, one could also bring lithium insertion materials and carbonaceous materials together in one capacitor cell and build hybrid capacitors which can benefit from the high energy density of lithium insertion materials and great power capability of carbon materials at the same time. However, in this case the performance of carbon electrodes in Li containing electrolyte (e.g. $LiPF_6$ in carbonate solvent) has to be firstly investigated in detail (especially the long term cycling stability).

Bibliography

[1] International Energy Agency, “World Energy Outlook 2013,” Nov. 2013.

[2] D. Stover, “The myth of renewable energy,” *Bulletin of the Atomic Scientists*, Nov-2011.

[3] M. Winter and R. J. Brodd, “What are batteries, fuel cells, and supercapacitors?,” *Chem. Rev.*, vol. 104, no. 10, pp. 4245–69, Oct. 2004.

[4] P. Simon and Y. Gogotsi, “Materials for electrochemical capacitors.,” *Nat. Mater.*, vol. 7, no. 11, pp. 845–54, Nov. 2008.

[5] B. E. Conway, *Electrochemical Supercapacitors Scientific Fundamentals and Technological Applications*. New York: Kluwer Academic/Plenum Publisher, 1999.

[6] J. R. Miller and A. F. Burke, “Electrochemical Capacitors : Challenges and Opportunities for Real-World Applications,” *Electrochem. Soc. Interface*, 2008.

[7] A. G. Pandolfo and A. F. Hollenkamp, “Carbon properties and their role in supercapacitors,” *J. Power Sources*, vol. 157, no. 1, pp. 11–27, Jun. 2006.

[8] “Homepage of Maxwell Technologies.” [Online]. Available: http://www.maxwell.com. [Accessed: 17-Feb-2014].

[9] B. Xu, S. Hou, H. Duan, G. Cao, M. Chu, and Y. Yang, “Ultramicroporous carbon as electrode material for supercapacitors,” *J. Power Sources*, vol. 228, pp. 193–197, Apr. 2013.

[10] J. C. Ellenbogen and M. S. Halper, “Supercapacitors : A Brief Overview,” 2006.

[11] K. Naoi and P. Simon, “New Materials and New Configurations for Advanced Electrochemical Capacitors,” *Electrochem. Soc. Interface*, vol. 17, no. 1, pp. 34–37, 2008.

[12] J. P. Zheng, P. J. Cygan, and T. R. Jow, “Hydrous Ruthenium Oxide as an Electrode Material for Electrochemical Capacitors,” vol. 142, no. 8, pp. 3–7, 1995.

[13] K. Naoi, O. Nobuhiro, and I. Shuichi, “REACTION METHOD, METAL OXIDE NANOPARTICLE OR METAL OXIDE NANOPARTICLE-DEPOSITED CARBON OBTAINED THEREBY, ELECTRODE CONTAINING THE CARBON AND ELECTROCHEMICAL ELEMENT USING THE ELECTRODE,” JP 2007-160151.

[14] a. Laforgue, P. Simon, J. F. Fauvarque, M. Mastragostino, F. Soavi, J. F. Sarrau, P. Lailler, M. Conte, E. Rossi, and S. Saguatti, “Activated Carbon/Conducting Polymer Hybrid Supercapacitors,” *J. Electrochem. Soc.*, vol. 150, no. 5, p. A645, 2003.

[15] D. Cericola and R. Kötz, “Hybridization of rechargeable batteries and electrochemical capacitors: Principles and limits,” *Electrochim. Acta*, vol. 72, pp. 1–17, Jun. 2012.

[16] D. Bresser, E. Paillard, M. Copley, P. Bishop, M. Winter, and S. Passerini, “The importance of ‘ going nano ’ for high power battery materials,” *J. Power Sources*, vol. 219, pp. 217–222, 2012.

[17] A. Du Pasquier, I. Plitz, J. Gural, S. Menocal, and G. Amatucci, “Characteristics and performance of 500 F asymmetric hybrid advanced supercapacitor prototypes,” *J. Power Sources*, vol. 113, no. 1, pp. 62–71, Jan. 2003.

[18] A. Du Pasquier, I. Plitz, J. Gural, S. Menocal, G. Amatucci, and A. Du Pasquier, “A comparative study of Li-ion battery, supercapacitor and nonaqueous asymmetric hybrid devices for automotive applications,” *J. Power Sources*, vol. 115, no. 1, pp. 171–178, Mar. 2003.

[19] K. Naoi, S. Ishimoto, Y. Isobe, and S. Aoyagi, “High-rate nano-crystalline Li 4 Ti 5 O 12 attached on carbon nano-fibers for hybrid supercapacitors,” *J. Power Sources*, vol. 195, no. 18, pp. 6250–6254, 2010.

[20] H. Li, L. Cheng, and Y. Xia, “A Hybrid Electrochemical Supercapacitor Based on a 5 V Li-Ion Battery Cathode and Active Carbon,” *Electrochem. Solid-State Lett.*, vol. 8, no. 9, p. A433, 2005.

[21] J.-H. Yoon, H. J. Bang, J. Prakash, and Y.-K. Sun, “Comparative study of Li[Ni1/3Co1/3Mn1/3]O2 cathode material synthesized via different synthetic routes for asymmetric electrochemical capacitor applications,” *Mater. Chem. Phys.*, vol. 110, no. 2–3, pp. 222–227, Aug. 2008.

[22] R. Vasanthi, D. Kalpana, and N. G. Renganathan, “Olivine-type nanoparticle for hybrid supercapacitors,” *J. Solid State Electrochem.*, vol. 12, no. 7–8, pp. 961–969, Nov. 2007.

[23] D. Cericola, P. Novák, a. Wokaun, and R. Kötz, “Segmented bi-material electrodes of activated carbon and LiMn2O4 for electrochemical hybrid storage devices: Effect of mass ratio and C-rate on current sharing,” *Electrochim. Acta*, vol. 56, no. 3, pp. 1288–1293, Jan. 2011.

[24] N. Böckenfeld, T. Placke, M. Winter, S. Passerini, and a. Balducci, “The influence of activated carbon on the performance of lithium iron phosphate based electrodes,” *Electrochim. Acta*, vol. 76, pp. 130–136, Aug. 2012.

[25] Y. Lei, Z.-H. Huang, W. Shen, F. Kang, and Y. Zheng, “Bi-material anode based on porous graphitic carbon for Li4Ti5O12-PGC/LiFePO4 hybrid battery capacitor,” *Electrochim. Acta*, vol. 107, pp. 413–418, Sep. 2013.

[26] H.-T. Fang, M. Liu, D.-W. Wang, X.-H. Ren, and X. Sun, “Fabrication and supercapacitive properties of a thick electrode of carbon nanotube–RuO2 core–shell hybrid material with a high RuO2 loading,” *Nano Energy*, vol. 2, no. 6, pp. 1232–1241, Nov. 2013.

[27] X. Andrieu, “Energy storage syst,” *Electron. New Trends Electrochem. Technol*, vol. 1, p. 521, 2000.

[28] J. Garche, C. K. Dyer, P. T. Moseley, Z. Ogumi, D. A. J. Rand, and B. Scrosati, *Encyclopedia of Electrochemical Power Sources*. Newnes, 2013.

[29] M. Okamura, *Electric double layer capacitor and its charging system*. Nikkan Kogyo Shimbun, 2001.

[30] L. Zhang, R. Zhou, and X. Zhao, “Graphene-based materials as supercapacitor electrodes,” *J. Mater. Chem.*, no. 20, pp. 5983–5992, 2010.

[31] R. A. Rightmire, “Electrical energy storage apparatus,” US Patent 3288641, 1966.

[32] “DEC IMPIANTI - Activated Carbon.” [Online]. Available: http://www.decimpianti.com/dec-impianti/activated-carbon_en.html. [Accessed: 22-Jun-2014].

[33] P. Sharma and T. S. Bhatti, “A review on electrochemical double-layer capacitors,” *Energy Convers. Manag.*, vol. 51, no. 12, pp. 2901–2912, Dec. 2010.

[34] L. L. Zhang and X. S. Zhao, “Carbon-based materials as supercapacitor electrodes,” no. March, pp. 2520–2531, 2009.

[35] G. Salitra, A. Soffer, L. Eliad, Y. Cohen, and D. Aurbach, “Carbon Electrodes for Double-Layer Capacitors I. Relations Between Ion and Pore Dimensions,” *J. Electrochem. Soc.*, vol. 147, no. 7, p. 2486, 2000.

[36] E. Raymundo-Piñero, K. Kierzek, J. Machnikowski, and F. Béguin, “Relationship between the nanoporous texture of activated carbons and their capacitance properties in different electrolytes,” *Carbon N. Y.*, vol. 44, no. 12, pp. 2498–2507, Oct. 2006.

[37] C. Largeot, C. Portet, J. Chmiola, P. Taberna, Y. Gogotsi, and P. Simon, “Relation between the Ion Size and Pore Size for an Electric Double-Layer Capacitor,” *J. Am. Chem. Soc.*, vol. 130, pp. 2730–2731, 2008.

[38] V. Choudhary and A. Gupta, “Polymer / Carbon Nanotube Nanocomposites,” in *Carbon Nanotubes - Polymer Nanocomposites*, 2001.

[39] E. Frackowiak, S. Delpeux, K. Jurewicz, and K. Szostak, “Enhanced capacitance of carbon nanotubes through chemical activation,” *Chem. Phys. Lett.*, vol. 361, no. July, pp. 35–41, 2002.

[40] T. Bordjiba, M. Mohamedi, and L. H. Dao, “New Class of Carbon-Nanotube Aerogel Electrodes for Electrochemical Power Sources,” *Adv. Mater.*, vol. 20, no. 4, pp. 815–819, Feb. 2008.

[41] A. D. Roberts, X. Li, and H. Zhang, “Porous carbon spheres and monoliths: morphology control{,} pore size tuning and their applications as Li-ion battery anode materials,” *Chem. Soc. Rev.*, vol. 43, no. 13, pp. 4341–4356, 2014.

[42] E. Frackowiak, “Carbon materials for supercapacitor application.,” *Phys. Chem. Chem. Phys.*, vol. 9, no. 15, pp. 1774–85, Apr. 2007.

[43] J. Huang, B. G. Sumpter, and V. Meunier, “A universal model for nanoporous carbon supercapacitors applicable to diverse pore regimes,

carbon materials, and electrolytes.," *Chemistry*, vol. 14, no. 22, pp. 6614–26, Jan. 2008.

[44] D.-W. Wang, F. Li, M. Liu, G. Q. Lu, and H.-M. Cheng, "3D aperiodic hierarchical porous graphitic carbon material for high-rate electrochemical capacitive energy storage.," *Angew. Chem. Int. Ed. Engl.*, vol. 47, no. 2, pp. 373–6, Jan. 2008.

[45] AlexanderAIUS, "Graphene - Wikipedia." [Online]. Available: http://en.wikipedia.org/wiki/Graphene.

[46] K. S. Novoselov, a K. Geim, S. V Morozov, D. Jiang, Y. Zhang, S. V Dubonos, I. V Grigorieva, and a a Firsov, "Electric field effect in atomically thin carbon films.," *Science*, vol. 306, no. 5696, pp. 666–9, Oct. 2004.

[47] M. F. El-Kady, V. Strong, S. Dubin, and R. B. Kaner, "Laser scribing of high-performance and flexible graphene-based electrochemical capacitors.," *Science*, vol. 335, no. 6074, pp. 1326–30, Mar. 2012.

[48] S. Kannappan, K. Kaliyappan, R. ~K. Manian, A. Samuthira Pandian, H. Yang, Y. ~S. Lee, J.-H. Jang, and W. Lu, "Graphene based Supercapacitors with Improved Specific Capacitance and Fast Charging Time at High Current Density," *ArXiv e-prints*, Nov. 2013.

[49] E. Frackowiak and Q. Abbas, "Carbon / carbon supercapacitors," *J. Energy Chem.*, vol. 22, pp. 226–240, 2013.

[50] Q. T. T. Qu, B. Wang, L. C. C. Yang, Y. Shi, S. Tian, and Y. P. P. WU, "Study on electrochemical performance of activated carbon in aqueous Li2SO4, Na2SO4 and K2SO4 electrolytes," *Electrochem. commun.*, vol. 10, no. 10, pp. 1652–1655, Oct. 2008.

[51] K. Fic, G. Lota, M. Meller, and E. Frackowiak, "Novel insight into neutral medium as electrolyte for high-voltage supercapacitors," *Energy Environ. Sci.*, vol. 5, no. 2, p. 5842, 2012.

[52] A. Jänes, H. Kurig, T. Romann, and E. Lust, "Novel doubly charged cation based electrolytes for non-aqueous supercapacitors," *Electrochem. commun.*, vol. 12, no. 4, pp. 535–539, Apr. 2010.

[53] H. Yu, Q. Tang, J. Wu, Y. Lin, L. Fan, M. Huang, J. Lin, Y. Li, and F. Yu, “Using eggshell membrane as a separator in supercapacitor,” *J. Power Sources*, vol. 206, pp. 463–468, May 2012.

[54] C. Portet, P. . Taberna, P. Simon, and C. Laberty-Robert, “Modification of Al current collector surface by sol–gel deposit for carbon–carbon supercapacitor applications,” *Electrochim. Acta*, vol. 49, no. 6, pp. 905–912, Mar. 2004.

[55] R. Zhou, C. Meng, F. Zhu, Q. Li, C. Liu, S. Fan, and K. Jiang, “High-performance supercapacitors using a nanoporous current collector made from super-aligned carbon nanotubes.,” *Nanotechnology*, vol. 21, no. 34, p. 345701, Aug. 2010.

[56] A. Sumboja, X. Wang, J. Yan, and P. S. Lee, “Nanoarchitectured current collector for high rate capability of polyaniline based supercapacitor electrode,” *Electrochim. Acta*, vol. 65, pp. 190–195, Mar. 2012.

[57] “Capabuses - ten-year-experimental in Shanghai, Aowei Technology.” [Online]. Available: http://www.aowei.com/article_view.php?typeid=9&id=219. [Accessed: 24-Mar-2014].

[58] “Maxwell Technologies Ultracapaitors and supercapacitors as a green, alternative energy resource.” [Online]. Available: http://www.maxwell.com/ultracapacitors/. [Accessed: 24-Mar-2014].

[59] “Supercapacitor buses - Aowei Technology.” [Online]. Available: http://www.aowei.com/case_view.php?typeid=1&id=4. [Accessed: 24-Mar-2014].

[60] “Helium Bluetooth speakers powered by supercapacitors.” [Online]. Available: http://www.gizmag.com/helium-capacitor-powered-speakers/29938/. [Accessed: 24-Mar-2014].

[61] “Coleman FlashCell Cordless Screwdriver Recharges In Just 90 Seconds.” [Online]. Available: http://www.ohgizmo.com/2007/10/01/coleman-flashcell-cordless-screwdriver-recharges-in-just-90-seconds/. [Accessed: 24-Mar-2014].

[62] “Light For Life Flashlight | The future of things | Science and technology of tomorrow.” [Online]. Available: http://thefutureofthings.com/6275-light-for-life-flashlight/. [Accessed: 24-Mar-2014].

[63] P. W. Ruch, D. Cericola, M. Hahn, R. Kötz, and A. Wokaun, “On the use of activated carbon as a quasi-reference electrode in non-aqueous electrolyte solutions,” vol. 636, pp. 128–131, 2009.

[64] A. Varzi, “Investigations on Multi-Walled Carbon Nanotubes for Lithium-Ion Battery Applications,” Ulm University, 2012.

[65] K. S. W. Sing, D. H. Everett, R. A. W. Haul, L. Moscou, R. A. Pierotti, J. Rouquérol, and T. Siemieniewska, “INTERNATIONAL UNION OF PURE COMMISSION ON COLLOID AND SURFACE CHEMISTRY INCLUDING CATALYSIS * REPORTING PHYSISORPTION DATA FOR GAS / SOLID SYSTEMS with Special Reference to the Determination of Surface Area and Porosity,” *Pure Appl. Chem.*, vol. 57, no. 4, pp. 603–619, 1985.

[66] S. Brunauer, P. H. Emmett, and E. Teller, “Adsorption of gases in multimolecular layers,” *J. Am. Chem. Soc.*, vol. 60, pp. 309–319, 1938.

[67] “auto sorb iQ and ASiQwin GAS SORPTION SYSTEM,” 2012.

[68] R. Evans, U. M. B. Marconi, and P. Tarazona, “Capillary Condensation and Adsorption in Cylindrical and Slit-like Pores,” *J. Chem. Soc. Faraday Trans. 2*, vol. 1787, pp. 1763–1787, 1986.

[69] P. I. Ravikovitch, G. L. Haller, and A. V. Neimark, “Density functional theory model for calculating pore size distributions: pore structure of nanoporous catalysts,” *Adv. Colloid Interface Sci.*, vol. 76–77, pp. 203–226, Jul. 1998.

[70] J. H. de Boer, B. G. Linsen, T. van der Plas, and G. J. Zondervan, “Studies on pore systems in catalysts: VII. Description of the pore dimensions of carbon blacks by the t method,” *J. Catal.*, vol. 4, no. 6, pp. 649–653, 1965.

[71] P. Magelhaes, S. Ram, and M. Abramoff, “Image processing with ImageJ,” *Biophotonics Int.*, vol. 11, no. 7, pp. 36–42, 2004.

[72] A. Mahmoud, J. M. Amarilla, K. Lasri, and I. Saadoune, “Influence of the synthesis method on the electrochemical properties of the Li4Ti5O12 spinel in Li-half and Li-ion full-cells. A systematic comparison,” *Electrochim. Acta*, vol. 93, pp. 163–172, Mar. 2013.

[73] S. Dsoke, X. Tian, C. Täubert, S. Schlüter, and M. Wohlfahrt-Mehrens, “Strategies to reduce the resistance sources on Electrochemical Double Layer Capacitor electrodes,” *J. Power Sources*, vol. 238, pp. 422–429, Sep. 2013.

[74] X. LIU, R. ZHANG, L. ZHAN, D. LONG, W. QIAO, J. YANG, and L. LING, “Impedance of carbon aerogel/activated carbon composites as electrodes of electrochemical capacitors in aprotic electrolyte,” *New Carbon Mater.*, vol. 22, no. 2, pp. 153–158, Jun. 2007.

[75] D. Qu, “Studies of the activated carbons used in double-layer supercapacitors,” *J. Power Sources*, vol. 109, no. 2, pp. 403–411, Jul. 2002.

[76] M. Gaberscek, J. Moskon, B. Erjavec, R. Dominko, and J. Jamnik, “The Importance of Interphase Contacts in Li Ion Electrodes: The Meaning of the High-Frequency Impedance Arc,” *Electrochem. Solid-State Lett.*, vol. 11, no. 10, p. A170, 2008.

[77] B. A. Boukamp, “A NONLINEAR LEAST SQUARES FIT PROCEDURE FOR ANALYSIS OF,” *Solid State Ionics*, vol. 20, pp. 31–44, 1986.

[78] E. Lust, A. Jänes, T. Pärn, and P. Nigu, “Influence of nanoporous carbon electrode thickness on the electrochemical characteristics of a nanoporous carbon|tetraethylammonium tetrafluoroborate in acetonitrile solution interface,” *J. Solid State Electrochem.*, vol. 8, no. 4, pp. 224–237, Mar. 2004.

[79] C. Portet, P. L. Taberna, P. Simon, E. Flahaut, and C. Laberty-Robert, “High power density electrodes for Carbon supercapacitor applications,” *Electrochim. Acta*, vol. 50, no. 20, pp. 4174–4181, Jul. 2005.

[80] X. Li, J. Rong, and B. Wei, “Electrochemical Behavior of Single- Walled Carbon Nanotube Supercapacitors under Compressive Stress,” *ACS Nano*, vol. 4, no. 10, pp. 6039–6049, 2010.

[81] H. Zhang, W. Zhang, J. Cheng, G. Cao, and Y. Yang, “Acetylene black agglomeration in activated carbon based electrochemical double layer capacitor electrodes,” *Solid State Ionics*, vol. 179, no. 33–34, pp. 1946–1950, Oct. 2008.

[82] C. Dangler, M. Rane-Fondacaro, T. S. Devarajan, S. Higashiya, J. Snyder, and P. Haldar, “Role of conducting carbon in electrodes for electric double layer capacitors,” *Mater. Lett.*, vol. 65, no. 2, pp. 300–303, Jan. 2011.

[83] G. Wang, Z. Shao, and Z. Yu, “Comparisons of different carbon conductive additives on the electrochemical performance of activated carbon,” *Nanotechnology*, vol. 18, no. 20, p. 205705, May 2007.

[84] J. Sánchez-González, a. Macías-García, M. F. Alexandre-Franco, and V. Gómez-Serrano, “Electrical conductivity of carbon blacks under compression,” *Carbon N. Y.*, vol. 43, no. 4, pp. 741–747, Jan. 2005.

[85] V. Khomenko, E. Raymundo-pi, and F. Béguin, “A new type of high energy asymmetric capacitor with nanoporous carbon electrodes in aqueous electrolyte,” vol. 195, pp. 4234–4241, 2010.

[86] M. Ue, “Electrochemical Properties of Organic Liquid Electrolytes Based on Quaternary Onium Salts for Electrical Double-Layer Capacitors,” *J. Electrochem. Soc.*, vol. 141, no. 11, p. 2989, 1994.

[87] L. Mariachiara, “Electrode Materials for Ionic Liquid Based-Supercapacitors,” 2010.

[88] K. Xu, “Toward Reliable Values of Electrochemical Stability Limits for Electrolytes,” *J. Electrochem. Soc.*, vol. 146, no. 11, p. 4172, 1999.

[89] K. Xu, M. S. Ding, and T. Richard Jow, “A better quantification of electrochemical stability limits for electrolytes in double layer capacitors,” *Electrochim. Acta*, vol. 46, no. 12, pp. 1823–1827, Mar. 2001.

[90] D. Weingarth, H. Noh, A. Wokaun, and R. Kötz, “A reliable determination method of stability limits for electrochemical double layer capacitors,” *Electrochim. Acta*, vol. 103, pp. 119–124, 2013.

[91] Y. Zhang, H. Feng, X. Wu, L. Wang, A. Zhang, T. Xia, H. Dong, X. Li, and L. Zhang, “Progress of electrochemical capacitor electrode materials: A review,” *Int. J. Hydrogen Energy*, vol. 34, no. 11, pp. 4889–4899, Jun. 2009.

[92] L. Wang, T. Morishita, M. Toyoda, and M. Inagaki, “Asymmetric electric double layer capacitors using carbon electrodes with different pore size distributions,” *Electrochim. Acta*, vol. 53, no. 2, pp. 882–886, Dec. 2007.

[93] O. Barbieri, M. Hahn, a. Herzog, and R. Kötz, “Capacitance limits of high surface area activated carbons for double layer capacitors,” *Carbon N. Y.*, vol. 43, no. 6, pp. 1303–1310, May 2005.

[94] S. J. Gregg and K. S. W. Sing, *Adsorption, surface area, and porosity*. Academic Press, 1991.

[95] K. Kaneko and C. Ishii, “Superhigh surface area determination of microporous solids,” *Colloids and surfaces*, vol. 67, pp. 203–212, 1992.

[96] L. Wei and G. Yushin, “Nanostructured activated carbons from natural precursors for electrical double layer capacitors,” *Nano Energy*, vol. 1, no. 4, pp. 552–565, Jul. 2012.

[97] J. Chmiola, G. Yushin, Y. Gogotsi, C. Portet, P. Simon, and P. L. Taberna, “Anomalous increase in carbon capacitance at pore sizes less than 1 nanometer.,” *Science*, vol. 313, no. 5794, pp. 1760–3, Sep. 2006.

[98] J. Segalini, E. Iwama, P.-L. Taberna, Y. Gogotsi, and P. Simon, “Steric effects in adsorption of ions from mixed electrolytes into microporous carbon,” *Electrochem. commun.*, vol. 15, no. 1, pp. 63–65, Feb. 2012.

[99] G. Sun, W. Song, X. Liu, D. Long, W. Qiao, and L. Ling, “Capacitive matching of pore size and ion size in the negative and positive electrodes for supercapacitors,” *Electrochim. Acta*, vol. 56, no. 25, pp. 9248–9256, Oct. 2011.

[100] J. Segalini, B. Daffos, P. L. L. Taberna, Y. Gogotsi, and P. Simon, “Qualitative Electrochemical Impedance Spectroscopy study of ion transport into sub-nanometer carbon pores in Electrochemical Double Layer Capacitor electrodes,” *Electrochim. Acta*, vol. 55, no. 25, pp. 7489–7494, Oct. 2010.

[101] R. Lin, P. Huang, J. Ségalini, C. Largeot, P. L. Taberna, J. Chmiola, Y. Gogotsi, and P. Simon, “Solvent effect on the ion adsorption from ionic liquid electrolyte into sub-nanometer carbon pores,” *Electrochim. Acta*, vol. 54, no. 27, pp. 7025–7032, Nov. 2009.

[102] H. Shi, “Activated carbons and double layer capacitance,” *Electrochim. Acta*, vol. 41, no. 95, p. 1633, 1996.

[103] E. Ito, S. Mozia, M. Okuda, T. Nakano, M. Toyoda, and M. Inagaki, “Nanoporous carbons from cypress II. Application to electric double layer capacitors,” *New Carbon Mater.*, vol. 22, no. 4, pp. 321–326, Dec. 2007.

[104] L. Wang, M. Fujita, and M. Inagaki, “Relationship between pore surface areas and electric double layer capacitance in non-aqueous electrolytes for air-oxidized carbon spheres,” *Electrochim. Acta*, vol. 51, pp. 4096–4102, 2006.

[105] L. J. Kennedy, J. J. Vijaya, and G. Sekaran, “Electrical conductivity study of porous carbon composite derived from rice husk,” *Mater. Chem. Phys.*, vol. 91, no. 2–3, pp. 471–476, Jun. 2005.

[106] M. Inagaki, K. Ishihara, M. Kato, T. Morishita, and A. I. Tech, “Mesoporous carbons for energy storage.”

[107] L. Li, H. Song, and X. Chen, “Pore characteristics and electrochemical performance of ordered mesoporous carbons for electric double-layer capacitors,” *Electrochim. Acta*, vol. 51, no. 26, pp. 5715–5720, Aug. 2006.

Publication list

Xu Tian, Bettina Fuchs, Sonia Dsoke, Margret Wohlfahrt-Mehrens, Towards the realization of powerful and energetic electrochemical double layer capacitors, 14th Ulm Electrochemical Talks (UECT), Ulm, June 24-26, 2014.

S. Dsoke, X. Tian, C. Täubert, S. Schlüter, M. Wohlfahrt-Mehrens, Strategies to Reduce the Resistance Sources on EDLCs Electrodes, Journal of Power Sources, Volume 238, 2013, 422-429.

X. Tian, S. Dsoke, C. Täubert, M. Wohlfahrt-Mehrens, An asymmetric electrochemical capacitor with activated carbon electrodes in organic electrolyte, Pacific RIM Meeting on Electrochemical and Solid-State Science 2012, Honolulu, Hawaii, October 7-12, 2012.

X. Tian, S. Dsoke, C. Täubert, A. Rota, T. Kirschbaum, M. Wohlfahrt-Mehrens, High capacitance Activated Carbon for Double Layer Supercapacitors, GDCh-Electrochemistry 2012, Munich, September 17-19, 2012.

X. Tian, S. Dsoke, C. Täubert, M. Wohlfahrt-Mehrens, Evaluation of Electrode Components Contributions on the Total Impedance of a Symmetric Electrochemical Double Layer Capacitor, 124th BASF International Summer Course, Ludwigshafen, August 14-24, 2012.

X. Tian, S. Dsoke, C. Täubert, M. Wohlfahrt-Mehrens, Investigation on improving the electrical contact between carbon and current collector for double layer supercapacitors, 13th Ulm Electrochemical Talks (UECT), Ulm, July 3-5, 2012.

Lebenslauf

Xu Tian

Persönliche Angaben

Geburtsdatum:	25.09.1985
Geburtsort:	Nei Mongol, China

Arbeitserfahrungen

09/2014 - heute

Entwicklungsingenieur

International Project Management, Akkumulatorenfabrik MOLL, Bad Staffelstein

- Entwicklung von neuen Formationsverfahren für Blei Batterien
- Inbetriebnahme neuartigen Batterie Formationsanlage und Finish-linie in China und auch in Deutschland
- International Project Management (besonders die Zusammenarbeit mit dem chinesischen Partner Chaowei)

Ausbildung

03/2011 - 08/2014

Promotion (Chemie)

Zentrum für Sonnenenergie- und Wasserstoff-Forschung Baden-Württemberg (ZSW), Ulm

(Projekt mit diversen Industriepartnern)

- Rohmaterialcharakterisierung (N_2 und CO_2 Adsorption, REM, Hg-porosimetrie) von verschiedenen Aktivmaterialien (Aktivkohlen, Ruße, $LiFePO_4$, $Li_4Ti_5O_{12}$, etc.)

- Prozessentwicklung und -optimierung für die Elektroden-präparation in Li-Ion Batterie- und Superkondensatorfertigung;
  Erfahrungen mit Viskosimeter, Kneter, Heißpresse, Laminator, Extruder, Zweiwalzenmühle und Kalander in drei verschiedenen Fertigungsmaßstäben
- Elektrochemische Charakterisierungen der Zellen aus diversen Aktivmaterialien

10/2008 - 12/2010 **Master of Science (Energiewissenschaft und -technik)**
Universität Ulm; Note: 1,5

- Schwerpunkt Materialwissenschaft und Elektrochemie

Masterarbeit am ZSW, Ulm
Titel der Masterarbeit: "Investigation of naturally and artificially ageing processes of gas diffusion layers for PEM-Fuel Cells"

09/2003 - 06/2008 **Bachelor of Engineering (Werkstoffwissenschaft und -technik)**
Tongji Universität, Shanghai, China; Note: 2,5

- Schwerpunkt Polymer

Titel der Bachelorarbeit: "Preparation and characterization of natural-fiber-reinforced poly lactic acid composite for aeronautic applications"

06/2003 **Abitur**
1. Baogang Mittelschule, Nei Mongol, China

Stipendien

04/2013 - heute E-fellows.net Stipendium